CONTENTS

	Page	
SUMMARY	1	1/A9
INTRODUCTION	3	1/A11
SYMBOLS AND ABBREVIATIONS	5	1/A13
CONFIGURATION DEFINITION	12	1/B6
Engine Definition	12	1/B6
969-512B Configuration	12	1/B6
Stability and Control	14	1/B9
Longitudinal Control	14	1/B9
Longitudinal Stability	14	1/B9
Lateral-Directional Stability and Control	16	1/B11
Fuel Tank Arrangements	17	1/B12
STRUCTURAL DESCRIPTION	19	1/B14
Materials Evaluation and Selection	20	1/C1
Metals	20	1/C1
Advanced Composites/Adhesives	20	1/C1
Fuel Tank Sealant	21	1/C2
Fuel Tank Insulation	21	1/C2
Structural Concepts	22	1/C3
Wing Skin Panel Concepts	27	1/C11
Wing Spar Concepts	29	1/C13
Fuselage Panel Concepts	30	1/C14
STRUCTURAL ANALYSIS AND DESIGN	32	1/D2
The Integrated Computer Program System	32	1/D2
The ATLAS System	32	1/D2
FLEXSTAB System	34	1/D4
Flutter Modules	36	1/D6
Analytical Models	36	1/D6
Structural Model	36	1/D6
Structural Model Verification	37	1/D7
Mass Model	38	1/D8
Aerodynamic Model	38	1/D8
Structural Design Loads	38	1/D8
Structural Design Airspeeds	38	1/D8
Design Gross Masses	39	1/D9
Engine Thrust	39	1/D9
Maneuver and Gust Criteria	39	1/D9
Landing, Taxi, and Ground Handling Loads Criteria	41	1/D11
Aerodynamic Loads Analysis	41	1/D11

CONTENTS (Concluded)

	Page
Structural Load Conditions	43 1/D14
Jig Shape	45 1/E2
Thermal Analyses	45 1/E2
Aerodynamic Heating	45 1/E2
Solar Absorptance and Surface Emittance	46 1/E3
Transient Thermal Analysis	46 1/E3
Fuel Temperature Analysis	48 1/E5
Mission Description	48 1/E5
Temperature Limits	49 1/E6
Fuel System	49 1/E6
Fuel Temperature	49 1/E6
Stress Analysis and Strength Sizing	52 1/E10
Flutter Analysis and Resizing	55 1/E13
Flutter Analysis Procedure	55 1/E13
Preliminary Flutter Analysis and Stiffness Resize	55 1/E13
Final Flutter Analysis and Stiffness Redesign	57 1/F1
Mass Analysis	58 1/F2
Wing and Contents	59 1/F3
Correction of Mass Analysis	59 1/F3
Body and Contents	62 1/F6
Empennage and Wing-Mounted Fin	62 1/F6
Fuel	62 1/F6
Wing Box Mass Estimation Method	62 1/F6
Mass Changes Resulting From Redesign for Strength	63 1/F7
Additional Mass Required to Satisfy Flutter Criteria	65 1/F10
Final Group Mass Statement	65 1/F10
EFFECTS OF REDESIGN ON AIRPLANE PERFORMANCE	67 1/F13
RECOMMENDATIONS	69 1/G1
Further Applications of the Arrow Wing Model	69 1/G1
Research on Prediction of Aerodynamic Pressure Distributions	69 1/G1
Advanced Titanium Alloys	70 1/G2
Fabrication Techniques	70 1/G2
CONCLUDING REMARKS	72 1/G4
REFERENCES	74 1/G6

Item No. 830-H-14

NAS 1.26:2743

JAN 24 1978

NASA Contractor Report 2743

COMPLETED
ORIGINAL

Study of Metallic Structural Design Concepts for an Arrow Wing Supersonic Cruise Configuration

M. J. Turner and D. L. Grande

CONTRACT NAS1-12287
DECEMBER 1977

NASA

150

NAS1.26:2743

NASA Contractor Report 2743

Study of Metallic Structural Design Concepts for an Arrow Wing Supersonic Cruise Configuration

M. J. Turner and D. L. Grande
Boeing Commercial Airplane Company
Seattle, Washington

Prepared for
Langley Research Center
under Contract NAS1-12287

National Aeronautics
and Space Administration

Scientific and Technical
Information Office

1977

Blank Page

TABLES

No.		Page
1.	Configuration Characteristics, Model 969-512B	13
2.	Group Mass and Balance Statement, Model 969-512B	15
3.	969-512B Estimated Lateral Control Power	16
4.	Structural Concepts Evaluated	22
5.	Structural Concept Evaluation, Wing Skin Panels, Point 269	23
6.	Structural Concept Evaluation, Wing Skin Panels, Point 431	24
7.	Structural Concept Evaluation, Wing Spar	25
8.	Structural Concept Evaluation, Body	26
9.	A Summary of ATLAS 2.2 Capabilities	34
10.	Boeing Program to Improve Efficiency and Reliability of Aeroelastic Loads Analysis	35
11.	Design Gross Mass	40
12.	Installed Maximum Thrust ATAT-1 Afterburner Operative	40
13.	Limit Load Factors	40
14.	Limit Loads for Ground Handling Conditions	42
15.	Load Conditions for Design	44
16.	Thermal Analysis Conditions	47
17.	Mission Profile	48
18.	Fuel Tank Conductance	50
19.	Fuel Temperatures for Various Trip Conditions	51
20.	Preliminary Symmetric Wing Flutter Results	56
21.	Modifications – Model 969-512B	58
22.	Group Mass and Balance Statement, Model 969-512B	60
23.	Wing Structural Mass Change, Model 969-512B	64
24.	Mass Changes for Flutter	66
25.	Structural Design Impact on Mission Range	67
26.	Structural Design Impact on Performance	68

FIGURES

No.		Page
1.	Configuration for structural analysis, model 969-512B	77
2	Longitudinal HSAS functional diagram	79
3.	Alpha limiter functional diagram	80
4.	Lateral – directional HSAS functional diagram	81
5.	Fuel tank layout, model 969-512B	82
6.	Wing structural arrangement, model 969-512B	83
7.	Body structural arrangement, model 969-512B	84
8.	Materials selection process, 1975 technology	85
9.	Panel/tank conductance characteristics	86
10.	Potential insulating materials	87
11.	Wing structural control panel locations and design conditions	88
12.	Body control panel locations	89
13.	Wing baseline skin panels	90
14.	Wing skin panel, aluminum, brazed titanium honeycomb	91
15.	Wing skin panel, integrally machined and welded – sheet stiffener	92
16.	Wing spar, baseline, PT 249	93
17.	Wing spar, baseline, PT 269 and 431	94
18.	Body baseline shell arrangement	95
19.	Structural analysis and design process	96
20.	ATLAS, an integrated structural analysis and design system	97
21.	Basic structural model	98
22.	Resonance of landing gear	99
23.	Mass paneling for flutter	100
24.	Aerodynamic paneling for subsonic loads	101
25.	Design speed-altitude envelope	102
26.	Maneuver envelope at sea level for maximum flight mass	103
27.	Geometry and gear reactions for ground loads	104
28.	Forward body ultimate shear force, landing impact	105
29.	Forward body ultimate bending moment, landing impact	106
30.	Jig shape deflections	107
31.	Solar and emittance effects	108
32.	Control points for thermal analysis	109
33.	Mission profile – 6190 km (3340 nmi)	110
34.	Fuel tank nos. 1 and 2, fuel management	111
35.	Fuel tank no. 1, point 249	112
36.	Fuel tank no. 1 temperatures, point 249, case 1	113
37.	Fuel tank no. 1 thermal stresses, point 249, case 1	114
38.	Effect of panel thermal conductance on fuel tank conductance	115
39.	Maximum temperature of fuel in main tanks at end of second supersonic cruise mission, baseline configuration	116
40.	Maximum temperature of fuel in main tanks at end of supersonic cruise, second trip, compartmented configuration	117
41.	Wing structur. regions	118

FIGURES (Concluded)

No.		Page
42.	Wing cover element subsets	119
43.	Wing spar element subsets	120
44.	Lower bound data	121
45.	Typical mechanical properties (including thermal stress decrements) Ti-6Al-4V, condition 1	122
46.	Typical instability allowables (including thermal stress decrements), Ti-6Al-4V, condition 1	123
47.	Typical wing panel resizing results	124
48.	Effect of resizing on theoretical wing mass	126
49.	Preliminary flutter speeds	127
50.	Effect of nacelle beam stiffening on modal coupling	128
51.	Arrow wing flutter boundary, 969-512B	129
52.	Final design modification for stiffness	130
53.	Wing leading edge and trailing edge structure, mass input elements	131
54.	Wing contents, mass input elements	132
55.	Body structure and contents, mass distribution	133
56.	Body payload, mass distribution	134
57.	Fuel management – model 969-512B	135
58.	Structural mass estimation	136
59.	Typical nonoptimum wing panel elements	137
60.	Aluminum brazed titanium honeycomb panels – skin t vs nonoptimum mass	138
61.	Structural wing box mass estimation method	139
62.	Range sensitivity to OEM and supersonic drag	140
63.	SST performance climb placards	141

STUDY OF METALLIC STRUCTURAL DESIGN CONCEPTS FOR AN ARROW WING SUPERSONIC CRUISE CONFIGURATION

M. J. Turner and D. L. Grande
Boeing Commercial Airplane Company

SUMMARY

The principal objectives of the present study were to assess the relative merits of various metallic structural concepts and materials suitable for an advanced supersonic aircraft cruising at Mach 2.7, to select the structural approaches best suited for the Mach 2.7 environment, and to provide construction details and structural mass estimates based on in depth structural design studies of representative wing and fuselage structures. During the first part of the study, an arrow-wing configuration was analyzed in considerable detail for compliance with criteria derived from the National SST program. An advanced technology afterburning turbojet engine concept developed under contract NAS1-11938 was used for propulsion.

A study of the internal structural arrangement was conducted based on the arrangement developed in a previous study of an arrow-wing supersonic cruise aircraft (NASA SCAT-15F). A series of structural variations were evaluated. The wing structure that was selected consisted of a multispar internal structure with aluminum brazed titanium sandwich panels for the wing surfaces, except for a machined skin on the lower surface of the main wing box. The fuselage was of skin stringer construction. Titanium was used throughout.

A single basic finite element model of the structure was developed for aeroelastic loads, stress, and flutter analyses containing approximately 2000 nodes, 4200 elements, and 8500 active degrees of freedom. Analyses were performed by an integrated structural analysis and design system interfaced with loads and flutter analysis systems. The elements in the wing covers were resized using an automated resizing module in the integrated system, with convergence, measured in terms of total mass change, occurring in three cycles. Nine flutter analyses were conducted to evaluate a series of stiffness changes to remedy a flutter deficiency in the strength design. Stiffness changes were based on engineering judgment and experience from the National SST program.

The resulting configuration, designated the 969-512B, meets most of the specified study requirements, having a maximum taxi gross mass of 340 200 kg (750 000 lbm), and a payload of 22 200 kg (49 000 lbm) representing 234 passengers in tourist accommodations, and a cruise Mach number of 2.7. The structure, stability and control characteristics, and systems meet the appropriate requirements of *Federal Aviation Regulations, Part 25, Airworthiness Standards: Transport Category Aircraft, and the Tentative Airworthiness Requirements for Supersonic Transports.*

It is concluded that a major advantage of the integrated flutter analysis and design system is the reduction in resources and cycle time required to perform analyses. This improved efficiency permits stiffness requirements to be imposed earlier in the design cycle. Also, the study contributes to structural analysis and design methodology and provides a detailed mathematical model of the baseline airplane that can be used to evaluate design improvements and advances in technology for supersonic cruise aircraft. Recommendations for further development of integrated design tools and applications methodology are discussed.

INTRODUCTION

This document presents a general description of a study conducted by the Boeing Commercial Airplane Company as a part of the NASA Supersonic Cruise Aircraft Research program. The principal objectives of the study were to assess the relative merits of various concepts and materials suitable for an advanced supersonic aircraft cruising at Mach 2.7, to select the structural approaches best suited for the Mach 2.7 environment, and to provide construction details and structural mass estimates based on in-depth structural design studies of representative wing and fuselage structures. A brief description of the study has been presented previously in reference 1.

The airplane configuration on which the structural analysis was conducted is an arrow-wing concept representative of a 1975 technology level. A Mach 2.7 arrow wing configuration was selected for these baseline studies because previous investigations have shown it to be one of the most promising aerodynamic configurations for supersonic cruise. It is derived from a configuration presented by NASA (see ref. 2), and is similar to the Model 969-336C that was studied during the National SST program (ref. 3). Since arrow wing aircraft tend to be large and flexible, aeroelasticity is a major design consideration, and realistic aeroelastic considerations based on analysis of finite-element structural models and sophisticated aerodynamic loading analysis are required even in a preliminary design study of such a vehicle. The amount of interaction between the various technical disciplines in aeroelastic problems requires the use of computer-aided design methods to improve and expedite the aeroelastic and structural resizing cycle (ref. 4).

A detailed multidisciplinary analysis of the configuration was conducted, and further modifications and refinements to the airframe were introduced. This effort focused on those aspects of the configuration that are likely to impose significant constraints on structural design. Engine locations were dictated largely by performance requirements. Also pitching moment characteristics related to stability and control were given careful consideration in establishing horizontal tail size.

Basic objectives of the evaluation of the metallic structure were to select materials and structural concepts that were consistent with the requirements of an aircraft designed to cruise at Mach 2.7 and based on a 1975 level of technology. In assessing the various structural concepts and materials, such factors as mass, ease of fabrication, sealing of fuel tanks, maintenance and servicing, material and fabrication costs, and fail safety were considered.

The analytical design studies were conducted to evaluate the importance of factors such as: variations of structural concepts, including sandwich panels, stiffened thin sandwich panels, skin-stringer construction, and variations in frame, rib, and spar construction; variations in landing gear and engine location and the effect of variations in engine support beam stiffness; effects of temperature on material allowables and temperature gradients on stresses; flutter; static aeroelastic effects; control systems interactions with the loads; and volume and insulation requirements for fuel storage. Particular emphasis was put on flutter, aeroelasticity, and practical design considerations such as fail safety

and fastener requirements. In addition to the usefulness of the results obtained for the specific configuration, these studies provided a unique opportunity to appraise the computer-aided design methods that have been developed by the contractor during the past few years, and to bring into sharper focus those problems and technology areas requiring structural evaluation.

The following sections of this report present an abbreviated account of the configuration definition study, followed by a detailed exposition of the structural analysis and design. This latter account discusses the concept selection process and the selected concepts, followed by an account of the analysis and design process. In addition to a description of the analytical methods for loads, stress, and flutter, the iterative design process is described, leading to the final member sizes that satisfy strength and flutter criteria.

Recommendations are presented for necessary improvements in prediction of aerodynamic pressure distributions, advanced titanium alloys, and improved structural concepts.

SYMBOLS AND ABBREVIATIONS

A	Area
ALT	Altitude
A/P	Airplane
APP	Approach
APU	Auxiliary power unit
AR	Aspect ratio
AST	Advanced supersonic technology
ATAT	Advanced technology afterburning turbojet
a	Acceleration
BL	Buttock line
Btu	British thermal unit
b_w	Wing span
C_D	Drag coefficient
$\mathbb{C}_L$	Centerline
C_L	Lift coefficient
C_{ℓ}	Rolling moment coefficient
$C_{L_{APP}}$	Lift coefficient for landing approach
$C_{L_{MAX}}$	Maximum value of lift coefficient
$C_{L_{MAXDEM}}$	Maximum demonstrated lift coefficient
$C_{L_{MIN}}$	Minimum value of lift coefficient
C_{M_o}	Pitching moment coefficient at zero lift
$C_{M_{TAIL}}$	Pitching moment coefficient due to horizontal tail
C_m	Pitching moment coefficient

$C_{N_{MAXDEM}}$	Maximum demonstrated normal force coefficient
C_{n_β}	Static directional stability derivative
C_n	Yawing moment coefficient
$\bar{c}$	Mean aerodynamic chord
c/4	One quarter chord
c.g.	Center of gravity
D	Drag
D_M	Main gear drag reaction
D_N	Nose gear drag reaction
dB	Decibels
E	Modulus of elasticity
EAS	Equivalent airspeed
ECS	Environmental control system
EPNdB	Effective perceived noise decibels
F	Fahrenheit
F_N	Engine net thrust
FAR	Federal Aviation Regulation
ft	Feet
G	Control elements in a block diagram
g	Gravitational acceleration
H/C	Honeycomb
HSAS	Hardened stability augmentation system
h_α	Rate of change of heat transfer coefficient with angle of attack

hr	Hours
in.	Inches
K	Kelvin
KEAS	Knots-equivalent airspeed
kg	Kilograms
km	kilometers
kn	Knots
L	Lift
LE	Leading edge
Ldg	Landing
lbf	Pound force
lbm	Pound mass
ℓ_H	Horizontal tail arm length
ℓ_V	Vertical tail arm length
M	Mach number
M_C	Design cruise Mach number
M_D	Design dive Mach number
M_{MO}	Maximum operational Mach number
M_δ	Pitching moment derivative with respect to control surface deflection
MAC	Mean aerodynamic chord
m	Meters
N	Newtons
N_x	Inplane stress resultant in the x direction
N_{xy}	Shear stress resultant
n	Normal load factor

n_z	Vertical acceleration
nmi	Nautical miles
OEM	Operational empty mass
PPD	Prototype Point Design
PR	Percent radius
PT	Prototype
p	Roll rate
psf	Pounds per square foot
q	Dynamic pressure
q_0	Freestream incompressible dynamic pressure
R	Rankine
r	Yaw rate
RFP	Request for proposal
RT	Room temperature
rad	Radians
ref	Reference
S	Laplace transform
S & C	Stability and control
S_H	Horizontal tail area
S_M	Main gear side load
S_N	Nose gear side load
S_{ref}	Reference area (usually wing area)
S_V	Vertical tail area
S_W	Wing area

SFC	Specific fuel consumption
SOB	Side of body
S/S	Sound suppressor
SST	Supersonic transport
Sta	Station
Std	Standard
s, sec	Seconds
sq	Square
T	Temperature, Time
T_W	Wall temperature
TE	Trailing edge
TO	Takeoff
T/R	Thrust reverser
t	Thickness
$\bar{t}$	Equivalent thickness
t/c	Thickness ratio (thickness over chord)
u	Forward velocity increment
V	True velocity (speed)
V_A	Design maneuver speed at a positive load factor
V_{APP}	Approach speed
V_B	Design speed for maximum gust intensity
V_{BAL}	Speed for engine out yawing moment
V_C	Design cruise speed
V_c	Calibrated cruise speed

V_D	Design dive speed
V_E, V_e	Calibrated equivalent speed
V_F	Design flap speed
V_H	Design maneuver speed
V_M	Main gear vertical reaction
$V_{MAX_{DEM}}$	Maximum demonstrated speed
$V_{MIN_{DEM}}$	Minimum demonstrated speed
V_{MO}	Maximum operation speed
V_N	Nose gear vertical reaction
V_R	Takeoff rotation speed
V_1	Takeo-off safety speed
$\overline{V}$	Tail volume coefficient
$\overline{V}_H$	Horizontal tail volume coefficient
W	Watts
W/	With
WL	Waterline
WRP	Wing reference plane
w	Vertical velocity increment
w/o	Without
w_1	Mass per unit area of braze material, upper wing panel
w_2	Mass per unit area of braze material, lower wing panel
α	Angle of attack
α_{LOF}	Liftoff angle

α_{SOL}	Material absorptance for solar energy
α_{wrp}	Rotation angle in relation to wing reference plane
$\dot{\alpha}$	Time rate of change of angle of attack
β	Sideslip angle
Δ	Delta (increment)
δ	Deflection angle (usually control surface)
δ_a	Aileron deflection
δ_e	Elevator deflection
δ_H	Stabilizer deflection
δ_r	Rudder deflection
δ_{sp}	Spoiler deflection
ϵ	Surface emittance
η	Fraction of semispan
θ	Pitch angle
$\dot{\theta}$	Pitch rate of change
Λ	Sweep angle
λ	Taper ratio
ρ	Density
σ	Stefan-Boltzmann constant
σ_j	Stress in component j
ϕ	Bank angle or roll angle
ϕ_t	Bank angle achievable in time, t=sec
$\ddot{\phi}$	Rolling acceleration
ψ	Heading angle or yaw angle

CONFIGURATION DEFINITION

The airplane configuration on which the structural analysis was conducted is an arrow wing concept representative of a 1975 technology level. It was derived from a configuration presented by NASA (see ref. 2) and designated as model 969-510. This configuration is similar to the model 969-336C studied during the National SST Program (ref. 3) except for modifications to the wing leading edge sweep angle to provide additional wing chord and box depth in the outboard wing, and an outward shift of the engines to provide for a larger inboard flap to improve low speed lift. In addition to the above changes, the canard and "demand leading edge flap" systems which were present in the earlier configuration have been removed.

A detailed, multidisciplinary analysis of the configuration was conducted, focusing on those aspects of configuration that are likely to impose significant constraints on structural design. For example, engine locations were given considerable attention, and were largely dictated by performance considerations, with potential implications concerning wing flutter. Also pitching moment characteristics related to stability and control have been given sufficient attention to establish horizontal tail size.

ENGINE DEFINITION

The engine selected for this study is an advanced technology afterburning turbojet engine designated ATAT-1 developed under Contract NAS1-11938. This engine was based on the GE4/J6G afterburning turbojet, with modifications to geometry, mass, performance, and noise derived from data for more advanced technology designs. The total installed engine pod mass of 7570 kg (16 700 lbm) is representative of advanced technology variable cycle engines currently being studied under contract to NASA-Langley Research Center. To minimize pod weight, the engine is operated at the maximum afterburning temperature of 1644 K (2960° R) at takeoff.

The performance of the ATAT-1 is based on the GE4/J6G engine, the most advanced afterburning turbojet defined in the course of the U.S. National SST program. The installed performance was calculated accounting for all intake drag and recovery losses, environmental control system, secondary air system losses, and bleed and power extraction losses associated with the pod.

Prior work on engine/airframe integration for large supersonic airplanes indicates that a minimum drag installation is achieved when pod inlets are located behind the line of maximum wing thickness and the maximum pod area is close to the wing trailing edge. Lateral pod location is determined by spacing required to avoid mutual pod inlet interference and does not have a significant effect on cruise drag.

969-512B CONFIGURATION

The configuration used in the structural study, designated model 969-512B and incorporating the refinements resulting from the configuration review, is shown in figure 1. Geometric data and other characteristics are listed in table 1. The following modifications were made in defining the configuration for the structural study:

TABLE 1.–CONFIGURATION CHARACTERISTICS, MODEL 969-512B

Geometry			Wing	Wing vert. stabilizer	Vertical stabilizer	Horizontal stabilizer
Area	m^2	(sq ft)	915 (9,848)*	26.7 (287)/side	41.7 (449)	55.7 (600) exposed
Aspect ratio,	AR		1.78	0.493	0.848	1.32
Taper ratio,	λ			0.135	0.24	0.247
Sweep at LE	Rad	(deg)	1.29/1.23/1.05 (74/70.5/60)	1.30 (74.5)	0.89 (51)	0.94 (54)
Incidence	Rad	(deg)	–	–	–	-0.26/0.52 + 0.26/0.44 (-15/30 + 15/25)
Dihedral	Rad	(deg)	–	–	–	0
Root t/c	%		–	3	3	3
Tip t/c	%		–	3	3	3
Root chord	m	(in.)	47.8 (1881.1)	13.0 (510)	11.30 (445)	10.52 (414)
Tip chord	m	(in.)	5.18 (204)	1.75 (69)	2.72 (107)	2.59 (102)
MAC	m	(in.)	30.1 (1187)	8.79 (346)	7.90 (311)	7.34 (289)
Span	m	(in.)	40.4 (1590)	3.63 (143)	–	8.59 (338)
Tail arm	m	(in.)	–	17.70 (697)	24.82 (977)	26.97 (1062)
Tail vol coeff, $\bar{V}$			–	0.013	0.028	0.0545

*Reference area. Total wing area ABCDEFGH = 1045 m^2 (11 244 sq ft), see figure 1

Gross mass: 340 200 kg (750 000 lbm)

Body	Length, m (in.)	Max dia, m (in.)	Accommodation	
	92.4 (3640)	3.87 (152.2)	234 pass.	4/5 AB
Powerplants	Number	Type	Airflow	Inlet
	4	ATAT-1	287 kg/sec (633 lbm/sec)	Axisym
Landing gear wheels	Nose	Main	Loc % MAC	
	2–86 x 41 cm (34 x 16 in.)	24–103 x 36 cm (40.7 x 14 in.)	57.7 (pivot)	
Fuel capacity, kg (lbm)	Wing	Body	Total	
	143 970 (317 400)	32 660 (72 000)	176 450 (389 000)	
cg limits	Takeoff	Cruise	Landing	
% MAC Fwd			49.7	
% MAC Aft		55.5	53.0	

B

1. Reduction of wing tip leading edge sweep angle by 0.080 rad (4.6 deg) to increase wing tip lift capability and improve pitching moment characteristics

2. Alteration of planform and increase in area of horizontal stabilizer to increase effectiveness and satisfy nose-down control requirements

3. Replacement of all-movable vertical tail by a larger surface with fixed fin and segmented rudder to satisfy engine failure criteria.

4. Alteration of wing-to-fuselage location to reposition airplane center of gravity with zero fuel mass within acceptable limits

5. Increase of wing thickness over the wheel well to accommodate the landing gear without an out-of-contour fairing on the upper surface

6. 0.026 rad (1.5 deg) nose-down twist of wing tip to optimize cruise trim drag

7. Alteration of fuel tank arrangement to locate fuel in the aft body and deeper wing sections to reduce fuel heating during cruise

A group mass and balance statement for model 969-512B is presented in table 2.

STABILITY AND CONTROL

LONGITUDINAL CONTROL

The horizontal tail sizing for the 969-512B is based on updated low-speed stability and control characteristics. The minimum tail area that meets center-of-gravity range requirements is 50.44 m^2 (543 ft^2). A study was undertaken to determine the airplane mass sensitivity due to variations in horizontal stabilizer size. Although a smaller stabilizer satisfies control power requirements, a larger stabilizer results in a smaller operating empty mass and permits a c.g. range extending farther aft, thereby improving the airplane loadability. Consequently, a 55.74 m^2 (600 ft^2) horizontal stabilizer was retained for the 969-512B configuration.

LONGITUDINAL STABILITY

To meet minimum safe operational criteria throughout the flight envelope, longitudinal and lateral-directional flight-critical augmentation systems were incorporated in the design. The longitudinal augmentation system, shown in figure 2, produces a pitch rate feedback signal that is used to generate increased aerodynamic stiffness and damping. A second-order structural filter is used to prevent coupling between airplane dynamics and structural modes.

Wind tunnel data for flaps-down arrow wing configurations exhibit an unstable pitch break although the magnitude is dependent on the leading edge flap configuration, leading edge radius, basic wing planform, and trailing edge flap configuration. An alpha limiter system is used to prohibit angles of attack greater than that corresponding to $C_{L_{MAX\,DEM}}$.

TABLE 2.–GROUP MASS AND BALANCE STATEMENT, MODEL 969-512B

Group	Mass (kg)	Arm (m)	Mass (lbm)	Arm (in.)
Wing	**42 710**	**66.14**	**94 160**	2604
Horizontal tail	**2 962**	**92.02**	**6 530**	3623
Vertical tail (body and wing mtd)	**2 268**	**86.51**	**5 000**	3406
Body	**25 465**	**53.77**	**56 140**	2117
Main gear	**16 928**	**64.72**	**37 320**	2548
Nose gear	**1 705**	**29.92**	**3 760**	1178
Nacelle	**8 655**	**74.90**	**19 080**	2949
Total structure	**100,693**	**64.13**	**221 990**	2525.0
Engine (incl T/R, S/S and nozzle)	**20 502**	**78.13**	**45 200**	3076
Engine accessories	**612**	**74.78**	**1 350**	2944
Engine controls	**354**	**58.62**	**780**	2308
Starting system	**136**	**74.14**	**300**	2919
Fuel system	**3 806**	**63.37**	**8 390**	2495
Total propulsion	**25 410**	**75.55**	**56 020**	2974.3
Instruments	**846**	**43.43**	**1 865**	1710
Flight controls	**6 668**	**68.05**	**14 700**	2679
Hydraulics	**2 628**	**72.49**	**5 795**	2854
Electrical	**2 341**	**53.14**	**5 160**	2092
Electronics	**1 309**	**32.56**	**2 885**	1282
Furnishings	**8 623**	**46.15**	**19 010**	1817
ECS	**3 824**	**61.98**	**8 430**	2440
Anti-icing	**61**	**14.17**	**135**	558
APU	**113**	**75.84**	**250**	2978
Insulation	**1 315**	**48.59**	**2 900**	1913
Total systems and equipment	**27 728**	**56.13**	**61 130**	2209.7
Options	**1 134**	**63.27**	**2 500**	2491
Manufacturer's empty mass	**154 985**	**64.56**	**341 640**	2542.0
Standard items	**3 719**	**55.70**	**8 200**	2193
Operational items	**2 386**	**43.59**	**5 260**	1716
Operational empty mass	**161 070**	**64.05**	**355 100**	2521.7
Payload	22 200	**47.80**	49 000	1882
Zero fuel mass	**183 265**	**62.09**	**404 008**	2444.3

A conceptual block diagram of the selected alpha limiter system is shown in figure 3. This system will not affect airplane characteristics until the alpha limit is being approached. At this time it will modify the apparent airplane pitching moment by commanding nose-down elevator if the pilot has not already initiated recovery. A more detailed discussion of the alpha limiter system is published in reference 2.

LATERAL-DIRECTIONAL STABILITY AND CONTROL

The area of the wing-mounted vertical surfaces was selected to provide neutral stability at the cruise condition. This was achieved by maintaining the same ratio between the vertical surface area and the gross wing area as on the Langley wind tunnel model. The centerline vertical surface has the same geometry as the 1971 U.S. SST and is sized for engine-out control.

At M = 2.7, 1 g level flight, the yawing moments from an outboard engine seizure and inboard engine inlet unstart were balanced with rudder deflection and sideslip. The aerodynamic moments due to this failure mode were assumed to be the same as those for the 1971 U. S. SST (see ref. 2), adjusted for the new engine locations. The incremental change in thrust level due to this failure was also assumed to be the same as that for the 1971 U.S. SST.

At low speed the yawing moment from an outboard engine failure was balanced by rudder alone. The centerline vertical surface was sized to statically balance the engine-out moment at V_1 + 7.5 m/s (+15 kn). The centerline vertical surface yawing moment coefficients due to sideslip and rudder deflection were based on 1971 U.S. SST data.

The high-speed lateral controls for the 969-512B configuration consist of an inboard flaperon, an inboard and outboard plain spoiler, and an outboard inverted spoiler-slot-deflector. The estimated rolling moment contributions of the individual control surfaces are presented in table 3. These estimates are based on 1971 U.S. SST wind tunnel data where possible.

TABLE 3.–969-512B ESTIMATED LATERAL CONTROL POWER

$$\left(C_{\ell} = \frac{\text{rolling moment}}{qSb}\right)$$

Flight condition	Inboard flaperon	Inboard spoiler	Outboard spoiler	Inverted spoiler-slot deflector	Total control available
Mach 1.5, V_{MO}, climb mass, roll response (1.047 rad (60°) in 7 sec)	0.00066	0.00072	0.00028	0.00035	0.00201
Mach 2.7, V_{MO}, n_z = 1.0 engine failure (outbd seizure, inbd unstart)	0.00041	0.00035	0.00024	0.00037	0.00137
Mach 2.7, V_{MO}, n_z = 2.0 engine failure (double unstart)	0.00045	0.00053	0.00025	0.00037	0.00160

The design of the lateral control system considered two types of engine failure: (1) an outboard engine seizure in combination with an inlet unstart and total flameout of the adjacent inboard engine; (2) an inlet unstart and total engine flameout of both engines on the same side. The engine seizure case was considered only at 1 g level flight because of the low probability of its occurrence. Satisfactory control was available, since the greatest roll control requirement occurred at the instant of engine failure, before any sideslip angle had developed.

The double unstart, having a relatively higher probability of occurrence, was considered at all load factors up to 2.0 g. In this case the airplane exhibits large dihedral effects and a decrease in directional stability. This results in an unacceptable engine failure case where insufficient control exists to counter the steady state condition, much less control the peak overshoot condition. The large control requirements are primarily due to the high dihedral effect exhibited by the configuration at the angle of attack required for 2.0 g flight.

Three approaches were considered to control the 2.0 g double unstart case:

- Increase directional stability
- Increase roll control power
- Control engine failure with an automatic unstart system

Increasing directional stability required an increase in vertical tail size resulting in unacceptable increases in drag and weight. An increase in lateral control required a significant increase in lateral control surface area, exceeding the available space on the wing. Consequently it was decided to introduce an automatic unstart system. The automatic unstart system will sense the presence of an outboard engine inlet unstart in combination with a lateral acceleration. When this occurs it initiates an unstart on the opposite engine inlet, thereby reducing the yawing and rolling moments caused by engine failure. The unstart procedure is terminated when the inlet is stabilized in the unstart mode.

A flight-critical augmentation system is used to meet minimum safe operational criteria. Figure 4 shows a functional diagram of the lateral-directional augmentation system mentioned earlier. In this system yaw rate and lateral acceleration are fed back to the rudder for dutch roll damping and sideslip control following engine failure, respectively. Yaw rate to aileron feedback is used to reduce the divergence rate of the spiral mode and roll rate to aileron is used to improve the roll time constant. Structural mode filters are used in all feedback loops to prevent coupling between airplane dynamics and the structural modes.

FUEL TANK ARRANGEMENTS

The fuel tank arrangement selected for the 969-512B configuration is shown in figure 5. The temperature of the fuel in the tanks must be kept well below the boiling

temperature to prevent cavitation at the boost pumps. At supersonic cruise altitudes the average temperature of the fuel must remain below 344 K (160° F) for unpressurized tanks.

Fuel temperature for the basic tank arrangement used on the 1968 version of the arrow wing was analyzed during the AST Task III system study (Contract NAS1-11938) for typical flight profiles. These studies showed that the rear main tanks, tanks 2 and 3 in figure 5, were especially vulnerable to aerodynamic heating. The rear main fuel tanks together with the auxiliary tanks which feed them during supersonic cruise should have tank wall thermal conductances less than 14.2 W/m^2 K (2.5 $Btu/ft^2hr°R$). The forward main tanks are less vulnerable to heating requiring tank wall thermal conductances less than 38.4 W/m^2 K (6.77 $Btu/ft^2hr°R$).

In addition to the fuel temperature problem, the fuel tank boundaries were moved inboard and an auxiliary tank was added to the aft fuselage to position the c.g. within the airplane c.g. limits.

The total tank capacities are more than adequate to permit a mission starting at a maximum taxi mass of 340 194 kg (750 000 lbm) for any desired payload.

STRUCTURAL DESCRIPTION

The objective of the structural evaluation was to select structural concepts for the 969-512B configuration consistent with the requirements of a Mach 2.7 supersonic transport and a 1975 program go-ahead. The structural definition of the 969-512B was arrived at by considering materials and concepts for a 1975 design freeze. The concepts and materials were reviewed and selections made for primary structural applications based on Mach 2.7 performance requirements. The components of the airplane that were chosen for structural evaluation are those having the largest potential impact on the mass of the airplane. These are the wing skin panels, wing internal structure, and the fuselage shell. A baseline for comparison was established for each of these components from the previous study of the 969-336C airplane. Alternate structural concepts were designed for each of these major components and compared with the baseline design. The alternate structural concepts were assessed for mass, manufacturing complexity, stiffness, fatigue, thermal conductance and material cost, and qualitatively evaluated for maintainability and fail safety. This evaluation provided the basis for specific structural concept recommendations for the 969-512B configuration.

The selected materials and concepts were integrated into the structural arrangement for detail analysis and design. The basic airframe internal arrangement is derived from the 969-336C. Variations in this internal arrangement such as multirib construction and spar and post were considered but none showed significant advantages over the baseline multispar arrangement with a small number of ribs. A similar arrangement was employed on the National SST.

The following paragraphs describe the basic structural arrangement, materials, concepts, and trade studies of alternate structural concepts. The concept trade studies consisted of evaluating mass, manufacturing complexity, maintainability, fatigue, fail safety, and material cost. Also, the mass difference was evaluated for variations in wing spar spacing, a multirib arrangement with sheet-stiffener surfaces, and a wide spar spacing with intermediate posts to support the surfaces. Each of these studies led to a selection of the most efficient concepts and arrangements for use on the arrow wing aircraft.

As shown in figure 6 the wing is of multispar construction with a small number of ribs. The spar spacing is 88.90 cm (35.00 in.). The ribs are positioned to distribute the engine loads into the wing box, close out the outboard side of the wheel well, back up the outboard fin, and close out the wing tip. The engines are installed with front mounts attached to the rear spar of the wing, and beams to support the aft engine mounts are cantilevered off the rear spar. The wing spars aft of the wheel well form the main wing box, extending continuously across the fuselage. Spars forward of the wheel well are attached to fuselage frames that transmit bending and shear loads across the fuselage. The wing leading edge flaps function as high-lift devices for low-speed flight; they are supported from the front spar. The region immediately behind the rear spar, and bounded by an auxiliary trailing edge beam, is occupied by actuators, accessories, wires, and hydraulic lines. Apart from the portions of fixed surface adjacent to engine nacelles and the wing-mounted fin, the trailing edge region is occupied by flaps and ailerons.

The body structural arrangement, a portion of which is shown in figure 7, uses semimonocoque construction with frame spacing of 44.45 cm (17.5 in.), except in the forward areas. The lower lobe structure is continuous since the main landing gear is stowed in the wing rather than the body. Floor beams are transverse to the airplane centerline, except over the wing carry-through structure, where they are oriented longitudinally. The body has a double lobe cross section; the floor beams are located approximately at the body crease line dividing the two lobes.

The horizontal and vertical tail surfaces are of multispar construction supporting aluminum-brazed titanium honeycomb sandwich surfaces. The leading edges and the rudder and elevators are wedge-shaped surfaces, also made of aluminum-brazed titanium sandwich.

MATERIALS EVALUATION AND SELECTION

Structural materials for the wing and fuselage were reviewed and selections were made based on the assumption that the airplane design was to be frozen in 1975, using materials that would be available at that time. Materials are divided into three main categories – metals, advanced composites/adhesive bonding, and fuel tank sealant/insulation. Materials for various applications were selected by screening the potential candidates, considering a combination of availability, environmental effects, production capability, cost, and projected status of specifications and allowables. The chart in figure 8 summarizes this selection process. In this chart the factors evaluated are marked with a "yes" or "no" indicating acceptance or rejection, adequacy or inadequacy. Factors which were not evaluated are noted by a dash. The following paragraphs describe the selected materials.

METALS

Ti 6Al-4V has been modified and improved during the National SST program and the subsequent Department of Transportation (DOT) funded technology follow-on program. The improved Ti 6Al-4V beta-processed material possesses superior fracture and fatigue properties. These improved properties, however, are achieved at the expense of a 3% to 5% strength loss and 7% to 12% higher cost. Specifications for this improved Ti 6Al-4V have been written and are designated Advanced Supersonic Technology (AST) specifications. The AST Ti 6Al-4V material is recommended for high toughness and fatigue design applications, whereas conventional MIL specification materials are recommended for airframe components designed primarily by strength or stiffness.

PH15-7Mo (Th 1050 heat treat) steel is recommended for sheet and plate. 15-5 PH corrosion-resistant steel and Custom 455 corrosion resistant steel are recommended for forgings that are subject to high operating temperatures for hot structure. 300M low alloy steel is recommended for cooled structure such as landing gear.

ADVANCED COMPOSITES/ADHESIVES

Development of advanced composites has been actively supported by government and industry funding for the past several years. However, only a very limited amount of the

available data was considered applicable to Mach 2.7 commercial SST technology. None of the high-modulus, high-strength composites were developed sufficiently to be considered ready for primary structural applications requiring a 50 000 hr life with thermal cycling.

FUEL TANK SEALANT

Of 14 candidate materials screened the fluorosilicone DC-94-529 was the only fuel tank sealant developed sufficiently to be selected for use in the 1975 time period. It has been tested extensively under a contract with the Department of Transportation, with test specimens being exposed to three cyclic environments similar to the conditions experienced in flight. One test sequence duplicated a typical flight and another continuously imposed the most severe high temperature, i.e., 500 K, (440° F), and fuel vapor environment. A third test utilized a small sealed tank exposed to alternating cycles of environmental exposure and loading.

Unreliable adhesion to titanium and low strength and elongation after elevated temperature exposure are recognized deficiencies. There is no suitable injection or faying surface sealant for a Mach 2.7 SST.

FUEL TANK INSULATION

Insulation materials and concepts were reviewed to provide data for assessment of the fuel temperature problem and for estimation of insulation mass requirements. Since it was concluded that a substantial reduction in insulation requirements could be achieved by reduction of thermal conductivity of structure with improved fabrication techniques, it was not considered worthwhile to make detailed insulation design studies based on 1975 requirements.

Insulation is needed for the system lines routed through the fuel tanks to prevent heat transfer to the fuel, and for the tank walls and structure to prevent premature fuel vaporization. The amount of insulation needed depends, of course, on the conductance of the fuel tank structure. Figure 9 shows the total tank conductance as a function of panel conductance. The materials considered for fuel tank insulation are listed in figure 10.

The most practical conduit insulation is a foamed elastomeric fluorosilicone which may be wrapped around the tubing; joints may be sealed with the fluorosilicone fuel tank sealant. Thermal conductivity of the 320 kg/m^3 (20 lbm/ft^3) material was estimated to be 0.043 W/m K (0.3 Btu-in/ft^{2}hr°F). Further development of materials and methods can be expected to result in both the density and thermal conductivity being reduced by one-half.

The type and extent of insulation for tank structure will depend upon structural design. Sealed evacuated batts, consisting of titanium envelopes filled with dexiglass, may be used. They have a conductivity of 0.0058 W/m K (0.04 Btu-in/ft^{2}hr°F) and a density of 380 to 770 kg/m^3 (24 to 48 lbm/ft^3). The batts may be tack welded in place or bonded with fuel tank sealant. This concept is in an advanced stage of development.

A flexible foam insulation may be used for areas that are irregular in contour or too small for batts to be advantageous. It could also be used to cover stiffeners and other extensions into the fuel. A density as low as 270 kg/m^3 (17 lbm/ft^3) is attainable with a conductivity of 0.043 W/m K (0.3 Btu-in/ft^{2}hr$^\circ$ F). It can be attached to surfaces with fuel tank sealant.

STRUCTURAL CONCEPTS

The objective of the structural evaluation was to select structural concepts consistent with the requirements of Mach 2.7 and a 1975 program go-ahead.

The design loads and environmental conditions were established from the 969-336C study to provide a consistent basis for comparing each of the structural concepts. Structural concepts were evaluated at three locations on the wing, shown in figure 11, and four locations along the body, shown in figure 12. These points were selected to represent a typical range of structural requirements for an arrow-wing configuration. The critical design loads for each of these locations are presented in reference 2.

The concepts evaluated are identified in table 4. The initial selection of candidate structural concepts was generally based on previous evaluation experience on the National SST program.

TABLE 4.–STRUCTURAL CONCEPTS EVALUATED

Component	Location	Material	Concept
Wing skin panels	269,431	Ti	Corrugated core sandwich
	249, 269, 431	Ti	Al brazed Ti H/C
	269, 431	Steel	Brazed steel H/C
	269, 431	Ti	Sheet stiffener
	269, 431	Ti	Integrally machined sheet stiffener
	269, 431	Ti	Integrally machined waffles
Wing spars	249, 269, 431	Ti	Welded sine wave
		Ti	Riveted sheet stiffener
		Ti	Welded sheet stiffener
		Ti	Extruded sheet stiffener
		Ti	Brazed Ti H/C
Body skin covers	A, B, C, and D	Ti	Sheet stiffener Brazed Ti H/C Integrally machined

The concept evaluation utilized a rating system which included mass, manufacturing complexity, stiffness, maintenance, fatigue, fail safety, thermal conductance, and material cost. No concept with a major deficiency in any one characteristic was evaluated, regardless of other favorable considerations. As seen in tables 5 through 8, a rating factor was selected for each characteristic from a range of 0 to 100 (very poor to very good) based on the concept's merit relative to a baseline which was arbitrarily

TABLE 5.–STRUCTURAL CONCEPT EVALUATION, WING SKIN PANELS, POINT 269

Component	Item	Rating range	Baseline (corr core sandwich)	Al brazed Ti H/C	Brazed steel H/C	Sheet stiff Ti	Integrally mach and weld sheet-stiff	Integrally mach waffle
Upr surface	Mass	0-100	50	69	29	50	63	44
	Mfg complexity		50	40			52	
	Stiffness		50	53			50	
	Maintain		50	70			80	
	Fatigue (DFR)		50	–			–	
	Fail safety		50	–			–	
	Thermal conductance		50	27			1	
	Material cost	0-100	50					

Component	Item	Rating range	Baseline (sheet-stiff)	Al brazed Ti H/C	Brazed steel H/C	Integrally mach and weld sheet-stiff	Integrally mach waffle	
Lwr surface	Mass	0-100	50	56	10	57	57	
	Mfg complexity		50	33		45	41	
	Stiffness		50	60		62	33	
	Maintain		50	35		50		
	Fatigue (DFR)		50					
	Fail safety		50					
	Thermal conductance		50					
	Material cost	0-100	50					

Carry through to another level

A superior candidate established on basis of factors considered

TABLE 6.–STRUCTURAL CONCEPT EVALUATION, WING SKIN PANELS, POINT 431

Component	Item	Rating range	Baseline (corr core sandwich)	Al brazed Ti H/C	Brazed steel H/C	Sheet stiff Ti	Integrally mach and weld sheet-stiff	Integrally mach waffle
Upr surface	Mass	0-100	50	68	47	30	56	20
	Mfg complexity		50	40			52	
	Stiffness		50	57			55	
	Maintain		50					
	Fatigue (DFR)		50					
	Fail safety		50					
	Thermal conductance		50					
	Material cost	0-100	50					
Component	Item	Rating range	Baseline (corr core sandwich)	Al brazed Ti H/C	Brazed steel H/C	Sheet stiff Ti	Integrally mach and weld sheet-stiff	Integrally mach waffle
Lwr surface	M	0-100	50	49	17	38	58	47
	Mfg complexity		50	40			52	
	Stiffness		50	55			55	
	Maintain		50	70			80	
	Fatigue (DFR)		50	58			64	
	Fail safety		50					
	Thermal conductance		50					
	Material cost	0-100	50					

Carry through to another level

A superior candidate is established on basis of factors considered

24

TABLE 7.–STRUCTURAL CONCEPT EVALUATION, WING SPAR

Location	Item	Rating range	Baseline welded sine wave	Riveted sheet stiff	Welded sheet stiff	Extruded sheet stiff	Brazed Ti H/C
Pt 269	Mass	0–100	50	25	32.5	26.2	18.8
	Mfg complexity		50		48		
	Maintain		50		60		
	Fatigue (DFR)		50		48		
	Thermal conductance		50				
	Material cost	0–100	50				
Pt 431	Mass	0–100	50	33	40.5	37.5	22.5
	Mfg complexity		50		48	47	
	Maintain		50		50	55	
	Fatigue (DFR)		50		48	32	
	Thermal conductance		50				
	Material cost	0–100	50				
	Item	Rating range	Baseline riveted sheet stiff	Welded sine wave	Welded sheet stiff	Extruded sheet stiff	Brazed Ti H/C
Pt 249	Mass	0–100	50	58	57	56	23
	Mfg complexity		50	43	42	40	
	Maintain		50	40	40	45	
	Fatigue (DFR)		50	68	64	50	
	Thermal conductance		50	70	60		
	Material cost	0–100	50				

Carry through to another level

A superior candidate is established on basis of factors considered

TABLE 8.–STRUCTURAL CONCEPT EVALUATION, BODY

	Location	STA 1005		STA 1726			STA 2474		STA 3100		
		(1) Crown	(2) Side	(3) Crown	(4) Side	(5) Keel	(6) Crown	(7) Side	(8) Crown	(9) Side	(10) Keel
	Rating range	(0–100)	←							→	(0–100)
Mass	Sheet stiff (baseline)	50	50	50	50	50	50	50	50	50	50
	integrally mach	43	38	42	15	43	38	22	50	21	34
	Ti H/C	52	56	50	50	61	54	67	77	58	57
Mfg complexity	Sheet stiff (baseline)	50	50	50	50	50	50	50	50	50	50
	integrally mach								48		
	Ti H/C	28	28	29	28	33	33	33	33	28	33
Maintain	Sheet stiff (baseline)	50	50	50	50	50	50	50	50	50	50
	integrally mach								45		
	Ti H/C	40	40	40	40	40	40	40	40	40	40
Fatigue (DFR)	Sheet stiff (baseline)	50	50	50	50	50	50	50	50	50	50
	integrally mach								43		
	Ti H/C							33	28		
Fail safety	Sheet stiff (baseline)	50	50	50	50	50	50	50	50	50	50
	integrally mach										
	Ti H/C										
Material cost	Sheet stiff (baseline)	50	50	50	50	50	50	50	50	50	50
	integrally mach										
	Ti H/C										

Carry through to another level

A superior candidate is established on basis of factors considered

given a rating of 50. The concepts were screened through several levels of evaluation. Each level of evaluation considered a different characteristic starting with the most important (mass) and continuing in a descending order of importance to the lowest (material cost). Starting with two or three candidates from the first screening level, the best were evaluated through sufficient levels to establish a superior candidate. The ☐ symbols identify those concepts selected to carry through to another level of evaluation. The superior candidate is noted by ☐.

WING SKIN PANEL CONCEPTS

The baseline wing skin panels on the 969-336C at design point 249 and the lower surface at point 269 utilized titanium "stresskin honeycomb" with welded edge members as shown in figure 13. Stresskin is a spotwelded honeycomb configuration which has constant skin gages and no edge member when purchased from the supplier. The addition of welded edge members, milling of face sheets, and contouring of the wing skin panels was required to complete a typical skin panel assembly. A face sheet of 0.152-cm (0.060-in.) titanium was the upper limit of manufacturing capability as evaluated by Boeing. Since the loads at point 431 and the upper surface at point 269 require face sheet thicknesses greater than 0.152 cm (0.060 in.), the corrugated core sandwich was selected as the baseline. Panel face sheets are machined to provide integral edge attachments. The panels are assembled by spot welding at the corrugation nodes. These panels are structurally efficient for loads oriented axially with the corrugation but are relatively inefficient for transverse loads.

Five alternate structural concepts were designed for the wing skin panels. Each candidate specimen was designed and sized to maintain a margin of safety from 0% to 5% utilizing the material selections recommended from the material screening evaluation, and design loads and environmental conditions identical to those for the baseline skin panel. Static, thermal, and fail safe requirements were incorporated into the design of each specimen.

Silver-brazed steel honeycomb was investigated because of its potential structural efficiency at high temperatures and high end loads. This configuration was sized for both points 269 and 431. It was not investigated at point 249 because the low loads produce a minimum gage sizing which is heavier than similar concepts of minimum gage titanium.

These panels utilize PH15-7Mo steel face sheets with 0.635 cm (1/4 in.) cell 88 kg/m^3 (5.5 lbm/ft^3) honeycomb core also of PH15-7Mo steel. The steel-brazed honeycomb has good biaxial capability for N_x and N_y loads but is still less efficient than brazed titanium honeycomb configurations because of its lower strength to mass ratio.

The structural efficiency of aluminum-brazed titanium sandwich throughout the range of arrow wing end loads justifies its development as a candidate. The configuration was sized for all three control point locations, 249, 269, and 431. The configuration utilizes Ti 6Al-4V Condition I for the face sheets and 0.635 cm (1/4 in.) cell 78.5 kg/m^3 (4.9 lbm/ft^3) field core sandwich of Ti 3Al-2.5V. The aluminum-brazed titanium core

sandwich is structurally efficient in reacting combined N_x, N_y, and N_{xy} loads. This is a superior candidate because of the efficiency of honeycomb sandwich in the load ranges involved and the high strength to mass ratio of the titanium.

The waffle skin panel arrangement, fully machined from Ti 6Al-4V plate, was considered because of good biaxial capability compared to a conventional sheet stiffener arrangement. The waffle panel arrangements are of average structural efficiency for tension applications and below average efficiency for compression applications.

Riveted sheet stiffener construction was investigated for points 269 and 431 because of its manufacturing simplicity and relatively good tension efficiency. The sheet stiffener arrangement utilizes machined zee sections riveted to a machined skin. The stiffeners and skin material are made of titanium. This arrangement achieves a manufacturing rating of 54, the best of any concept investigated.

The integrally machined and welded sheet stiffener arrangements were designed to improve the transverse buckling capability. The configurations were sized for points 269 and 431 and utilized Ti 6Al-4V Condition I. The skin panel plate has machined elevated ridges and the machined stiffener angles are then butt welded to the outstanding ridges. The material which would normally be used in the stiffener skin flange has been redistributed into the sheet to improve the panel buckling allowable. The machined and welded sheet stiffener arrangement is a superior candidate for tension application but is not as efficient as honeycomb for compression application in the load ranges involved at points 269 and 431.

As discussed earlier, a candidate speciman was designed in detail for each structural concept at the points identified in figure 11. The specimen in each case was 30.48 cm (12 in.) in span and half the spar spacing in width. The establishment of specimen configurations included as many edge member and joint details as possible. It should be recognized, however, that total weight of a major component can only be accurately obtained by a complete design and analysis of all joints and components involved. The concept coupon weight represents an indicator of the relative effectiveness of various concepts; however, these cannot be extrapolated to find total weight differences between concepts for major airframe components.

The critical design conditions, loads, and thermal environment are shown in reference 2. For lower surface concepts, 40% bending reversal was assumed to obtain compressive design loads. For biaxial tension and shear, the panel was checked for maximum principal tension and maximum shear stress. A 10% allowance is provided for the combined effects of area-out and section net area efficiency. This is consistent with design practice for wing panel sizing. Design details for the spanwise splices are in accordance with design practices for integral fuel tank panels. Stiffener-to-panel attachments were designed to provide load transfer capability for fail safe requirements. With the limited loads data available, the fatigue evaluation of the strength-sized panels was based on ground-air-ground (GAG) cycle stresses with fatigue reliability factors, fatigue detail ratings, and GAG damage ratios estimated from the National SST program.

The structural concepts considered at points 431 and 269 on the wing are evaluated in tables 4 and 5. As described earlier, each factor that is considered is listed in the order of priority in the left hand column. Each factor is considered in order, and only the concepts that meet a factor reasonably well are carried on into the subsequent evaluations. For example, only the concepts that are reasonably competitive from a mass standpoint are evaluated for manufacturing complexity, and only those that have a reasonable manufacturing complexity are evaluated for stiffness, etc.

As can be seen from the tables, the aluminum-brazed titanium honeycomb, figure 14, was selected for the upper surfaces at all points, and the lower surface at points 269. The integrally machined and welded sheet stiffener, figure 15, was selected for the lower surface at point 269 and 431. In the former case, the aluminum-brazed sandwich had a significant mass advantage in the upper surface, while in the latter case, the sandwich and the integrally machined and welded sheet stiffener are about equal in mass, with the latter having a significant advantage in manufacturing complexity.

Although stresskin was considered for a time on the SST program it was not considered for the 969-512B because of unacceptable fatigue risks resulting from the manufacturing process. Also, the problem of designing and manufacturing an acceptable edge attachment for stressskin panels has not been satisfactorily resolved.

WING SPAR CONCEPTS

The baseline spar configuration at point 249 utilizes riveted sheet-stiffeners as shown in figure 16. At points 269 and 431 welded sine wave spars, as shown in figure 17, were utilized. The latter is a very efficient concept for both vertical shear and fuel crash loads when accessory attachments and cutouts are few in number.

Four alternate spar concepts were considered. The machined and welded sheet stiffener spar concept was conceived as a means of improving the structural efficiency by eliminating web-to-chord overlaps and stiffener-web overlaps. The configuration was sized for points 249, 269, and 431 utilizing Ti 6Al-4V Condition I. The web is pocket chem-milled with integral pads for joining chord members and stiffeners. The machined web stiffeners and spar chords are joined to the web by fusion welding. Because of the elimination of overlaps and efficient use of material, this configuration is the lightest sheet stiffener concept.

A machined extrusion spar was investigated because of the possibility that it would approach the structural efficiency of the machined and welded spar while minimizing cost by reducing welding requirements. The machined extruded spar was sized for points 249, 269, and 431 using Ti 6Al-4V. The titanium web stiffener extrusion requires 100% machining because of surface contamination and extrusion gage limitations. The maximum span per extruded web segment is approximately 53.3 cm (21 in.). Fusion butt welding would be utilized to join web segments. The mass of the rivet overlaps reduces the efficiency of this configuration.

The structural efficiency of both double edge and thin edge aluminum-brazed titanium honeycomb spar concepts was investigated. Both configurations utilized SS2-30 core with density of 224 Kg/m^3 (14.0 lbm/ft^3) at the periphery for bolt attachments. The thin edge configuration uses one welded chord attachment for minimum mass and one riveted to allow for buildup of tolerance. The double edge panel uses torque limited fasteners for spar chord installation.

The design and construction features of the silver-brazed steel honeycomb concept are similar to those described for aluminum-brazed titanium honeycomb. The skin and honeycomb core are of PH15-7Mo material. The manufacturing complexity rating is higher for steel construction than for titanium because the brazing cycle is more complex for steel.

Each of the spar configurations described above was analyzed for points 249, 269, and 431. Mass per unit spar length has been calculated for comparative purposes. At each of the locations considered the welded sine wave configuration is the lightest structural concept, followed by the sheet stiffener concepts, with the honeycomb concept the least efficient. Previous SST studies have established that hole and bracket reinforcements in the welded sine wave construction greatly reduce the mass efficiency and increase the complexity. This indicates that the number of holes provided for systems routing in various portions of the wing is an important consideration in the final choice of spar concept.

The evaluation of wing spar structural concepts is presented in table 7. As in the evaluation of the wing surfaces, the characteristics used in the evaluation are listed in the left-hand column in the order of priority, and the characteristics are evaluated sequentially. Only the concepts that are reasonably competitive in a given characteristic are included in the next evaluation.

The welded sine wave spar concept was selected as the superior candidate at points 269, 431, and 249 primarily because of the significant mass advantage over the other concepts.

FUSELAGE PANEL CONCEPTS

The riveted sheet stiffener baseline concept and the 10 fuselage panel control points are shown in figure 18. Design conditions identical to those used for the baseline were used to size each of the alternate concepts at the 10 control points.

The use of aluminum-brazed titanium honeycomb skin panels for the body was investigated for the following reasons:

- Efficiency in carrying combined shear and compression is a requirement through most of the body end load range.
- A large portion of the body structure is critical for compression load conditions.
- The high degree of inherent stability of honeycomb skins allows a reduction in support structure to meet general instability requirements.

The aluminum-brazed titanium body skin design utilizes fabrication techniques similar to those required for the wing skins. The panels utilize integrally machined Ti 6Al-4V face sheets with SC4-20 titanium core. Dense core is used along the panel edge to resist bolt crushing loads. The outer skins are recessed for flush installation of circumferential splice straps only. Longitudinal splice straps are installed external to contour. The frame-to-panel attachments have been made by bolts which require densified core and skin pads locally at every frame. This requirement greatly complicates the fitup of core to face sheet. The superior stability of the honeycomb panels permitted a frame spacing of 88.9 cm (35 in.).

Integrally machined body skin panels have been investigated as a means of improving structural efficiency by tailoring of the cover material to the bending and shear requirements of the body. Stiffener spacing and intervening nodes have been sized and spaced to optimize compression and shear allowables. Integrally machined nodes for stiffener attachment eliminate the requirement for a flange to rivet the stiffener to the skin. Machined angle stiffeners have been welded to the face sheet node by fusion butt welding. Integral circumferential skin pads are utilized as part of body frame outer chords. A separate frame fail-safe chord is located inside of the skin stiffeners. All skin and frame components have been designed of Ti 6Al- 4V Condition I. The assembly of the monolithic panels by machining and welding represents a slightly more complex manufacturing procedure than the machining and riveting sequence utilized in sheet stiffener fabrication, as indicated by the manufacturing complexity rating in table 8.

The above three body structural concepts have been designed in detail for the baseline structural loads and environmental conditions at the 10 control point locations. The total mass of each panel specimen was calculated and reduced to an average mass per unit area for comparative purposes.

The evaluation of the fuselage structural concepts is presented in table 8. The factors on which the evaluation is based are listed in the left column. In each case the baseline sheet stiffener concept is evaluated in comparison with integrally machined skin stiffener and aluminum-brazed titanium honeycomb concepts. The procedure was the same as that used for the wing surfaces and wing spars.

The integrally machined concept was eliminated in the mass evaluation at all four evaluation points, except the crown at station 7874 (3100). Subsequent evaluation, with respect to manufacturing complexity, maintainability, and fatigue, established the superiority of the baseline skin stringer concept over the other two candidates. Consequently the baseline concept was selected for the entire fuselage.

STRUCTURAL ANALYSIS AND DESIGN

This section provides a general overview of the detailed analyses and computational procedures that were used to establish an efficient distribution of structural material to satisfy strength and flutter criteria. The computerized system that was used in performing this work was organized around an interim version of the ATLAS Structural Analysis and Design System (ref. 5), interfaced with external programs for flutter analysis, and with the FLEXSTAB System for loads analysis, (ref. 6).

The major subtasks that make up the structural analysis and design process are identified in figure 19. This may be visualized as three interconnected discipline-oriented segments with the interconnection being provided by the ATLAS system. On the left of the figure is FLEXSTAB, used for prediction of steady aeroelastic loads which provide input to the strength design segment shown in the center of the figure. On the right is a group of operations associated with the flutter analysis and design to satisfy flutter criteria. The computer programs performing the various functions are shown in the upper portion of the boxes.

Basic data describing the aircraft were developed early in the program. This information, comprising aircraft geometry, structural arrangement, structural concepts, and structural materials, was then used to develop structural, aerodynamic, and mass models of the aircraft and other input data to initiate the analysis and design cycle.

THE INTEGRATED COMPUTER PROGRAM SYSTEM

THE ATLAS SYSTEM

ATLAS is an integrated structural analysis and design system operational on the Control Data Corporation (CDC) 6600/CYBER computers. It is a modular system of computer codes, controlled by one executive module and with a common data base. The arrow wing analysis used a preliminary version of ATLAS. Hence, the system description that follows reports an evolving capability as it existed during the detailed analyses in the arrow wing study. The system's capabilities are broad in scope, supporting analyses in many different but related aeroelastic technologies. Execution of modules is controlled by the user by means of a technically oriented language. Input data are written in a problem-oriented language which provides versatile automatic data generating capabilities. Additionally, the various data preprocessors provide capabilities to reduce the amount of input data and flowtime required to define the structural problem. Data postprocessors allow selected data to be extracted, manipulated, and displayed to facilitate the evaluation of either input data or analysis results.

The ATLAS problem size limitations for stiffness and mass models are:

Number of stiffness nodes	4 095
Number of stiffness elements	32 767
Number of loadcases	4 095
Number of mass nodes	4 095
Number of mass elements	32 767
Number of mass conditions	200

Problems generally become critical for bulk storage or hardware reliability before these limitations are reached. For substructured stiffness and mass models there is no practical limit to the total problem size.

There are two basic types of modules in the ATLAS system: executive modules and computational modules. There are two executive modules, ATLAS(0,0) and Control. ATLAS(0,0) monitors the job execution. Control, which is generated by the user, performs such functions as selecting the sequence of computations, selecting analysis results to be displayed, and handling execution. In general, the Control module is generated from the control deck at execution time by the precompilers and compilers.

Computational modules are grouped into three types according to their function:

- Preprocessors read, decode, generate, and interrogate the input data or load data for a restarted job.
- Processors perform technical, analytical computations in the following disciplines:
  - Stiffness
  - Mass
  - Design
  - Linear matrix algebra
- Postprocessors extract and display input data or analysis results and save data for a later restart of the job.

Table 9 provides a summary of the capabilities of the ATLAS 2.2 system used during Arrow Wing Task II. The table is divided into three sections representing the Executive, Technical, and Pre- and Postprocessor modules.. The structure of Version 2.2 of the ATLAS System, which was used in the present study, is depicted schematically in figure 20.

TABLE 9.–A SUMMARY OF ATLAS 2.2 CAPABILITIES

Module	Function
ATLAS (0,0) Control	Initializes loading of module overlays, and closes system data files. Defines the sequence of execution of modules.
Aerodynamics	Generates aerodynamic influence coefficients using three-dimensional linearized potential flow theory for general planar surfaces.
Design	Calculates margins of safety, and resizes the structure using a fully-stressed approach.
Airloads	Generates steady-state loads using AIC's from "AERODYNAMICS," mass matrices from "MASS," and flexibility matrix from "STIFFNESS."
Loads	Prepares finite element static and thermal loads.
Mass	Generates finite element mass matrices for primary and secondary structure, fuel, and payload.
Stiffness	Generates the finite element stiffness and stress matrices.
Stress	Calculates the finite element stresses.
Interpolation	Establishes mode shape interpolation functions to be used by the airload generators.
Vibration	Calculates frequencies and mode shapes of a structure undergoing free, undamped vibrations.
Preprocessor	Reads the ATLAS Problem Deck, and loads the restart tape.
Plot	Prepares SC4020, Gerber and Calcomp plot data.
Report	Prepares printed reports of results generated by technical and utility modules.
Output	Saves all problem data on a checkpoint file to enable subsequent problem restart.

FLEXSTAB SYSTEM

FLEXSTAB (ref. 6) is a system of programs developed by Boeing under contract NAS2-5006, to NASA-Ames Research Center It was designed to predict the stability characteristics of flexible airplanes based on the geometry, mass distribution, and flexibility of the airframe, using linear aerodynamic and structural theories. Although not principally designed as a loads analysis tool, FLEXSTAB generates pressure distributions in the process of performing a stability analysis, hence its use for loads analysis was a fairly simple task.

In preparation for the arrow wing contract a contractor development effort was directed at producing a version of FLEXSTAB that would produce design loads. The changes and additions made to FLEXSTAB during this time are shown in table 10. These changes were subsequently incorporated in the NASA version of FLEXSTAB 1.2.

TABLE 10.–BOEING PROGRAM TO IMPROVE EFFICIENCY AND RELIABILITY OF AEROELASTIC LOADS ANALYSIS

	Reason for modification	
	Improved efficiency	Improved capability
Addition of cycling capability for balanced maneuvers or unit solutions		
For unit solutions on $\alpha, \beta, q, \dot{\theta}, \dot{\phi}, \dot{\psi}, \delta_E, \delta_R, \delta_A, V_{TAS}$, THRUST ALTITUDE and ATTITUDE	●	
For balanced maneuvers on: $n, q, \theta, V_{TAS}, U_{de}$, THRUST and ALTITUDE	●	
Added capability to generate rigid and flexible solutions in one computer run	●	
Capability to select the degrees of freedom retained at the structural nodes	●	●
Addition of the static gust solution based on the revised gust load formula		●
Addition of the capability to superimpose an externally generated pressure distribution on that computed by SD&SS** (nacelles, for example)		●
Added capability to generate in SD&SS the airloads and the inertia loads at the nodes separately		●
Added capability to specify load factor rather than pitch rate for balanced maneuvers	●	●
Added capability to put user-specified matrices on the SD&SS output tape		●
Print out the equivalent airspeed and C_{N_α} in SD&SS		●
Develop interfaces: ATLAS ⇔ FLEXSTAB and FLEXSTAB ⇔ ATLAS	●	
*Develop a program (VAMAT) providing the capability to generate net shear, moment, and torsion along wing, body, and horizontal tail in user-specified cross sections (using SD&SS tape output)		●
*Develop a program (VMTSCM) providing the capability to scan through the loads and select critical loads	●	●
*Develop a plotting program providing plots of shear, moment, and torsion along wing, body, and horizontal tail	●	●

*These programs are not part of the FLEXSTAB program

**Stability derivatives and static stability

The modifications to FLEXSTAB were carried out with two major purposes in mind – improvement in program efficiency and improved analytical capability – and table 10 identifies in which of these categories the various changes fall.

FLUTTER MODULES

As indicated in figure 19, the flutter modules were also linked to the ATLAS system through a tape interface. Modal data, flexibility matrices, and mass matrices were transmitted from ATLAS to the flutter modules. RHO III, (ref. 7) was used to calculate unsteady aerodynamic loadings caused by motions of lifting surfaces based on the subsonic kernel function approach, utilizing the modal data supplied by ATLAS. These loadings were then used to calculate generalized aerodynamic airforces for use in subsonic flutter analysis. Similar airload calculations for supersonic flutter analysis were obtained from the Mach Box program (ref. 8). Generalized aerodynamic force matrices, together with generalized mass and stiffness matrices from ATLAS, were incorporated in the flutter equations and solved to define the flutter stability envelope by utilization of a V-g solution program based on the QR algorithm.

ANALYTICAL MODELS

STRUCTURAL MODEL

One finite element model of the structure was developed as the source of basic structural data for aeroelastic loads, stress, vibration, and flutter analyses. Consistency of geometric data was found to be particularly critical. Geometry of an individual component was generally defined in a convenient local reference frame. Hence, particular care had to be taken in defining coordinate transformations between these local reference systems and the global system that was used in defining the assembled model of the complete structure.

Close coordination between stress, flutter, and loads specialists was required to provide a single basic model from which special-purpose models could be derived to satisfy the requirements of each individual discipline. This interdisciplinary coordination is particularly important in the design of large supersonic aircraft that tend to be slender and very flexible, in which aeroelasticity is a major design consideration. Dynamic loadings associated with flutter often exhibit distributions that are vastly different from strength-critical loadings. Hence, requirements exist for detailed representation of structural characteristics in different regions of the aircraft to satisfy requirements for stress analysis, strength design, flutter analysis, and stiffness design. Prior experience on the National SST program provided useful background for modeling the arrow wing structure. Initial structural sizing to start the aeroelastic cycle was derived from the 969-336C design study, with appropriate adjustments to reflect the increase in maximum taxi gross mass to 340 194 kg (750 000 lbm). Since program constraints permitted only a single cycle of aeroelastic loads analysis, it was considered necessary to develop an initial sizing to match strength requirements reasonably well. Automated resize capability had not been provided in the ATLAS system when the initial sizing had to be done. Hence, this initial sizing was performed manually. Availability of automated resize capability will make it possible to employ a crude estimate of the initial sizing with considerable savings of time and effort on future jobs of this kind. A detailed description of the model and an account of model development and checkout are presented in reference 2.

The major portions of the structural model used in this study are shown in figure 21. The finite element model contains approximately 2000 nodes, 4200 elements, and 8500 active degrees of freedom. For dynamic analyses, a much smaller number of degrees of freedom are retained (225 for symmetric conditions and 260 for antisymmetric conditions). The loads analysis used a reduced model having 164 retained nodes and 192 degrees of freedom. The complexity of the model results from (1) the use of one model for stress, loads, and flutter analyses, and (2) the detail requirements for meaningful flutter analysis. For the wing, these requirements include structural modeling of the engine beams (allowing complete c.g. motion of the engines), leading and trailing edge controls, wing secondary structure, landing gear and wheelwell cutouts, major access doors, and wing-mounted fins as well as wing primary structure. For the rest of the aircraft, they include a detailed body idealization for wing attachment and a less sophisticated model of the remaining fuselage and the empennage.

STRUCTURAL MODEL VERIFICATION

The structural model was generated and initial checks made over a period of about five months. During this period a maximum of three people worked on the model. About 17 man-weeks of effort were required to define and size the elements in the body. About 18 man-weeks of effort were involved in formulating the wing model, distributed equally between model definition and sizing. Four additional months were required to accomplish the following tasks: connect the wing and fuselage models, verify the accuracy of design data, check local modeling details, conduct a preliminary vibration analysis to review mode shapes and frequencies, make a preliminary flutter check, and revise portions of the wing structure to relieve a severe flutter deficiency before strength sizing.

The preliminary vibration analysis showed that there was a local resonance involving the main landing gear, which was supported in the stowed position on shallow beams extending across the top of the wheel well region. This resulted in a low-frequency, high-amplitude resonance of this local area, illustrated in figure 22. Several changes were made to suppress the objectionable mode by stiffening the landing gear uplock restraint. These included the addition of a full-depth rib on the inboard side of the wheel well, addition of lower surface honeycomb skin panels extending from the added rib to the side of the body rib, and an increase in depth of the uplock beam.

Provision was also required to restrain the mathematical model at the center of gravity in order to calculate the flexibility matrix for use in the airloads analysis. This restraint was provided by adding special nodes and massless structural elements to prevent rigid body motions, both symmetrical and antisymmetrical. The added structure is statically determinate; its sole purpose is to transfer the support reactions to frames and body shell. It does not contribute to the mass or stiffness of the model; hence it does not affect the loads or flutter analysis.

The initial stress analysis, while done primarily for model verification, also afforded an early opportunity to check the operation of the ATLAS program when executing a

problem of this size. The arrow wing model is about 40% larger than the largest previously executed model and its stiffness matrix has a relatively large "half-band width."

The length of time required for model generation and validation was a result of the small size of the study team, the limited experience using ATLAS on a model of this size and geometric complexity, and lack of a "body" geometry package in the program. While experience gained from this study and programming improvements will decrease both the effort and time required to generate and validate a complex structural model, it is evident that model generation should begin as soon as possible in a design study to obtain maximum benefit from an automated design system.

MASS MODEL

Different sets of retained freedoms describing structural deformation were required for aeroelastic loads analysis and for flutter analysis since the numbers and distributions of retained structural freedoms were different. Hence, it was necessary to develop two different sets of mass panels. To "lump" the masses at the retained nodes an "automated cookie cutter" technique (ref. 9) was used. For this process the location of the retained node is selected and the boundaries of the space that contributes mass to this node define a vertical prism ("cookie"). Figure 23 shows the retained nodes and panels used for modeling the flutter mass matrix. An external boundary as shown in the figure is required by the "PLOT GRID" ATLAS program.

AERODYNAMIC MODEL

A basis for the aerodynamic analysis is provided by the loft contours that define the envelope of the airframe. This loft is used to produce the geometrical description of the surfaces of the airplane, and the associated slopes for use in the steady state loads analyses, as described later. These panels are illustrated in figure 24.

STRUCTURAL DESIGN LOADS

The selection of loads conditions for analysis was based on the requirements of the *Federal Aviation Regulations, Part 25*, and the *Tentative Airworthiness Standards for Supersonic Transports (TAS)*. Loads analysis experience on the National SST program and on a previous study, performed by the contractor, of the 969-336C configuration was used as the basis for selecting design conditions. Where appropriate, recourse was made to the extensive analyses performed for the National SST design in the selection of design parameters.

STRUCTURAL DESIGN AIRSPEEDS

The maximum operating speed and Mach number, V_{MO} and M_{MO}, are established to include all normal climb, cruise and descent conditions. The speeds chosen for the arrow wing were those determined for the National SST.

The design cruising speed, V_C, is equal to V_{MO}. Supersonic cruise Mach number is $M_C = 2.7$. The selected design cruising speeds exceed the requirements of FAR 25.

The design dive speed and Mach number, V_D and M_D, are the same as those used on the National SST, which provide an adequate speed margin between the cruise and dive placards.

The design maneuvering speed, V_A, is based on the following equation:

$$V_A = V_{MIN\ DEM} \sqrt{2.5}$$

where $V_{MIN\ DEM}$ is the minimum demonstrated speed with flaps retracted or a lesser speed based on a rational selection of $C_{L_{MAX}}$ for structural design.

The design speed for maximum gust intensity, V_B, is established in the subsonic regime in accordance with FAR 25 and TAS. The V_B concept is not used for supersonic flight where slowdown or gust avoidance may not be operationally feasible.

The design flap speed, V_F, is derived in compliance with FAR 25. The design flap speed for each position is sufficiently greater than the operating speed recommended for the corresponding stage of flight to allow for probable variations in airspeeds and for transition from one flap position to another.. The structural design airspeeds for the arrow wing are shown in figure 25.

DESIGN GROSS MASSES

Pertinent gross masses are presented in table 11.

ENGINE THRUST

The maximum installed thrust values for the ATAT-1 engine are presented in table 12.

MANEUVER AND GUST CRITERIA

Flight loads for symmetrical balanced maneuvers are established within the maneuvering envelope in accordance with FAR 25. Except as limited by maximum design lift coefficients, the design limit load factors are as shown in table 13.

The airplane is assumed to be in equilibrium with zero pitching acceleration. The effects of pitching velocity are accounted for in the analysis. The airplane is analyzed for maneuvers at all points on or within the maneuver envelope for both maximum and minimum gross masses at the appropriate altitude.

The following maneuver time histories are also considered:

1. Maximum Stabilizer Displacement – The airplane is assumed to be flying in a steady level flight attitude at speeds from V_A to V_D and the pitch control is suddenly deflected in an up or down direction at the maximum rate available to a deflection consistent with pilot effort.

TABLE 11.–DESIGN GROSS MASS

Condition	Mass	
	kilograms	(pounds mass)
Maximum flight mass	337 727	(743 000)
Maximum zero fuel mass	185 112	(407 246)
Minimum mass and ballast	157 427	(346 340)
Maximum takeoff mass	340 000	(748 000)
Maximum landing mass	218 182	(480 000)

TABLE 12.–INSTALLED MAXIMUM THRUST ATAT-1 AFTERBURNER OPERATIVE

Mach no.	Altitude		Installed thrust per engine	
	Meters	(Feet)	Newtons	(Pounds force)
0	0	(0)	252 570	(56 767)
0.6	1 523	(5 000)	240 330	(54 028)
0.9	4 572	(15 000)	249 100	(56 000)
1.2	10 667	(35 000)	136 120	(30 600)
1.6	12 190	(40 000)	139 770	(31 421)
2.0	13 713	(45 000)	161 600	(36 329)
2.2	13 713	(45 000)	190 170	(42 751)
2.7	18 287	(60 000)	130 490	(29 336)
2.9	18 287	(60 000)	102 490	(23 040)

TABLE 13.–LIMIT LOAD FACTORS

Condition	Positive limit load factor	Negative limit load factor
All speeds up to V_C	2.5	-1.0
At V_D	2.5	0.0
Flaps down condition	2.0	0.0

2. **Checked Maneuvers** – The airplane is assumed to be subjected to checked maneuvers for balanced conditions at any load factor within the design maneuver envelope and at all speeds between V_A and V_D. The elevators are checked back to a position such that the airplane pitching accelerations meet or exceed the FAR requirements.

A maneuver envelope for sea level altitude at the maximum flight mass is shown in figure 26.

Loads due to yawing maneuvers are established in compliance with FAR 25. The following time histories are considered:

1. From a condition of steady level flight at zero sideslip, displace the rudder control to the maximum position as limited by stops, boost capability, or pedal force.

2. With the rudder control displaced as in (1), allow the airplane to yaw to a maximum sideslip angle.

3. With the airplane yawed to the sideslip angle consistent with (2), return the rudder abruptly to neutral.

4. With the airplane yawed to the static sideslip angle consistent with the control displacement in (1), return the rudder control abruptly to the maximum value in the opposite direction.

Loads due to both vertical and lateral gust are computed at all speeds and altitudes on and within the flight envelope. Use is made of the revised gust load formula (ref. 10) in computing airplane load factors due to gusts. The design airspeed for maximum gust intensity, V_B, is not considered at supersonic speeds.

LANDING, TAXI, AND GROUND HANDLING LOADS CRITERIA

Design landing impact loads were determined for the National SST using a dynamic analysis which included the significant elastic modes of the airframe, rigid body degrees of freedom, and a representation of the energy absorption characteristics of the landing gear shock strut and tires. Landing impact loads for the 969-512B configuration were obtained by applying the load factors obtained for the National SST to the mass distribution of the 969-512B. Aerodynamic forces acting during landing impact were neglected.

The air and ground handling loads are computed in compliance with the requirements of FAR 25. The taxi loads are computed on the assumption that the airplane experiences a 2 g acceleration at the center of gravity while taxiing. In each of these conditions, the external loads are placed in equilibrium with the linear and angular inertia loads in a rational manner. Ground handling loads are summarized in table 14.

The definition of geometry and forces for the ground load conditions is shown in figure 27.

AERODYNAMIC LOADS ANALYSIS

The linearized potential flow method developed by Woodward is utilized in FLEXSTAB to generate aerodynamic influence coefficients for aeroelastic loads analysis. This system has the capability of treating a wide variety of configurations, and it may be applied at subsonic and supersonic speeds.

TABLE 14.–LIMIT LOADS FOR GROUND HANDLING CONDITIONS

Max ramp mass = 340 300 kg (750 000 lbm)
Body station of cg = 62.97 m (2479.16)

See figure 27 for sign convention

a. SI Units

	Main gear			Main gear			Nose gear			Main gear torque, kN · m
	V_M kN	D_M kN	S_M kN	V_M kN	D_M kN	S_M kN	V_N kN	D_N kN	S_N kN	
Static reaction	1549			1549			239			
Taxi	3097			3097			478			
2-pt braked roll	1663	1334		1668	1334					
3-pt braked roll	1384	1107		1384	1107		568			
Turning	2784		1392	314		157	237		120	
Nose wheel yaw	1483	1186	62.6	1438		59.7	415		121	
Reverse braking	1549	-852		1709	-852		239			
Pivoting	1549			1549			239			1515
Towing	1549			1549			239	F_{Tow} = 500		

b. U.S. Customary Units

	Main gear			Main gear			Nose gear			Main gear torque, in. lbf
	V_M lbf	D_M lbf	S_M lbf	V_M lbf	D_M lbf	S_M lbf	V_N lbf	D_N lbf	S_N lbf	
Static reaction	348 135			348 135			53 730			
Taxi	696 270			696 270			107 460			
2-pt braked roll	375 000	300 000		375 000	300 000					
3-pt braked roll	311 105	248 885		311 105	248 885		127 790			
Turning	625 790		312,895	70 480		35 240	53 700		26 865	
Nose wheel yaw	333 300	266 640	13 840	323 305		13 430	93 395		27 270	
Reverse braking	348 135	-191 475		384 135	-191 475		53 730			
Pivoting	348 135			348 135			53 730			13 407 000
Towing	348 135			348 135			53 730	F_{Tow} = 112 500		

Accurate analytical techniques are required for the prediction of steady and unsteady aerodynamic load distributions, including the effects of structural deformation on large flexible aircraft. Accurate load prediction becomes particularly acute when critical structural or control design conditions occur in the transonic speed range.

Experience in design of the SST prototype identified a number of problem areas associated with aeroelastic analysis, the principal one being the need to develop a practical means of incorporating wind tunnel pressure data in the analysis to account for effects of separated flow and formation of strong leading edge vortices on this type of configuration.

The wing structural weight which resulted from the structural analysis for the delta wing of reference 11 was based on loads which were adjusted to reflect wind tunnel test results. The adjustments led to significant reductions in the loads relative to linear potential flow theory. The technique used in applying wind tunnel data to the loads analysis was based on two major assumptions:

1. Panel pressure coefficient slopes used to calculate incremental aeroelastic loads can be adjusted by a single factor per panel.

2. The location of the upper surface vortex is not affected by wing deformation.

Wind tunnel tests described in reference 12 of a flat and twisted wing of the same section and planform, and test-theory comparisons for this wing, have shown that these assumptions probably are not valid, since the vortex streaming aft over the wing alters the pressure distribution as a function of wing twist.

For the arrow wing loads analysis, only theoretical solutions were obtained involving the assumptions inherent in the linearized potential flow theory - thin wings, slender bodies, small angle of attack, small control surface deflections, and attached flow. Work is continuing to develop a means of incorporating wind tunnel data in the loads analysis, but such a method is not yet available.

STRUCTURAL LOAD CONDITIONS

A structural model with 164 retained nodes and 192 degrees of freedom was selected from the complete structural mathematical model. Analysis conditions were selected on and within the maneuver envelope to cover the complete range of Mach numbers, design speeds, and load factors. Maximum flight mass at the appropriate altitude, and maximum zero fuel mass plus reserve fuel, were considered for all maneuver conditions. In addition, the minimum flight mass, which occurs in the ferry flight configuration, was considered for the gust conditions.

The following conditions were analyzed:

1. Symmetric, balanced maneuvers at maximum flight mass
2. Symmetric, balanced maneuvers at maximum zero fuel mass plus reserve fuel
3. Design vertical gusts at maximum flight mass
4. Design vertical gusts at the ferry flight mass

5. Checked and unchecked elevator maneuvers as specified in FAR 25.331(c)

6. Design lateral gusts at the maximum flight mass

7. Rudder maneuvers as in FAR 25.351(a)

8. Landing impact

9. Taxi

10. Ground handling as specified in FAR 25.471 through 25.509

Loads were calculated for a total of 154 flight conditions. The critical design conditions selected for use in the resizing are shown in table 15. Ultimate shear and bending moment off the forward body due to landing impact are presented in figures 28 and 29. The forward body is the only portion of the structure for which landing impact is the critical condition.

TABLE 15.–LOAD CONDITIONS FOR DESIGN

Symmetrical Loads

Column number	Condition number	Condition description
1	0.4-01-02-05-20E	Flaps down maneuver at V_F
2	0.6-01-19-06-25E	Positive maneuver at V_A
3	0.9-01-34-06-25E	Positive maneuver at V_A
4	1.2-01-52-07-1NE	Negative maneuver at V_H
5	1.2-01-39-06-25E	Positive maneuver at V_A
6	2.0-01-48-03-1NE	Negative maneuver at V_C
7	2.7-01-67-07-1NE	Negative maneuver at V_H
8	0.4-05-02-05-20E	Flaps down maneuver at V_F
9	0.6-05-07-07-1NE	Negative maneuver at V_C
10	1.2-05-35-03-1NE	Negative maneuver at V_C
11	0.9-01-34-36-10E	Abrupt elevator maneuver

Asymmetrical Loads

1		Lateral gust at Mach = 0.9
2		Rudder maneuver no. 1
3		Rudder maneuver no. 2
4		Rudder maneuver no. 3

JIG SHAPE

The jig shape represents the stress-free condition for the aircraft structure and corresponds to a state of zero applied loads. The analysis of design loads is based on the camber slopes for this jig shape. On the other hand, the performance of the configuration is optimized for a shape corresponding to a particular flight condition, normally a mid-cruise condition. Before calculating design loads, therefore, the jig shape must be computed from the shape defined for use in the performance calculations.

This was accomplished in FLEXSTAB by first trimming the airplane for the mid-cruise design condition, with the airplane treated as a rigid body. The resulting loads were then applied to the flexible airplane and the increments of camber and displacement due to this loading were subtracted from those defined for the design condition to yield the jig shape. The wing and body vertical displacements from the mid-cruise design condition to the jig shape are shown in figure 30.

THERMAL ANALYSES

Supersonic aircraft are subjected to heating effects from several external and internal sources. Structural thermal analysis is required to determine resulting temperature gradients which produce thermal stresses, and to establish temperature limits for material selection. Internal heat sinks provided by the structure and the fuel must be considered in the analysis in order to predict temperature and stress distributions. These are then used in the design and sizing of the structural elements, in the selection of suitable structural materials, and in determining insulation requirements for fuel tanks.

The thermal analysis initially requires the establishment of criteria, a mission profile, a fuel management plan, and external and internal environments to predict heating rates to the various regions of the aircraft. The next phase is the determination of the thermal response of the particular structural cross section yielding the required temperature distributions, gradients, and stresses.

The criteria and methods used in the present analysis are identical to those employed on the National SST program. In determining the structural temperatures, no factors of safety were applied. However, a factor of safety of 1.25 was applied on thermal strains to account for uncertainties.

The major sources of external heating for a commercial supersonic transport are aerodynamic and solar heating. Both were considered in the present analysis. The analysis methods and results are described in the following paragraphs.

AERODYNAMIC HEATING

Based on studies of several alternate procedures conducted on the National SST program, Eckert's reference temperature method was selected for determining heat transfer coefficients for this study. The Reynolds analogy and the Blasius skin friction relationship were used for laminar flow regions, a modified Reynolds analogy, the

Prandtl-Schlichting-Wieghardt skin friction relation, and Rubesin correction factor (ref. 13) were used for turbulent flow regions. Flat plate approximations were used in calculating heat transfer coefficients for the large external surfaces having small curvature.

SOLAR ABSORPTANCE AND SURFACE EMITTANCE

The effects of solar absorptance and surface emittance on the equilibrium wall temperature are shown in figure 31. For this study the titanium solar absorptance was assumed to be $\alpha_{SOL} = 0.7$, and the surface emittance was assumed to be $\epsilon = 0.2$. It was further assumed that the lower surfaces of the aircraft received 10% of the solar energy reflected from the earth (albedo).

TRANSIENT THERMAL ANALYSIS

The externally generated heat flows into the aircraft through the skin surfaces and adjoining structural members mostly by conduction and radiation. There is a certain time lag in the structural temperature response due to thermal resistance, resulting in temperature gradients which produce thermal stresses. A thermal analyzer computer program was used in generating the thermal gradient and the temperature time histories required for the selection and sizing of various structural members. The program is based on a finite difference solution of the heat flow equation using a three-dimensional nodal network. Effects of conduction, convection, radiation, external and internal heat sources, and property variations with time, temperature, and direction are included.

For transient thermal analyses structural members, such as a wing spar and upper and lower panel combination, are divided into a suitable number of elements, represented by lumped masses at the centroids. The thermal model is then represented by a passive electrical network for analysis. This network of capacitors, resistors and radiators, in conjunction with sources, sinks, and the aerodynamic heating boundary conditions are used to calculate the thermal response.

The thermal stresses in the structural members were calculated using a stress subroutine that solves the following equation:

$$\sigma_j = \alpha_j E_j \Delta T_j - E_j \frac{\sum_{i=1}^{n} \alpha_i E_i A_i \Delta T_i}{\sum_{i=1}^{n} A_i E_i}$$

This equation predicts the thermal stress in each of n uniaxial elements. The n elements are assumed to be of equal length at a reference temperature as in a stiffened panel. When subjected to temperature differentials from the reference temperature, the members are constrained against rotation but allowed to translate to a common length at which the total axial load of the n members is zero.

The thermal analysis of the arrow wing SST configuration was conducted for selected locations shown in figure 32. These locations and structural arrangements are listed in table 16.

TABLE 16.–THERMAL ANALYSIS CONDITIONS

Configuration	Point	Case	Description	Insulation
Fuel tank no. 1 (Spar area)	249	1	Tank height = 1.10 m (43.3 in.) Upper panel does not touch fuel	None
		2	Tank height = 0.89 m (35.0 in.) Upper panel touches fuel	None
Fuel tank no. 2 (Stringer area)	269	1	Upper panel touches fuel	0.63 cm (0.25 in.)
		2	Upper panel touches fuel	1.27 cm (0.50 in.)
		3	Upper panel does not touch fuel	0.63 cm (0.25 in.)
		4	Upper panel does not touch fuel	1.27 cm (0.50 in.)
Intermediate and rear spars	431	1	Spar fwd of point 431	None
		2	Spar aft of point 431	None
Wing panel dry bay area	431	1	Fwd of point 431	None
		2	Aft of point 431	None
Body stringers	5	1	Lower crown	None
	6	2	Upper crown	None

The aerodynamic heating rates were calculated using a 6190 km (3340 nmi) mission profile, as shown in figure 33, for the 1962 U.S. standard atmosphere. Since the flow along the wing and the body is mostly turbulent, turbulent heat transfer rates were used in the analysis. Solar heating and radiation to outer space was included in the calculation of the transient skin temperatures. The thermal conductance of the 25.4 mm (1 in.) deep honeycomb panel was assumed to be 34 W/m^2K(6.0 $Btu/ft^2\ hr\ °R$). For the denser honeycomb core, at the joint with the spar, a value of 216 W/m^2K (38.0 $Btu/ft^2\ hr\ °R$) was used.

To determine the effect of fuel on tank structures, the fuel management scheme shown in figure 34 was used in the transient analysis. This fuel management is consistent with the flight performance of the 969-512B. The thermal conductance between the structure and the fuel was assumed to be 170 W/m^2K (30.0 $Btu/ft^2\ hr°R$) It was further assumed that the panel and the spars of tank no. 1 were not internally insulated. Insulation with a thermal conductivity of 0.058 W/m K (0.4 $Btu\text{-}in/ft^2hr°R$) was used only for the tank no. 2 area which contained integrally stiffened lower panels.

The initial temperature before the aircraft flight was assumed as 288.8 K (60° F). Typical temperature time histories for a representative wing section, figure 35, are shown in figure 36. Thermal stresses are shown in figure 37. For complete results of the thermal analysis see reference 2.

FUEL TEMPERATURE ANALYSIS

The environmental control system for the SST relies heavily on the fuel as a heat sink to cool the passenger cabin and certain equipment. Therefore, control of the fuel temperature is a critical factor in the design of the environmental control system and the engine fuel system. The fuel temperatures for the 969-512B missions were calculated using a thermal analyzer program developed during the National SST program.

MISSION DESCRIPTION

The mission profile that was used for fuel temperature analysis consists of 106 minutes of Mach 2.7 cruise flight on a standard day. Significant points on the profile are listed in table 17.

TABLE 17.–MISSION PROFILE

Condition	Time from start of taxi, minutes	Mach no.	Altitude	
			Meters	(Feet)
Start of taxi	0	0	0	(0)
Takeoff	10.66	0.32	10.7	(35)
Start of cruise	35.68	2.7	18 600	(60 973)
End of cruise	141.22	2.7	20 600	(67 484)
Start of descent	142.54	2.4	20 600	(67 484)
Touchdown	167.08	0.22	0	(0)

The fuel temperature analysis considers single trips as well as two consecutive legs of a New York-Paris round trip flight using the most adverse combinations of fuel usage and bulk fuel temperature. The initial fuel temperature in the tanks is assumed to be 306 K (90° F) as discussed in reference 2. Bulk fuel temperatures greater than 306 K(90° F) were estimated to occur less than 2.5% of the time. Prior to the second leg of the flight, all auxiliary tanks were refilled with 306 K(90° F) fuel. The main tanks, containing the hot reserve fuel left from the first leg of the flight, were also refilled with 306 K (90° F) bulk fuel, resulting in a somewhat higher initial temperature. Subsequently during climbout the main tank temperature decreases as cooler fuel is pumped in from the auxiliary tanks.

It was assumed that the fuel usage during the first leg of the flight was normal for the flight profile and that the airplane landed with normal reserves aboard. The fuel usage during the second leg of the flight was assumed to increase uniformly throughout the flight to reflect the use of the trip fuel allowance. This combination provides a worst-case situation in that the greater amount of hot fuel left from the first leg of the flight results in a higher initial fuel temperature in the main tanks for the beginning of the second leg. Also, the use of the reserve fuel during the second flight results in larger temperature increases in the main tanks by the end of the cruise segment.

TEMPERATURE LIMITS

The critical fuel temperature occurs at the end of the cruise segment at an altitude of 20 600 m (67 500 ft). At this altitude the boiling temperature of maximum volatility kerosene is 353 K (175° F). Allowing a margin of 8 K (15° F) to account for pressure uncertainties, temperature stratification of the fuel in the tanks, and pump cavitation, a bulk temperature of 344 K (160° F) is established as the maximum allowable temperature of fuel remaining in any tank.

An engine/airframe interface fuel temperature limit of 394 K (250° F) is established assuming engine electronics will be cooled with another coolant, and that a burner nozzle fuel temperature limit of 436 K (325° F) is reasonable.

FUEL SYSTEM

An important factor influencing fuel temperature is the amount of wetted area in each fuel tank as a function of quantity of fuel in the tank. The wing and body surface coordinates and fuel tank boundaries were analyzed to determine both fuel volume and hot surface area of the fuel tanks including corrections for unusable fuel volume.

The fuel tanks on the 969-512B shown in figure 5 are primarily aluminum-brazed titanium honeycomb sandwich panels except for the rear fuselage auxiliary tank, 14A, which was riveted sheet stiffener construction, and the lower surface of the main wing box which has integrally stiffened skin stiffener construction. The thermal conductance of the aluminum-brazed titanium honeycomb sandwich was estimated to be 34 W/m²K (6 Btu/ft² hr °F). A previous analytical study estimated that the effect of additional heat paths due to the panel edge members, access holes, and fasteners increased the net average fuel tank conductance to 62.4 W/m²K (11 Btu/ft²hr°F). This relationship is illustrated in figure 38. The conductance of the skin stiffener areas in tank 14A and the aft wing is estimated to be 3400 W/m²K (600 Btu/ft² hr °F).

FUEL TEMPERATURE

The maximum temperature of the fuel in the main tanks at the end of a second supersonic cruise mission is shown as a function of fuel tank conductance in figure 39. For the purposes of this trade study, the conductances of all main and auxiliary tanks were considered equal. As indicated, tank conductances of about 22.7 W/m²K (4 Btu/ft² hr °F) are required to keep the rear main tank fuel temperature below the 344 K (160° F) maximum, and conductances of about 34 W/m²K (6 Btu/ft² hr °F) would be required for the forward main tanks. All auxiliary tanks except the rear fuselage auxiliary tank 14A are emptied early in the flight before much fuel heating can occur. Since the brazed aluminum honeycomb structure used in auxiliary tank walls provides reasonable insulation, it was determined that the fuel temperatures would be maintained below the 344 K (160° F) maximum and that no insulation was required for these auxiliary tanks. Based upon the above study the tank conductances shown in table 18 were established as requirements and used in subsequent analysis. To attain this level of tank conductance additional insulation will be required in main tanks 1, 2, 3, and 4 and in auxilary tank 14A.

TABLE 18.–FUEL TANK CONDUCTANCE

Tanks	Tank conductance, $W/m^2 K$ (Btu/hr $ft^2 °F$)
Forward mains 1 and 4	28.3 (5)
Rear mains 2 and 3	17.0 (3)
Auxiliary 1A and 2A	62.4 (11)
Auxiliary 2A and 3A	62.4 (11)
Auxiliary 5A and 6A	62.4 (11)
Auxiliary 14A	62.4 (11)
Ballast	62.4 (11)

It should be noted, however, that significant improvements have been achieved in low-conductivity brazed core design and in diffusion-bonded sandwich panel manufacturing techniques subsequent to completion of this study. These improvements will result in net fuel tank conductances about 50% lower than those used in the fuel temperature analysis reported herein, and should virtually eliminate the need for adding extra fuel tank insulation.

The problem of excessive fuel temperatures is largely associated with flights which combine adverse thermal conditions such as high onloaded fuel temperatures and/or consecutive trips with hot reserve and/or ballast fuel remaining from the earlier trip combined with trips which used fuel reserves in an adverse manner. Table 19 shows the fuel temperatures at the end of cruise or start of descent (whichever is higher) in the main fuel tanks, at the engine/airframe interface, and at the fuel nozzles for a series of conditions using the tank conductances listed above. On a first trip with onloaded fuel at 289 K (60° F), trip condition 1, excessive fuel temperatures do not occur. When the onloaded fuel temperature is increased to 305 K (90° F) the end-of-mission fuel temperatures increase significantly but are still satisfactory. On a second consecutive trip with 305 K (90° F)) onloaded fuel, the main tank temperatures increase to above 344 K (160° F). If the second trip uses trip fuel reserve, the forward fuel tank temperature rises to over 347 K (165° F). In all cases the engine/airframe interface fuel temperature remains less than 394 K (250° F), and the engine nozzle temperature remains less than 436 K (325° F) maximum.

The temperatures in table 18 were determined for the 969-512B airplane, which had a mission duration of 2.8 hours. A longer duration at supersonic cruise will tend to aggravate the fuel temperature problem. However, increased mission range does not affect fuel temperature as adversely as might be expected, because the amount of onloaded fuel would have to be increased, which also increases the available fuel heat sink. Previous studies of the 969-336C airplane indicated that the fuel temperature rise with increasing range was a function of tank conductance, and for the conductances recommended herein the rate of increase would be about 0.0045 K/km (0.015° F/nmi).

TABLE 19.–FUEL TEMPERATURES FOR VARIOUS TRIP CONDITIONS

Trip condition	On loaded fuel temp, K (°F)	Maximum temperatures at end of cruise or start of descent (whichever is higher), K (°F)			
		Forward main tanks 1 or 4	Rear main tanks 2 or 3	Engine/ airframe interface	Burner nozzle
1. Normal, first trip	289 (60)	324 (130.3)	328 (129.9)	376 (217.4)	414 (285)
2. Higher on-loaded fuel temp., first trip	306 (90)	340 (153.0)	340 (153.3)	388 (238.6)	425 (306)
3. Same as 2, except second trip; reserve plus ballast fuel discharged to main tanks after first trip	306 (90)	345 (159.8)	345 (161.1)	392 (246.4)	430 (315)
4. Same as 3, except second trip used excess fuel (trip reserves) during trip	306 (90)	318 (165.5)	346 (163.7)	394 (250.0)	433 (320)
5. Same as 4, except with earlier discharge of rear auxiliary tank 14A at 3.03 kg/sec (400 lbm/min) per main tank	306 (90)	345 (160.2)	344 (157.5)	392 (246.0)	425 (307)
6. Same as 5, except discharge of tank 14A at 6.06 kg/sec (800 lbm/min) per main tank	306 (90)	344 (158.2)	342 (156.0)	391 (244.0)	426 (308)

*Conductances per table 18

51

Two possible alternatives to additional tank insulation were investigated to reduce fuel temperature. The first of these was to compartment the main tanks so that the inboard portions of all main tanks would have a capacity of 13 659 kg (30 000 lbm) fuel each, and the outboard portion would be converted into additional auxiliary tanks. The results of this concept are shown in figure 40. This compartmenting scheme would reduce final fuel temperature about 4.4 K (8° F), but would introduce the additional weight of bulkheads, pumps, gages, etc. required for the additional auxiliary fuel tanks.

Another possibility is to start discharging the fuel from the rear fuselage auxiliary tank (14A) prior to the end of cruise. This is effective only when tank 14A has sufficient insulation to keep the fuel cool. The results of this concept are shown in table 18, conditions 5 and 6. In both cases the transfer from tank 14A started 15 minutes before the end of cruise. For condition 5 the transfer rate was 3.03 kg/sec (400 lbm/min) per main tank, and for condition 6 the rate was 6.06 kg/sec (800 lbm/min) per main tank. As can be seen, this results in tank fuel temperature reductions of 3.05 K (5.5° F) and 4.16 K (7.5° F) respectively. The penalty for early discharge of tank 14A is that the c.g. moves forward during supersonic cruise, which would require moving the forward c.g. limit and would result in increased trim drag with the associated performance penalty. The magnitude of this performance penalty has not been established, nor has the increase in forward c.g. limit been identified.

STRESS ANALYSIS AND STRENGTH SIZING

The stress analysis and resizing of the structural members is the culmination of structural design for strength. These analyses involve a number of activities relating to the preparation of external loads in a form to be applied to the airframe to produce internal loads, preparation of many sets of data necessary to properly utilize allowable stresses and recognize practical design limitations on the structural members, and checking of the data and programs to assure proper operation and accurate results. This last item, checkout of data and programs, is perhaps the most critical requirement for producing analyses of the type described herein. Experience on analyses of large finite element models has shown that flow time and manpower requirements for this checking function are often underestimated.

The following paragraphs describe these activities as carried out on the arrow wing, followed by the description of the stress analysis and results of resizing.

The initial effort consisted of a thorough checkout of the mathematical model to verify correctness of initial data and transfer to the computer. This checkout took the form of checking listings and plots of the many input parameters, locations of members and nodes, classification of members, etc. Following this, sample vibration analyses, deflection, and stress analyses were conducted, and equilibrium and reactions were checked.

The wing was divided into a number of regions, illustrated in figure 41, based on commonality of skin panel construction, spar web construction, spar spacing, and fuel tankage. These regions were defined to expedite the analysis of effects of high structural temperatures and associated thermally induced stresses for each load

condition. Allowable stresses were established for these structural elements by reducing the room temperature allowables by an amount equal to 1.25 times the calculated thermal stresses. The 1.25 factor on the thermal stresses is consistent with the requirements on the National SST program. In cases where thermal stresses relieved the mechanical stresses induced by the airloads, the thermal stresses were conservatively neglected.

A number of subsets of structural members were defined for convenience in specifying design data necessary for stress analysis and resizing. The types of information specified in this manner are: properties of elements used to convert internal loads into stresses, definition of upper and lower bounds on areas or skin gages to limit the redesign for practical reasons, and specification of elements that are not to be resized for special reasons. A number of these subsets are depicted in figures 42 and 43. Figure 44 summarizes the lower bound data for surface panels and spars.

The analytical model represents the right half of the airplane. Deflections were calculated for the symmetric and antisymmetric load components for a given load condition with appropriate boundary conditions applied in the plane of symmetry to specify either symmetric or antisymmetric elastic behavior with respect to this plane. These deflections were then superposed to form the deflections for the design conditions. For unsymmetric conditions, deflections are determined for both sides of the airplane. These superposed deflections then form the basis for the stress analysis of the selected design conditions.

The strength design requires evaluation of: (1) stresses due to the various load conditions, (2) the relation between imposed and allowable stresses, i.e., margins of safety, and (3) structural member size changes necessary to obtain the desired values of the margins of safety.

The stability interaction equation used for evaluation of margins of safety in biaxial compression and shear in the honeycomb sandwich wing covers is:

$$R = \left[\frac{R_x}{1 - R_{xy}^2}\right]^4 + \frac{R_y}{1 - R_{xy}^4}$$

where R_x, R_y, R_{xy} are the ratios of actual to allowable inplane load for axial and shear loads. For strength-critical loading conditions, a modified Hill's yield criterion was used. The influence of temperature on elastic moduli and allowable stresses was included in the analysis.

Structural elements that were not restrained by minimum gage requirements were resized to obtain new member sizes. Automated resizing of the fuselage elements was not attempted because of the problem posed by buckled skins and the smaller structural weight savings expected in the fuselage. Elements in the fuselage were resized by hand and the resizing process for these elements converged in two cycles. Since lumped areas used in model beam elements in the fuselage are composed in part of effective skin areas and these are influenced by buckling, body pressurization, and thermal stresses, iterative procedures were employed in resizing these elements. Effects of body

pressurization and thermal stresses on effective areas were included in the analysis. Stringer spacing, fastener sizes, and stringer geometry were also defined to establish compression allowables. The relevant design parameters, effective areas, and allowables were adjusted in successive analysis cycles until overall consistency was achieved, with the margins of safety near zero. Figure 45 presents typical material properties as a function of temperature, and figure 46 presents typical compression allowables for various temperatures.

Elements in the wing covers were resized using the ATLAS automated resizing module, with convergence, as measured by total mass change, occurring in three cycles. The resizing module uses the interaction equation given above, and an iterative solution technique. Margins of safety were calculated considering stability, allowable stress level, and fail safety for multiple load cases. Elements were grouped in sets as indicated previously in figures 42 and 43 to allow imposition of common constraints, such as panel minimum face sheet thickness, spar web, minimum gage, spar chord minimum areas, and mechanical properties and instability allowables with appropriate thermal stress decrements. Constraints between element types, such as maintaining cap areas of at least one-quarter of the area of the larger adjacent panels for fail safety, were manually determined after a given cycle and imposed as lower bound data in the next resizing cycle.

The stress analysis was run for eleven symmetrical and four unsymmetrical flight conditions, and three symmetrical and two unsymmetrical ground load conditions. Resizing of the body and the wing carry-through structure was completed manually following the first cycle of stress analysis. Subsequent resizing of body structure was confined to the region containing wing carry-through structure.

Typical initial wing panel gages and those resulting from successive cycles of automated resizing are presented in figure 47. For each upper and lower surface panel, three gages are shown. Reading from top to bottom, the first set of values are the upper/lower surface panel gages derived manually from the SCAT-15F as the initial sizes. The second and third sets of gages were obtained from successive cycles of automated resizing.

For lower surface panels of integrally stiffened skin construction, the initial value is the area per inch of skin plus stiffener, while the second value, in parentheses, is the skin gage. For upper and lower surface panels of honeycomb sandwich construction, the single value shown is the sum of the inner and outer face sheet gages.

In the wing region having integrally stiffened lower surface panels, where skin gages are shown in parentheses, it should be noted that the initial sizing of the upper surface panels was larger than required because of the effect of the improved chordwise compressive load allowables of the honeycomb panels relative to that of the corrugated core sandwich on which the initial sizing was based.

The total theoretical masses of the wing box, spars, and panels were evaluated at the end of each successive cycle of stress analysis and resize. The criterion for convergence of the design was based on the total wing box mass. Figure 48 presents the normalized mass of the wing box and illustrates that at the end of the third cycle the mass had essentially converged to a constant value.

FLUTTER ANALYSIS AND RESIZING

Initial sizing of the arrow wing structure was based on design loads from the early design study of the 969-336C configuration, reported in reference 3, suitably modified to account for the increased gross mass in the present study. However, it was anticipated that a significant increase in structural stiffness, beyond the level provided by the strength design, would be required to satisfy flutter prevention criteria. Since program cost constraints limited aeroelastic loads analysis to one cycle, it was considered necessary to conduct a preliminary flutter analysis with initial sizing and to make some adjustments in stiffness prior to the loads analysis, in order to obtain a set of design loads that would be reasonably consistent with the final design.

FLUTTER ANALYSIS PROCEDURE

Flutter results were obtained in a single computer run including the generation of stiffness and mass matrices, vibration mode analysis, generation of unsteady air forces for all lifting surfaces, and solution of the flutter equations. A generalized coordinate approach was used in formulating the flutter equations, with a truncated set of airplane vibration modes, together with the relevant rigid airplane degrees of freedom for symmetric and antisymmetric cases. Subsonic kernel-function and supersonic Mach box versions of unsteady lifting surface theory were used to calculate generalized air forces on the wing. The Q-R algorithm was used to solve the complex eigenvalue flutter problem. Constant altitude classical V-g flutter solutions were cross plotted to match the Mach number of the unsteady air forces, and this result was confirmed by an automated flutter solution routine based on the Nyquist criterion. A supplementary study of energy balance at neutral stability was made to provide insight into the flutter mechanism, and to assist in defining changes to increase the flutter speed.

The stiffness modifications which were made in meeting flutter criteria were based on engineering judgment. These judgments were aided by interpretation of the energy balance at the onset of flutter, which identified the vibration modes important to the flutter mechanism. Plots of frequency vs airspeed showed which of these modes required stiffening, and inspection for high strain regions, in those mode shapes, indicated the areas where increased stiffness was required.

PRELIMINARY FLUTTER ANALYSIS AND STIFFNESS RESIZE

The preliminary flutter analysis was confined to the symmetric high gross mass condition and to a high subsonic Mach number, M = 0.9, based on the flutter results for the National SST program. The same analytical detail and procedures were employed in this preliminary study as in the final analysis. Airplane plunge and pitch and the first 18 symmetric airplane vibration modes were used as generalized coordinates in setting up the flutter equations. Results of the preliminary flutter analyses and the effects of the preliminary stiffness resize are summarized in figure 49 and table 20.

TABLE 20.–PRELIMINARY SYMMETRIC WING FLUTTER RESULTS

M = 0.9 – High Gross Mass Condition

Wing structure	Flutter speed, m/s (kn) EAS	Frequency, Hz
Bare wing flutter speed (no nacelles and fin)	212 (413)	5.7
Initial structural design 1.05 MN/m (6 kips/in.) engine beams	93 (181.0[a]) 143 (278.0)	2.18 3.58
Initial design with stiffened tip and aileron 1.58 MN/m (9 kips/in.) engine beams	112 (217.0) 216 (420.0)	2.29 3.67
Initial design with stiffened tip and aileron 4.72 MN/m (27 kips/in.) engine beams	224 (436.0) 224 (435.0)	1.90 3.72

[a]6100 m (20,000 ft) solution; Mach number not matched.
Clearance speed (1.2 V_D): 259 m/s (504 kn) EAS

The flutter speed with initial sizing of the structural model was 93 m/s (181 kn) EAS at a frequency of 1.9 Hz, which was 166 m/s (323 kn) EAS below the design requirement at M = 0.9. An appraisal of the flutter mode showed large amplitude nacelle motion as well as large energy inputs from excessive wing tip distortion and windup of the low-speed aileron relative to the inboard location of its actuators. These flexibilities were also very apparent in the flexibility influence coefficients and the vibration mode shapes.

As a result of the initial assessment of flexibilities and preliminary vibration analysis, it was decided to stiffen structure in three areas before initiating the FLEXSTAB aeroelastic loads analysis:

1. In the wing tip outboard of the wing-mounted fin, spars and covers of the main box and secondary structure behind the rear spar were doubled.

2. The low-speed aileron covers were quadrupled in thickness to minimize windup relative to the inboard location of the actuators.

3. The strength-designed nacelle support beams were stiffened by a factor of 1.5 to 1580 kN/m (9000 lb/in.), defined at the rear mount location with the beam cantilevered at the wing rear spar.

Little improvement in flutter speed of the critical low-frequency mode was obtained with this preliminary stiffness resize; it rose to 112 m/s (217 kn) EAS, still 148 m/s (287 kn) EAS below the M = 0.9 requirement. However, the flutter speed of the less critical overtone flutter mode did rise appropriately with the stiffened wing tip, as can be seen for this condition in table 20.

Experience on the National SST program indicated that the critical low-frequency flutter mode could not be controlled without further stiffening of the engine beams, which are cantilevered off the wing rear spar. This was further confirmed by large amplitude motions of the outboard nacelle in the calculated critical flutter mode of the arrow wing configuration. Since the trailing edge structure of the wing is attached to the nacelles and engine support beams, the wing deformations that are induced by large nacelle motions produce significant changes in the oscillatory wing airloads that have a destabilizing effect on the wing flutter mode. This was confirmed by wind tunnel tests on the National SST program. Vibratory displacements associated with the fifth airplane vibration mode were found to be an essential ingredient of the wing flutter motion. The shape of this particular mode is displayed in figure 50 for two different values of engine beam stiffness to illustrate the decoupling of the outboard nacelle resonance that occurs with increased engine beam stiffness. This decoupling effect is mainly responsible for the improved flutter speed with stiff engine beams.

FINAL FLUTTER ANALYSIS AND STIFFNESS REDESIGN

Following the automated resize of wing primary structure and prior to the final flutter analysis, some changes were made to the strength-designed structural model. These included locks on the low-speed aileron and outboard flaperon during high-speed flight, wing tip and low-speed aileron stiffening that had been adopted prior to the loads analysis, and engine beam stiffening to 4.5 times the strength design value. With these stiffness increments the effect of strength resizing was a slight decrease in flutter speed to 0.817 of the speed requirement at M = 0.9, compared with a flutter speed ratio of 0.865 prior to the strength resize (with the same stiffness increments, apart from the control locks). No reduction in gages or member sizes, below the values specified for strength, were allowed in defining further structural changes to meet flutter criteria. These changes are listed in table 21.

Six additional design modifications, based on engineering judgment, were analyzed in attempting to improve the wing flutter speed. This analytical work was first confined to the symmetric, high gross mass condition at M = 0.9. It was finally concluded that further efforts to increase the flutter speed of the critical 1.9 Hz wing flutter mode, via structural changes based on engineering judgment, would produce an unrealistically high mass penalty. Hence it was proposed that the subsonic dive placard be reduced by 26 m/s (50 kn) EAS to achieve flutter clearance. The reduced placard would impose a range decrease of 46 km (25 nmi) with fixed fuel loading, or an increase of 588 kg (1297 lbm) in fuel loading for constant range.

The structure with the final stiffness design modifications was then analysed for symmetric flutter at low gross mass and for antisymmetric flutter at both high and low gross masses and M = 0.9. This confirmed that the symmetric, high gross mass condition was critical. Flutter analyses were then conducted for that condition at other Mach numbers. The resulting flutter boundary for the 969-512B configuration with titanium structure (1975 technology) appears in figure 51.

TABLE 21.–MODIFICATIONS – MODEL 969-512B

Stiffness design modification	Modification number								
	(1)[a]	(2)	(3)	(4)	(5)	(6)	(7)	(8)	(9)[b]
Double wing tip spars and covers	X		X			X	X	X	X
Quadruple outboard aileron covers	X	X	X	X	X				
Aileron control locks	X	X		X	X	X	X	X	X
Stiffened engine beams	X	X	X	X	X	X	X	X	X
Double all wing box spars and ribs				X					
Triple wing tip spars and covers					X				
Increase spars, ribs, and covers 50% between vertical fin and kink rib					X				
Triple fin support rib						X	X	X	X
Stiffen trailing edge spar							X	X	
Add outboard nacelle diffusion ribs							X	X	
Increase outboard wing box depth (refair)								X	X
Add four outboard wing tip ribs									X
Add outboard and inboard nacelle diffusion ribs									X
Increase front spar web gage to average skin gage outboard of wing fin									X
Increase total rear spar web gage to average skin gage									X

[a]Initial design with preliminary stiffness

[b]Final stiffness

The stiffness design modifications to provide flutter clearance are summarized in figure 52. The penalty associated with the stiffness redesign is equivalent to 4637 kg (10 223 lbm), per aircraft including the 1339 kg (2953 lbm) equivalent of a 1.3 drag count increase for thickening the wing tip.

MASS ANALYSIS

The mass statement for Model 969-336C (see ref. 2) was revised early in the study to account for advances in subsystem design and in structures and materials technology that have occurred since the earlier study was made. This revision, data from the National SST program, and data from the AST study (Contract NAS1-19938) were then used to develop a preliminary mass and balance statement for the 969-512B configuration, and detailed mass distributions were defined for calculation of the mass matrices required for aeroelastic loads and flutter analyses.. The mass distribution and the mass matrix were revised as the design evolved, reflecting iterative design changes to satisfy strength and flutter criteria. A mass and balance statement for the final

configuration was prepared to provide a basis for assessment of the performance impact of the structural changes. This final mass statement and the preliminary mass statement from Task I are displayed together in table 22.

WING AND CONTENTS

Masses of wing structure and contents were introduced into the mass model in a number of ways. The theoretical masses of spars, ribs, and cover element skins were automatically calculated from the material density and volume required to satisfy the structural requirements. To these were added the masses of nonoptimum structure, consisting of padups, fasteners, fittings, etc., to arrive at total structural mass. The theoretical-to-actual mass increment was input as a percentage of the cover material, spar, rib, and beam masses. The derivation and a more detailed explanation of the theoretical-to-actual factor is discussed in later paragraphs.

Surface panel skins, honeycomb core and braze, and main landing gear doors were entered in the program as plate mass elements and distributed over the appropriate area. Some of the miscellaneous items in the wing box, such as fairing, fuel system provisions, aerodynamic fences, and jacking provisions were treated as rods, plates, or point masses, based on shape similarity.

Mass distributions for wing contents and secondary structure were determined from Model 969-336C data. Masses of leading and trailing edge structure and wing contents were defined for the mass panels shown in figures 53 and 54. Input data for these items were generated manually. Inertia data for the mass panels were generated automatically within the ATLAS analysis module.

CORRECTION OF MASS ANALYSIS

In conjunction with a later study, reported in references 14 and 15 and dealing with the application of advanced composite materials to the arrow wing structure, a detailed review of the structural mass analysis of the titanium arrow wing structure has been accomplished. In the course of this review some errors have been found. Principally these consisted of omission of spar and rib web stiffeners, inclusion of core and braze contributions in the integrally stiffened portion of the lower wing surface, and failure to fully account for spanwise edge padup masses in deriving theoretical-to-actual factors for wing surface panels. Detailed descriptions of these errors and revision of the mass analysis are presented in sections 5 and 9 of reference 14. In order to provide an adequate basis for derivation of theoretical-to-actual factors for composite wing panels it was found necessary to develop panel designs using both titanium and composite materials and including edge attachment details for five representative locations on the arrow wing. Design data for the five titanium panels from the later study were used in developing the theoretical-to-actual factors that were employed in correcting the mass analysis of the titanium structure.

Correction of the errors noted above has increased the mass of the titanium wing structure listed in table 22 by 930 kg (2050 lbm). The corrected value is 44 370 kg (97 810 lbm).

TABLE 22.–GROUP MASS AND BALANCE STATEMENT, MODEL 969-512B

a. SI Units

Group	Task I		Δ Mass, kg	Task II	
	Mass, kg	Arm, m		Mass, kg	Arm, m
Wing*	42 710	66.1	+ 730	43 440	66.1
Horizontal tail	2 960	92.0		2 960	92.0
Vertical tail (body and wing mounted)	2 270	86.5	+ 380	2 650	86.5
Body	25 460	53.8		25 460	53.8
Main gear	16 930	64.7		16 930	64.7
Nose gear	1 710	29.9		1 710	29.9
Nacelle	8 650	74.9		8 650	74.9
Total structure	100 690	64.14	+1110	101 800	64.23
Engine (incl T/R S/S and nozzle)	20 500	78.1		20 500	78.1
Engine accessories	610	74.8		610	74.8
Engine controls	350	58.6		350	58.6
Starting system	140	74.1		140	74.1
Fuel system	3 810	63.4	+320	4 130	63.4
Total propulsion	25 410	75.55	+320	25 730	75.39
Instruments	845	43.4		845	43.4
Flight controls	6 670	68.0		6 670	68.0
Hydraulics	2 630	72.5		2 630	72.5
Electrical	2 340	53.1		2 340	53.1
Electronics	1 310	32.6		1 310	32.6
Furnishings	8 620	46.2		8 620	46.2
ECS	3 820	62.0		3 820	62.0
Anti-icing	60	14.2		60	14.2
APU	110	75.6		110	75.6
Insulation	1 315	48.6		1 315	48.6
Total systems and equipment	27 720	56.13		27 720	56.13
Options	1 130	63.3		1 130	63.3
Manufacturer's empty mass	154 960	64.57	+1430	156 380	64.62
Standard items	3 720	55.7		3 720	55.7
Operational items	2 390	43.6		2 390	43.6
Operational empty mass	161 060	64.05	+1430	162 490	64.11
Payload	22 180	47.8		22 180	47.8
Zero fuel mass	183 240	62.09	+1430	184 670	62.15

*See text subsection: Correction of mass analysis

TABLE 22.–CONCLUDED

b. U.S. Customary Units

Group	Task I		Δ Mass, lbm	Task II	
	Mass, lbm	Arm, in.		Mass, lbm	Arm, in.
Wing*	94 160	2 604	+1600	95 760	2 604
Horizontal tail	6 530	3 623		6 530	3 623
Vertical tail (body and wing mounted)	5 000	3 406	+ 850	5 850	3 406
Body	56 140	2 117		56 140	2 117
Main gear	37 320	2 548		37 320	2 548
Nose gear	3 760	1 178		3 760	1 178
Nacelle	19 080	2 949		19 080	2 949
Total structure	221 990	2 525.0	+2450	224 440	2 528.9
Engine (incl T/R, S/S and nozzle)	45 200	3 076		45 200	3 076
Engine accessories	1 350	2 944		1 350	2 944
Engine controls	780	2 308		780	2 308
Starting system	300	2 919		300	2 919
Fuel system	8 390	2 495	+ 720	9 110	2 495
Total propulsion	56 020	2 974.3	+ 720	56 740	2 968.2
Instruments	1 865	1 710		1 865	1 710
Flight controls	14 700	2 679		14 700	2 679
Hydraulics	5 795	2 854		5 795	2 854
Electrical	5 160	2 092		5 160	2 092
Electronics	2 885	1 282		2 885	1 282
Furnishings	19 010	1 817		19 010	1 817
ECS	8 430	2 440		8 430	2 440
Anti-icing	135	553		135	558
APU	250	2 978		250	2 978
Insulation	2 900	1 913		2 900	1 913
Total systems and equipment	61 130	2 209.7		61 130	2 209.7
Options	2 500	2 491		2 500	2 491
Manufacturer's empty mass	341 640	2 542.0	+3170	344 810	2 544.3
Standard items	8 200	2 193		8 200	2 193
Operational items	5 260	1 716		5 260	1 716
Operational empty mass	355 100	2 521.7	+3170	358 270	2 524.1
Payload	48 906	1 882		48 906	1 882
Zero fuel mass	404 006	2 444.3	+3170	407 176	2 447.0

*See text subsection: Correction of mass analysis

BODY AND CONTENTS

The body structure and contents are plotted as a one-dimensional running load in figure 55. The concentrated masses of galleys and contents at the galley doors are identified, as well as the buildup of mass at the front spar. This plot does not include the wing-body intersection, passengers or cargo masses.

The wing-body intersection and carrythrough structure inboard of buttock line 55 are included in the mass model as part of the body. The passenger and cargo mass is shown as a one-dimensional load distribution in figure 56, for a full payload condition. Since the body structure was sized manually, as noted earlier, the mass input data for the body were also generated manually.

EMPENNAGE AND WING-MOUNTED FIN

The mass distributions of the wing-mounted vertical fin, the body-mounted vertical tail, and the horizontal tail were all represented as sets of concentrated masses in the mass model for aeroelastic loads analysis. For flutter analysis the body-mounted vertical tail and horizontal tail were represented as rigid inertias with mass, center of gravity, and three-axis moments of inertia. The wing-mounted vertical fin was represented as a set of concentrated masses, as in the aeroelastic loads analysis.

FUEL

The fuel tank arrangement and tank capacities for the model 969-512B are shown in figure 5. A balance diagram with c.g. limits and fuel management for the maximum gross mass condition is shown in figure 57. The fuel distribution by tank was calculated for each of the 27 design conditions, consistent with the c.g. limits and fuel management sequence. These fuel quantities were translated into percentages of tank capacities and distributed into consistent mass panels. The body fuel was treated as a set of point masses in the aerodynamic loads analysis and as a point mass and moment of inertia data in the flutter analysis.

WING BOX MASS ESTIMATION METHOD

The finite element analysis of the wing primary structure produced the masses of the theoretically designed structural elements. The mass of the nonoptimum structure was added to convert from theoretical to total structural mass, as shown in figure 58. Figure 59 gives an example of nonoptimum structural items in a honeycomb wing surface panel. These consist of: skin padups along the panel edges and access doors, basic honeycomb core, dense core along the panel edges, braze material, and miscellaneous items, such as access doors, fuel system provisions, fairings, etc.

The theoretical-to-actual structural factors used in the arrow wing program were derived from design details from the National SST program. The masses of the basic skin panels were compared with the calculated masses for the released structural drawings to arrive at the factors as shown in figure 60. Two sets of curves are shown, one for the Model 2707-300 prototype airplane (PT) and the other for the 2707-300

production airplane prototype point design (PPD). The lower theoretical-to-actual factor for the PPD airplane was used for Model 969-512B. The PT airplane was defined in greater detail, thus helping to substantiate the slope of the curve. These curves show that the factor is relatively high for the lighter skin gages, primarily due to fastener provisions and pad-ups at the panel edges. The correction factor for the lower surface is larger than for the upper surface because of more numerous cutouts. As can be seen on figure 60, outboard wing section 17 does not plot consistently with the remainder of the wing sections, due to additional wing tip cover material that was required to disperse concentrated loads from both leading edge and trailing edge flaps. The Model 969-512B has a similar outboard wing tip section, but these higher factors were not considered appropriate, since the basic skin gages in this area were doubled to help alleviate flutter.

A review of the honeycomb core masses on the National SST program showed that approximately 25% must be added to the upper surface and 30% to the lower surface basic core mass to account for the dense core around the panel edges and access holes. Similar percentages must be added to the basic braze mass to accommodate the dense core at the panel edges. A study similar to that for the surface panels was made to determine the theoretical-to-actual factors of the spars and ribs on the National SST program wing. It was found that the average mass increment for all spars was 15% of the theoretical structural mass and 18% for all ribs.

Figure 61 gives a summary of the method of estimating the total structural mass of the wing box starting with the theoretical structural mass generated by ATLAS.

MASS CHANGES RESULTING FROM REDESIGN FOR STRENGTH

Table 23 shows three wing masses: (1) the Task I wing mass estimate, 42 710 kg (94 160 lbm); (2) a re-estimate with preliminary stiffness, 46 180 kg (101 820 lbm); and (3) a structurally resized wing with preliminary stiffness, 41 870 kg (92 310 lbm).

The Task I wing mass in column (1) of table 22 was based on 969-336C masses with revisions added for changing material from stressskin to aluminum brazed titanium honeycomb, for changing the wing planform and flap configuration, increasing the gross mass from 288 030 kg (635 000 lbm) to 340 190 kg (750 000 lbm), and other miscellaneous design changes.

Column (2) is a revised estimate of Model 969-512B wing mass based on the ATLAS resized structural box, modified for preliminary stiffness increases. These increases consist of doubling the outboard wing tip spars and covers, quadrupling the outboard aileron cover material, and stiffening the engine beams.

The breakdown of the 3475 kg (7660 lbm) increment between columns (1) and (2) is as follows:

Outboard aileron stiffness increase	+ 381 kg	(+ 840 lbm)
Outboard wing tip stiffness increase	+1416 kg	(+3122 lbm)
Increase associated with initial sizing	+1677 kg	(+3698 lbm)
	+3474 kg	(+7660 lbm)

TABLE 23.–WING STRUCTURAL MASS CHANGE, MODEL 969-512B

	SI Units			U.S. Customary Units		
	(1) Task I mass estimate, kg	(2) Reestimate with prelim. stiffness, kg	(3) Resize with prelim. stiffness, kg	(1) Task I mass estimate, lbm	(2) Reestimate with prelim. stiffness, lbm	(3) Resize with prelim. stiffness, lbm
Theoretical cover material		10 996	8 850		24 242	19 510
Nonoptimum cover material		2 353	2 272		5 188	5 010
Theoretical spars		7 288	6 280		16 068	13 844
Nonoptimum spar material		1 089	938		2 400	2 068
Theoretical ribs		1 883	1 087		4 152	2 396
Nonoptimum rib material		331	190		730	420
Theoretical beams		288	297		634	654
Nonoptimum beam material		44	44		96	98
Total structural element mass	21 178	24 212	19 958	46 690	53 510	44 000
Core	2 694	2 694	2 694	5 940	5 940	5 940
Braze	1 456	1 456	1 456	3 210	3 210	3 210
Landing gear doors	1 860	1 860	1 860	4 100	4 100	4 100
Fairing, fence, and miscellaneous	435	435	435	960	960	960
Total wing box (less center section)	27 623	30 717	26 403	60 900	67 720	58 210
Wing center section	3 883	3 883	3 883	8 560	8 560	8 560
Wing leading edge	6 455	6 455	6 455	14 230	14 230	14 230
Wing trailing edge	4 749	5 130	5 130	10 470	11 310	11 310
Total wing structure	42 711	46 185	41 871	94 160	101 820	92 310
Δmass due to		+3474 kg Reestimate with preliminary stiffness; −4314 kg Wing structural resizing			+7660 lbm Reestimate with preliminary stiffness; -9510 lbm Wing structural resizing	

Column (3) is the mass of the wing as resized by ATLAS inboard of the wing-mounted fin, while retaining the sizing for stiffness in the outboard aileron and wing tip region.

The distribution of the 4314 kg (9510 lbm) reduction is as follows:

Reduction of cover material	−2227 kg	(−4910 lbm)
Reduction of spar material	−1159 kg	(+2556 lbm)
Reduction of rib material	− 937 kg	(−2066 lbm)
Increase of beam material	+ 10 kg	(+ 22 lbm)
	−4313 kg	(−9510 lbm)

ADDITIONAL MASS REQUIRED TO SATISFY FLUTTER CRITERIA

Nine wing flutter analyses were conducted at M = 0.9 with various stiffness combinations in order to satisfy flutter criteria. These structural configurations are identified in table 21, and the corresponding comparisons in wing structural mass are summarized in table 24.

Several revisions were also made to the wing-mounted vertical fins to satisfy the flutter requirements. These modifications included increased skin gages, spars, and ribs, as well as the addition of an intermediate horizontal rib. However, there was a decrease in the sizing of the base rib. The mass of the Task II wing-mounted fin with initial sizing was 1290 kg (2850 lbm). Stiffness design modifications added another 213 kg (470 lbm) for a total of 1503 kg (3320 lbm) per airplane.

FINAL GROUP MASS STATEMENT

Table 21 shows the Model 969-512B group mass statements for Task I and Task II and the mass increments.

The 726 kg (1600 lbm) increase in wing mass is the net change resulting from the ten cycles of analysis necessary for strength design and flutter prevention. This mass includes 822 kg (1812 lbm) reduction due to structural resizing for strength, and 1548 kg (3412 lbm) increase for the final modifications to satisfy flutter criteria.

The 316 kg (850 lbm) wing-mounted vertical tail mass increase includes 172 kg (380 lbm) for strength design and 213 kg (470 lbm) for the final stiffness modification for flutter.

As described earlier, a study was conducted to determine the fuel temperature rise during supersonic cruise on the Model 969-512B. This study indicated a minimum requirement of 694 kg (1530 lbm) of fuel tank insulation is required to keep the fuel temperature below the 344 K (160° F) limit. This is 327 kg (720 lbm) over the 367 kg (810 lbm) allowance in the initial mass estimate.

TABLE 24.–MASS CHANGES FOR FLUTTER

Structural component	Modification number								
	(1)[a] kg (lbm)	(2) kg (lbm)	(3) kg (lbm)	(4) kg (lbm)	(5) kg (lbm)	(6) kg (lbm)	(7) kg (lbm)	(8) kg (lbm)	(9)[b] kg (lbm)
Theoretical cover material	8 830 (19 470)	10 351 (22 820)	11 122 (24 520)	10 946 (24 132)	12 551 (27 670)	11 121 (24 518)	11 121 (24 518)	11 120 (24 514)	11 134 (24 547)
Nonoptimum cover material	2 272 (5 010)								
Theoretical spars	6 280 (13 844)	6 676 (14 718)	7 218 (15 912)	10 630 (23 434)	8 008 (17 655)	7 216 (15 909)	7 214 (15 904)	7 272 (16 031)	7 401 (16 317)
Nonoptimum spar material	938 (2 068)								
Theoretical ribs	1 087 (2 396)	1 219 (2 688)	1 277 (2 816)	1 697 (3 742)	1 378 (3 039)	1 337 (2 947)	1 625 (3 582)	1 633 (3 601)	2 729 (6 016)
Nonoptimum rib material	190 (420)								
Theoretical beams	297 (654)	341 (752)	341 (752)	384 (848)	341 (752)	341 (752)	341 (752)	341 (752)	341 (752)
Nonoptimum beam material	44 (98)								
Total structural element mass	19 958 (44 000)	18 587 (40 978)	19 958 (44 000)	23 657 (52 156)	22 278 (49 116)	20 015 (44 126)	20 301 (44 756)	20 366 (44 898)	21 605 (47 632)
Core	2 694 (5 940)	2 694 (5 940)	2 694 (5 940)	2 694 (5 940)	2 694 (5 940)	2 694 (5 940)	2 694 (5 940)	2 694 (5 940)	2 694 (5 940)
Braze	1 456 (3 210)	1 456 (3 210)	1 456 (3 210)	1 456 (3 210)	1 456 (3 210)	1 456 (3 210)	1 456 (3 210)	1 456 (3 210)	1 456 (3 210)
Landing gear doors	1 860 (4 100)	1 860 (4 100)	1 860 (4 100)	1 860 (4 100)	1 860 (4 100)	1 860 (4 100)	1 860 (4 100)	1 860 (4 100)	1 860 (4 100)
Fairing, fence and miscellaneous	435 (960)	435 (960)	435 (960)	435 (960)	436 (960)	435 (960)	435 (960)	435 (960)	435 (960)
Total wing box (less center section)	26 403 (58 210)	25 032 (55 188)	26 403 (58 210)	30 103 (66 366)	28 723 (63 326)	26 460 (58 336)	26 746 (58 966)	26 811 (59 108)	28 050 (61 842)
Wing center section	3 883 (8 560)	3 883 (8 560)	3 883 (8 560)	3 883 (8 560)	3 883 (8 560)	3 883 (8 560)	3 883 (8 560)	3 883 (8 560)	3 883 (8 560)
Wing leading edge	6 455 (14 230)	6 455 (14 230)	6 455 (14 230)	6 455 (14 230)	6 455 (14 230)	6 455 (14 230)	6 455 (14 230)	6 455 (14 230)	6 455 (14 230)
Wing trailing edge	5 130 (11 310)	5 130 (11 310)	5 130 (11 310)	5 130 (11 310)	5 130 (11 310)	4 736 (10 440)	4 903 (10 810)	4 903 (10 810)	5 048 (11 128)
Total wing structure	41 871 (92 310)	40 500 (89 288)	41 871 (92 310)	45 571 (100 466)	44 191 (97 426)	41 534 (91 566)	41 987 (92 566)	42 052 (92 708)	43 436 (95 760)

[a]Resize with preliminary stiffness

[b]Final stiffness

EFFECTS OF REDESIGN ON AIRPLANE PERFORMANCE

The mission performance of the arrow wing 969-512B configuration with the ATAT-1 engine was updated to reflect the changes in mass, drag, and climb placard which were necessary to satisfy strength, flutter, and thermal requirements. The total range decrement was 250 km (135 nmi), itemized in table 25.

TABLE 25.–STRUCTURAL DESIGN IMPACT ON MISSION RANGE

Change	Equivalent mass, kg (lbm)	Range km (nmi)
OEM	+1438 (+3170)	-109 (-59)
C_D +0.00013	+1275 (+2811)	-96 (-52)
Placard	+588 (+1287)	-44 (-24)
Total	+3301 (+7278)	-250 (-135)

The changes in range due to increased OEAS and drag were obtained from trades previously established and shown in figure 62. The placard change from the original climb speed of 180 m/s (350 kn) to 154 m/s (300 kn) to provide for adequate flutter margin, illustrated in figure 63 by the dotted line, gave a range decrement of 46 km (25 nmi), primarily due to reduced subsonic rate of climb at the reduced placard speed.

The updated performance is compared with the original 969-512B in table 26. The takeoff and approach data are unaltered by the changes.

TABLE 26.–STRUCTURAL DESIGN IMPACT ON PERFORMANCE

- Takeoff gross mass 340 194 kg (750 000 lbm)
- Payload 22 183.8 kg (48 906 lbm); 234 passengers, tourist
- Cruise M = 2.7, standard day

	969-512B, 1% LE rad + LE droop	969-512B update, 1% LE rad + LE droop
Propulsion		
• Type	ATAT-1	ATAT-1
• Airflow, kg/s (lb/s)	287 (633)	287 (633)
• Suppression	Plug and chutes	Plug and chutes
Weights		
• OEM relative to 969-512B kg (lb)	0	+1437 (+3170)
Range		
• Supersonic cruise, km (nmi) range relative to 969-512B	0	217 (–135)
• Supersonic cruise altitude, m (ft)	19 507 (64 000)	19 507 (64 000)
Cruise performance		
• Supersonic range factor, km (nmi) at M = 2.7	15 268 (8239)	15 061 (8113)
• L/D (L/D_{max})	8.29/8.63	8.22/8.53
• SFC, kg/sec/N (lbm/hr/lbf)	0.00004417 (1.559)	0.00004436 (1.566)
Takeoff		
• FAR field length, m (ft) (Std + 15 K)	3780 (12 400)	3780 (12 400)
• Lift-off speed, m/s (KEAS)	101 (197)	101 (197)
• Sideline noise, EPNdB	117	117
• Community noise, 6.49 km (3.5 nmi) from brake release, EPNdB	108	108
Approach		
• Approach speed, m/s (KEAS)	84 (163.5)	84 (163.5)
• Wet FAR field length, m (ft)	3200.4 (10 500)	3200.4 (10 500)
• L/D	4.23	4.23
• Approach noise, 1.85 km (1 nmi) threshold, EPNdB	117.5	117.5

RECOMMENDATIONS

Experience gained from this study has identified a number of problem areas where further work on automated design tools and basic technology is needed. These needs are discussed in the following paragraphs.

FURTHER APPLICATIONS OF THE ARROW WING MODEL

The mathematical model of the arrow wing configuration is a valuable resource that can be used in further studies to evaluate the effect of configuration changes and technology advances on supersonic cruise aircraft and to continue the development of procedures for structural design optimization.

As noted in the description of the flutter analysis, a number of trial-and-error attempts were required to arrive at the modifications for the flutter requirements. These structural variations were based on experience and judgment from the National SST program. The development of formal optimization techniques would not only improve the cycle time required to come up with such structural modifications, but would undoubtedly result in additional weight savings.

A study of finite element modeling criteria would be a valuable contribution to integrated analysis and design methodology. Essential structural details that have important effects on wing flutter speeds of supersonic cruise configurations were identified by analysis and wind tunnel model tests on the National SST program, and these details have been accounted for in this study. However, it has not been possible, within budget and schedule constraints, to determine how rapidly the flutter prediction deteriorates as the finite element model is simplified by decreasing the number of nodes, decreasing the number of structural elements, and thus increasing the size of individual finite elements. Such a study would be valuable for generating preliminary design modeling criteria that relate the fineness of the structural grid to the required quality of mass and aeroelastic predictions.

Design refinements were limited to variations instructural sizing with fixed concepts and materials and a fixed structural arrangement. Because of the mass penalties associated with flutter on the arrow wing configuration, the possibility that significant mass savings could be achieved by variations in structural arrangement should be explored. The ATLAS System provides an appropriate tool for conducting such a study on the arrow wing model. Consideration shoud be given, at least, to variations in rib spacing, spar spacing, and spar direction. A meaningful study would cover the entire aeroelastic cycle, including loads analysis, resizing for strength and flutter, and final mass analysis.

RESEARCH ON PREDICTION OF AERODYNAMIC PRESSURE DISTRIBUTIONS

For typical high aspect ratio configurations at subsonic speeds, methods of incorporating experimental data into the aeroelastic solution for static loads are well developed and

have been substantiated by flight tests. However, for typical low aspect ratio configurations where lifting surface aeroelastic solutions are required, no satisfactory methods of incorporating rigid experimental data into the solution have been developed. Similar uncertainties exist in the prediction of unsteady aerodynamic loads for prediction of flutter characteristics at transonic speeds and/or high angles of attack.

Limited work on these problems has been performed and is described in references 12 and 16. Research should be continued at high priority to develop theoretical and empirical methods for prediction of pressure distributions on complete vehicles, including effects of structural deformations and control displacements, with particular emphasis on the transonic regime.

ADVANCED TITANIUM ALLOYS

There is a definite possibility that new and more efficient titanium alloys will be available within the next five year period with some development effort. Two alloys currently under development, Ti-17 (Ti-5Al-2Sn-2Zr-4Mo-4Cr) and Ti-10V-2Fe-3Al, have the potential of providing 25% higher allowable stresses with the equivalent fracture toughness of Ti-6Al-4V, condition I. The use of these alloys as upper and lower surface cover material for the strength-designed portion of the wing is expected to produce significant weight reductions. In addition, the improvement in allowables would also apply to the strength-sized spar and rib chords. The associated improvement in structural mass of spar and rib chord areas is estimated to be about 650 kg (1400 lbm). The degree to which this mass reduction would be compromised by stiffness requirements related to flutter criteria is uncertain at this time.

During the quality control inspection of titanium extrusions, the tensile modulus of elasticity, E, is routinely checked. Boeing's experience shows that E for extrusions is significantly higher than for sheet and plate material, with the mean value being approximately 120.6 GN/m² (17.5 x 10^6 lb/in²). Maximum values as high as 137.9 GN/m² (20 x 10^6 lb/in²) have been observed. The development and selective use of high modulus titanium in areas requiring extra material for stiffness would reduce the mass increment for added material by about 15%. The higher tensile modulus of elasticity of the spar and rib chords would allow a reduction in the lower surface chord areas when the fail-safe minimums are critical.

Utilization of an advanced titanium alloy as primary structural material is one approach that may be used to achieve significant reductions in structural mass of a supersonic cruise aircraft. Development work on new titanium alloys, and testing to provide data on material properties for the design, should be continued.

FABRICATION TECHNIQUES

Aerodynamic heating has a significant impact on the design of the environmental control system that is used to cool the occupied areas of the airplane as well as the equipment and systems. Fuel is the primary heat sink used to remove heat from the environmental control system. Any improvement in insulating properties of the structure reduces the amount of extra insulation, retains the thermal capacity of the fuel to absorb heat from inside the airplane, and reduces the required capability of the

environmental control system. While titanium itself is a relatively poor conductor of heat, the presence of aluminum braze material in the wing cover panels provides a low resistance path through the sandwich, and increases the effect of aerodynamic heating on fuel temperature.

Boeing has developed a core configuration for use with aluminum-brazed titanium sandwich that eliminates the bridging effect of the aluminum braze alloy, and greatly reduces thermal conductivity. A new process is also being developed that uses diffusion bonding for sandwich panels instead of brazing and shows significant cost savings for manufacturing. The concepts have been demonstrated on laboratory samples, and additional development work is required to scale the process and designs up to full size hardware. It is recommended that sufficient funding be put into these developments to determine the ranges of panel sizes and loads for which the new process and concepts are efficient.

CONCLUDING REMARKS

An in-depth structural design study of an arrow wing supersonic cruise aircraft has been completed utilizing structural materials and concepts that are representative of the 1975 level of technology. The study requirements specified a gross takeoff mass of 340 000 kg (750 000 lbm), a payload of 22 200 kg (49 000 lbm), and a design range of 7800 km (4200 nmi).

The final configuration resulted from trade studies considering propulsion integration, wing-to-fuselage location, and horizontal tail shape and size. Wing twist and camber were optimized to give a maximum lift-to-drag ratio of about 8.6. An advanced-technology afterburning turbojet engine model developed in a previous Boeing study (Contract NAS1-11938) was selected for aircraft propulsion. Although this engine definition was considered satisfactory for the structural study, its performance parameters were not well enough defined to determine the absolute range of the aircraft. A conventional structural arrangement was optimized with respect to fuselage frame spacing and wing spar spacing to provide a near-minimum-mass structure. Sandwich panels with titanium face sheets aluminum brazed to a titanium honeycomb core are used throughout the upper wing surface. The forward, lightly loaded, portion of the wing lower surface and both surfaces of the stiffness-designed wing tip are also aluminum-brazed titanium honeycomb panels. The aft portion of the wing lower surface, which has large tensile loads, is an integrally machined and welded sheet stiffener construction in the wing outboard of the fuselage and an integrally machined waffle construction under the fuselage where large biaxial loads occur. Wing internal structure (spars and ribs) consists of stiffened sheet webs in the heavily loaded aft portion and sine wave webs in the forward portion. Fuselage structure is conventional sheet-stringer construction.

The ATLAS System, an advanced computerized analysis and design system, was used as the primary tool for the detailed structural analysis and design phase of the arrow wing study. Sizing of structural members for strength was accomplished by a combination of manual and automated methods, based on the fully stressed design principle. Deficiencies in wing flutter speed were corrected by an iterative improvement procedure based on prior experience on the National SST program and engineering judgment. The study provides a baseline aircraft design for assessment of current technology and for use in future studies of aerostructural trades, and application of advanced technology such as composite structural materials and active controls.

This design study using a large, complex mathematical model provided an opportunity to appraise the effect of the use of an advanced computerized structural design system on design methods.

The following conclusions have been drawn:

1. An integrated design system should be used in the preliminary design phase of a large supersonic aircraft development progam to reduce manpower and design cycle time and to provide sufficient modeling detail for aeroelastic analysis.

2. Static aeroelastic effects and flutter should be considered as early as possible in the design process so that stiffness-constrained members are identified and not unnecessarily resized for strength.

3. Generation and validation of a complex finite element model is a major item in the structural analysis effort, and the use of automated modeling methods and sophisticated graphics capability is desirable to decrease both manpower expenditure and flow time for this task.

4. Automated resizing for strength is an important factor in reducing design cycle time because the finite element model can be generated more quickly by using unrefined initial estimates of member sizes, and automated resizing during subsequent design cycles is much faster than manual methods.

5. Main fuel tanks should be located in the deeper portions of the wing to reduce the fuel temperatue rise due to aerodynamic heating.

6. Since the mass addition necessary to prevent flutter may be an appreciable fraction of the payload mass, efficient, automated structural optimization for flutter is desirable in computerized design systems.

REFERENCES

1. Robinson, James C.; Yates, E. Carson, Jr.; Turner, M. Jonathan; and Grande Donald L.: *Application of an Advanced Computerized Structural Design System to an Arrow-Wing Supersonic Cruise Aircraft*. AIAA paper 75-1038, August 1975.

2. Boeing Staff: *Study of Structural Design Concepts for an Arrow Wing Supersonic Transport Configuration*. NASA CR-132576-1 and -2, 1976.

3. Boeing Staff: *Mach 2.7 Fixed Wing SST Model 969-336C (SCAT 15F)*. D6A11666-1, The Boeing Company, 1969.

4. Swan, W. C.; and Kehrer, W. T.: "Design Evolution of the Boeing 2707-300 Supersonic Transport; Part I, Configuration Development, Aerodynamics, Propulsion, and Structures; Part II, Aircraft Design Integration and Optimization." Presented at the 43rd Meeting of the Flight Mechanics Panel of AGARD, Florence, Italy, October 1-4, 1974. *AGARD Conference Proceedings No. 147*.

5. Thomas, R. M.; Backman, B. F.; Flood, F. D.; Gray, R. P.; Hansteen, H. B.; Pratt-Barlow, C. R.; and Wahlstrom, S. O.: "Aircraft Strength and Stiffness Design Automation." U.S. – Japan Design Automation Symposium, Tokyo, Japan, August 1975.

6. Dusto, A. R.; Brune, G. W.; Dornfeld, G. M.; Mercer, J. E.; Pilet, S. C.; Rubbert, P. E.; Schwanz, R. C.; Smutny, P.; Tinoco, E. N.; and Weber, J. A.: *A Method for Predicting the Stability Characteristics of an Elastic Airplane, Vol. I – FLEXSTAB Theoretical Description*. NASA CR-114712, 1976.

7. Rowe, W. S.; Winther, B. A.; and Redman, M. C.: *Prediction of Unsteady Aerodynamic Loadings Caused by Trailing Edge Control Surface Motions in Subsonic Compressible Flow – Analysis and Results*. NASA CR-2003, 1972.

8. Ii, J. M.; Borland, C. J.; and Hogley, J. R.: *Prediction of Unsteady Aerodynamic Loadings of Non-Planar Wings and Wing-Tail Configuration in Supersonic Flow*. AFFDL TR-71-108, 1972.

9. Bendavid, D.: "Systematic Comparison of Lumped Weight and Inertia Representations of Arbitrary Structures." *Israel Journal of Technology*, vol. 7, no. 1-2, 1969, pp. 121-133.

10. Pratt, Kermit G.; and Walker, Walter G.: *A Revised Gust-Load Formula and a Re-Evaluation of V-G Data Taken on Civil Transport Airplanes from 1933 to 1950*. NACA Rep. 1206, 1954.

11. Boeing Staff: *Advanced Supersonic Configuration Studies Using Multicycle Engines for Civil Aircraft*. NASA CR-132723, 1975.

12. Manro, Marjorie E.; Manning, Kenneth J. R.; Halstaff, Thomas H.; and Rogers, John T.: *Transonic Pressure Measurements and Comparison of Theory to Experiment for an Arrow Wing Configuration*. NASA CR-2610, 1976.

13. Rubesin, M. W.: *A Modified Analogy for the Compressible Turbulent Boundary Layer on a Flat Plate*. NACA TN 2917, 1953.

14. Boeing Staff: *Study of Advanced Composite Structural Design Concepts for an Arrow Wing Supersonic Cruise Configuration*. NASA CR-145192, 1977.

15. Turner, M. J.; and Grande, D. L.: *Study of Advanced Composite Structural Design Concepts for an Arrow Wing Supersonic Cruise Configuration*. NASA CR-2825, 1978.

16. Manro, Marjorie E.: *Supersonic Pressure Measurements and Comparison of Theory to Experiment for an Arrow Wing Congiguration*. NASA CR-145046, 1976.

Blank Page

Microfilmed From
Best Available Copy

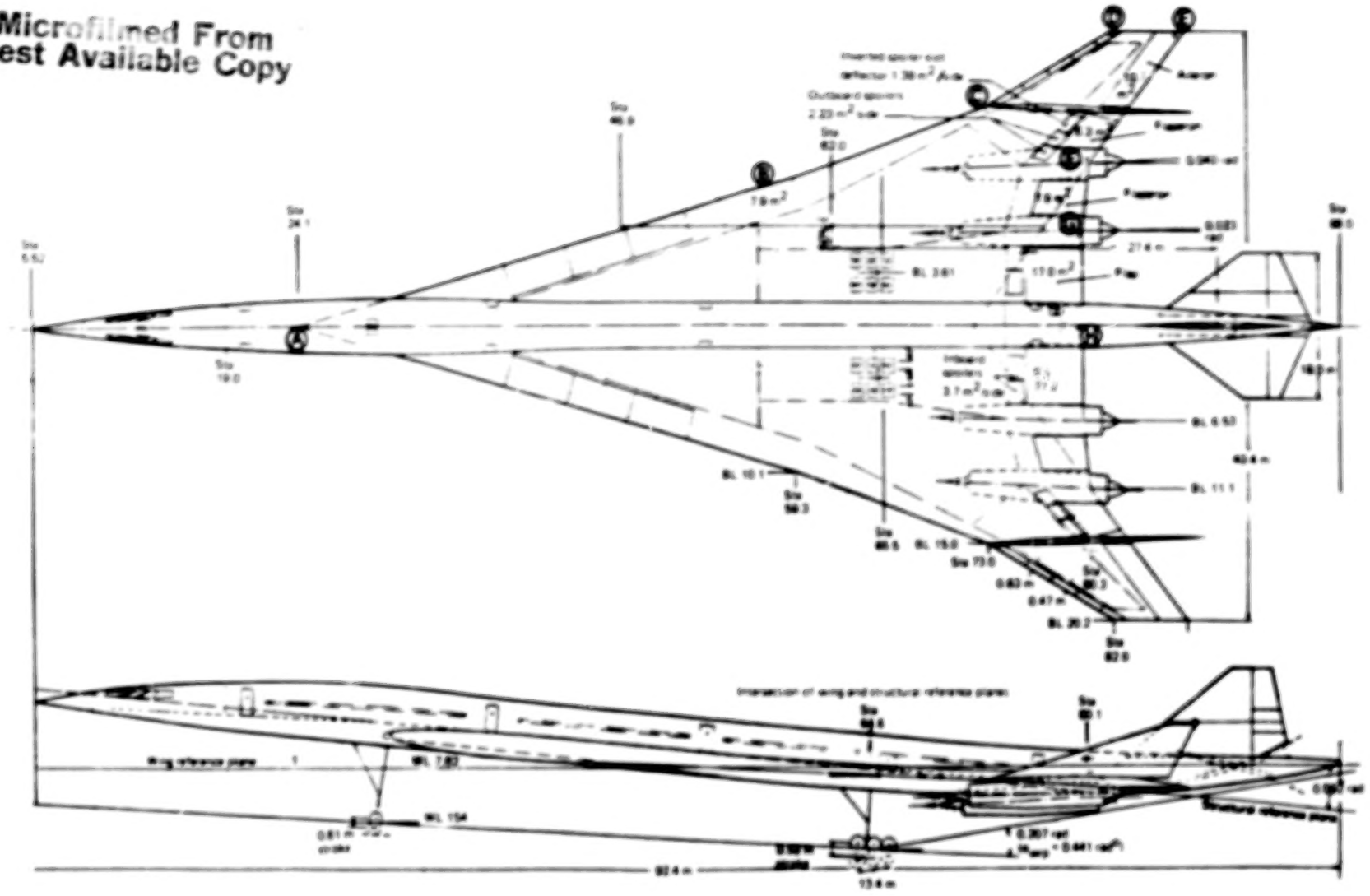

a. SI Units

Figure 1. – Configuration for structural analysis, model 969-512B

Microfilmed From
Best Available Copy

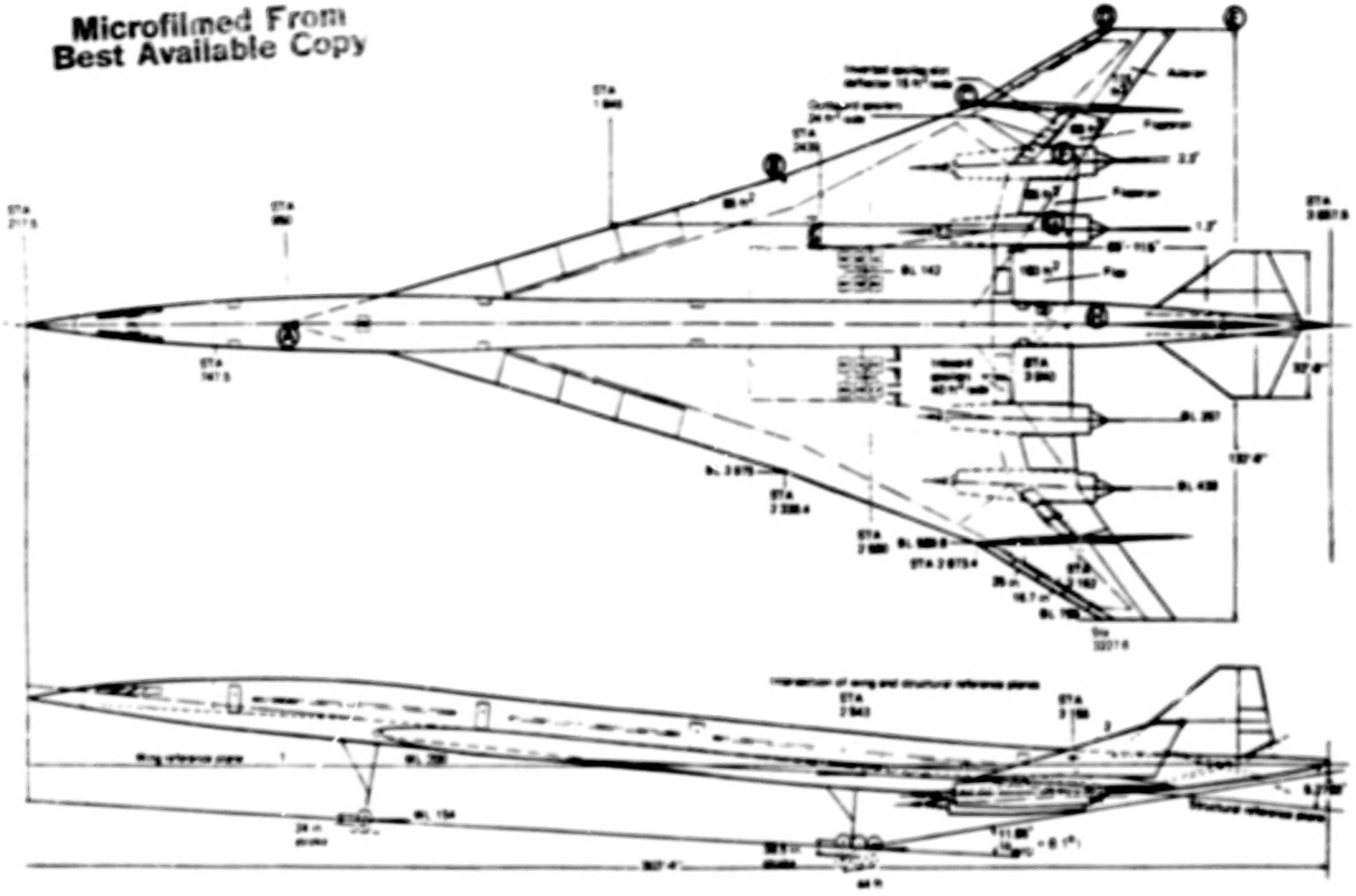

b. U.S. Customary Units

Figure 1. – (Concluded)

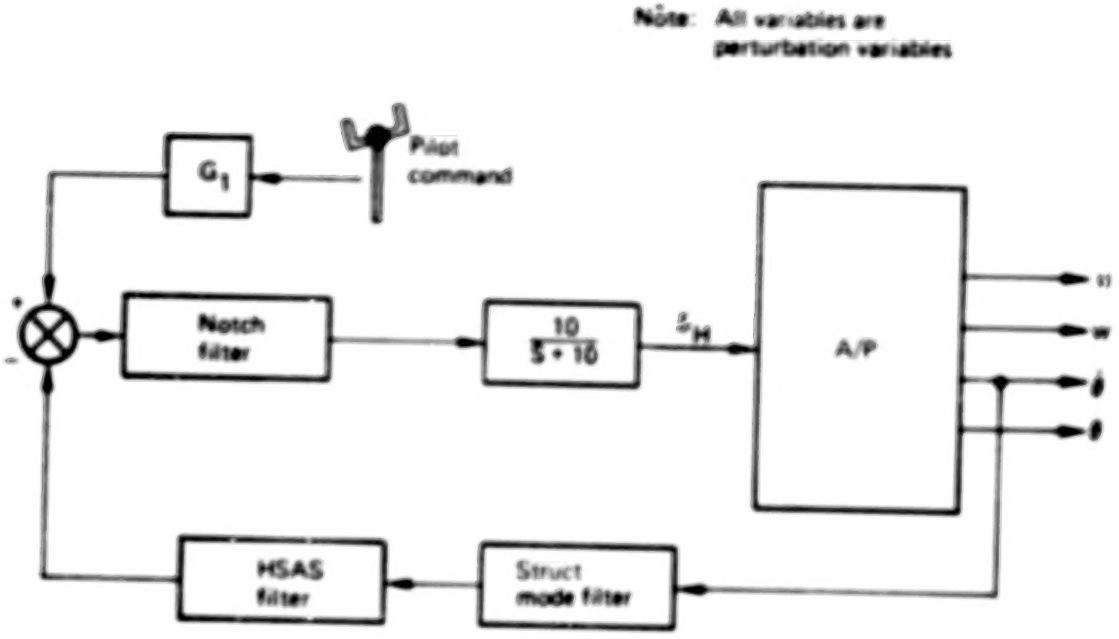

Figure 2. – Longitudinal HSAS functional diagram

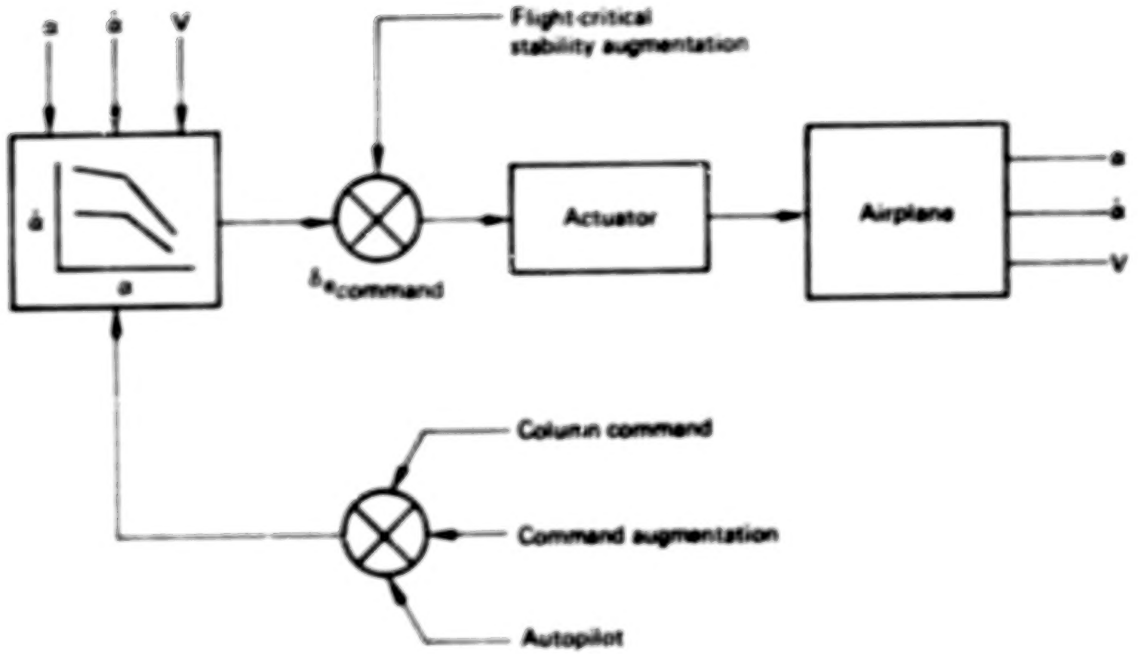

Figure 3. – Alpha limiter functional diagram

CONTENTS

	Page	
SUMMARY	1	1/A9
INTRODUCTION	3	1/A11
SYMBOLS AND ABBREVIATIONS	5	1/A13
CONFIGURATION DEFINITION	12	1/B6
Engine Definition	12	1/B6
969-512B Configuration	12	1/B6
Stability and Control	14	1/B9
Longitudinal Control	14	1/B9
Longitudinal Stability	14	1/B9
Lateral-Directional Stability and Control	16	1/B11
Fuel Tank Arrangements	17	1/B12
STRUCTURAL DESCRIPTION	19	1/B14
Materials Evaluation and Selection	20	1/C1
Metals	20	1/C1
Advanced Composites/Adhesives	20	1/C1
Fuel Tank Sealant	21	1/C2
Fuel Tank Insulation	21	1/C2
Structural Concepts	22	1/C3
Wing Skin Panel Concepts	27	1/C11
Wing Spar Concepts	29	1/C13
Fuselage Panel Concepts	30	1/C14
STRUCTURAL ANALYSIS AND DESIGN	32	1/D2
The Integrated Computer Program System	32	1/D2
The ATLAS System	32	1/D2
FLEXSTAB System	34	1/D4
Flutter Modules	36	1/D6
Analytical Models	36	1/D6
Structural Model	36	1/D6
Structural Model Verification	37	1/D7
Mass Model	38	1/D8
Aerodynamic Model	38	1/D8
Structural Design Loads	38	1/D8
Structural Design Airspeeds	38	1/D8
Design Gross Masses	39	1/D9
Engine Thrust	39	1/D9
Maneuver and Gust Criteria	39	1/D9
Landing, Taxi, and Ground Handling Loads Criteria	41	1/D11
Aerodynamic Loads Analysis	41	1/D11

CONTENTS (Concluded)

	Page
Structural Load Conditions	43 1/D14
Jig Shape	45 1/E2
Thermal Analyses	45 1/E2
Aerodynamic Heating	45 1/E2
Solar Absorptance and Surface Emittance	46 1/E3
Transient Thermal Analysis	46 1/E3
Fuel Temperature Analysis	48 1/E5
Mission Description	48 1/E5
Temperature Limits	49 1/E6
Fuel System	49 1/E6
Fuel Temperature	49 1/E6
Stress Analysis and Strength Sizing	52 1/E10
Flutter Analysis and Resizing	55 1/E13
Flutter Analysis Procedure	55 1/E13
Preliminary Flutter Analysis and Stiffness Resize	55 1/E13
Final Flutter Analysis and Stiffness Redesign	57 1/F1
Mass Analysis	58 1/F2
Wing and Contents	59 1/F3
Correction of Mass Analysis	59 1/F3
Body and Contents	62 1/F6
Empennage and Wing-Mounted Fin	62 1/F6
Fuel	62 1/F6
Wing Box Mass Estimation Method	62 1/F6
Mass Changes Resulting From Redesign for Strength	63 1/F7
Additional Mass Required to Satisfy Flutter Criteria	65 1/F10
Final Group Mass Statement	65 1/F10
EFFECTS OF REDESIGN ON AIRPLANE PERFORMANCE	67 1/F13
RECOMMENDATIONS	69 1/G1
Further Applications of the Arrow Wing Model	69 1/G1
Research on Prediction of Aerodynamic Pressure Distributions	69 1/G1
Advanced Titanium Alloys	70 1/G2
Fabrication Techniques	70 1/G2
CONCLUDING REMARKS	72 1/G4
REFERENCES	74 1/G6

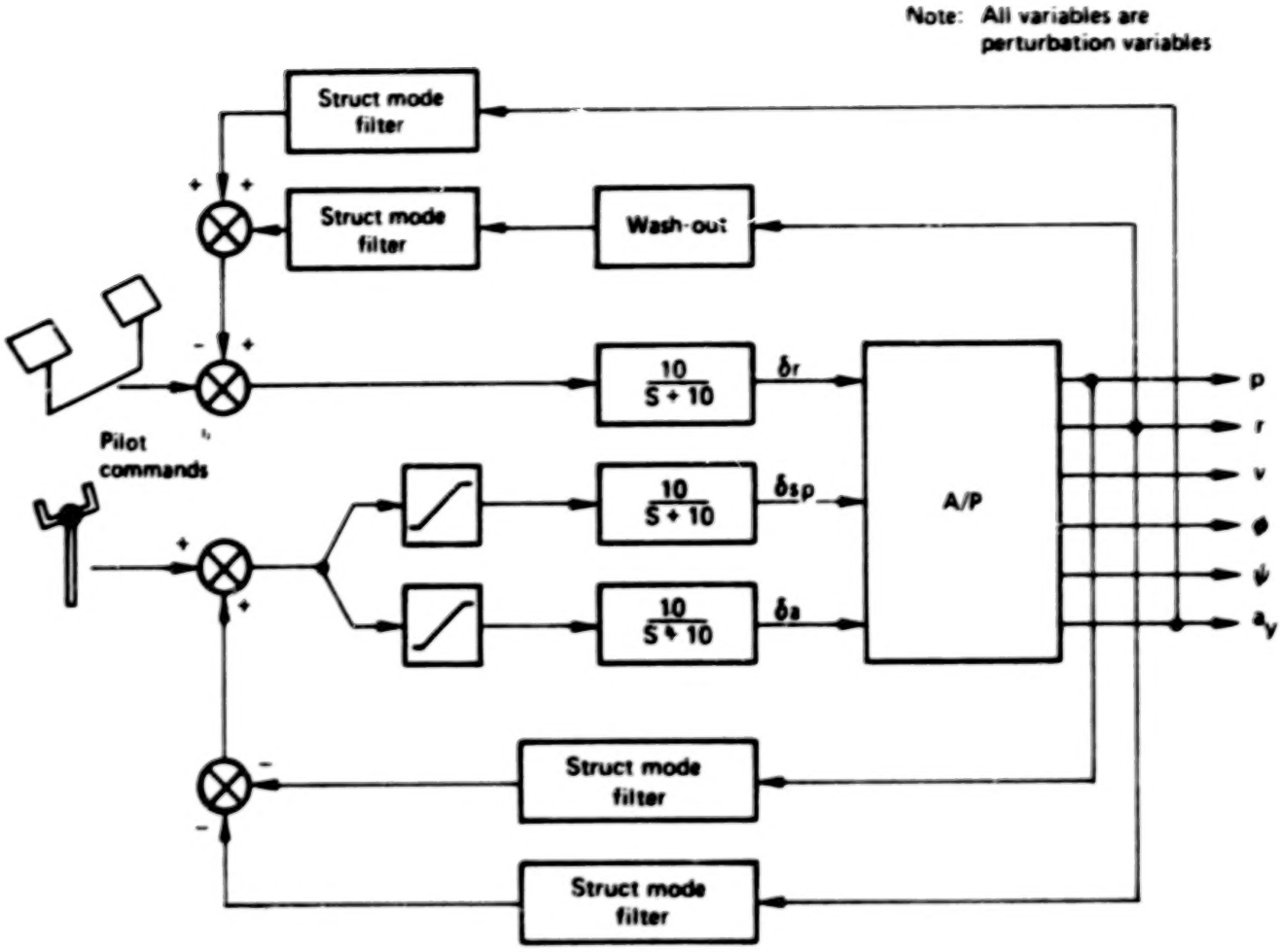

Figure 4. – Lateral – directional HSAS functional diagram

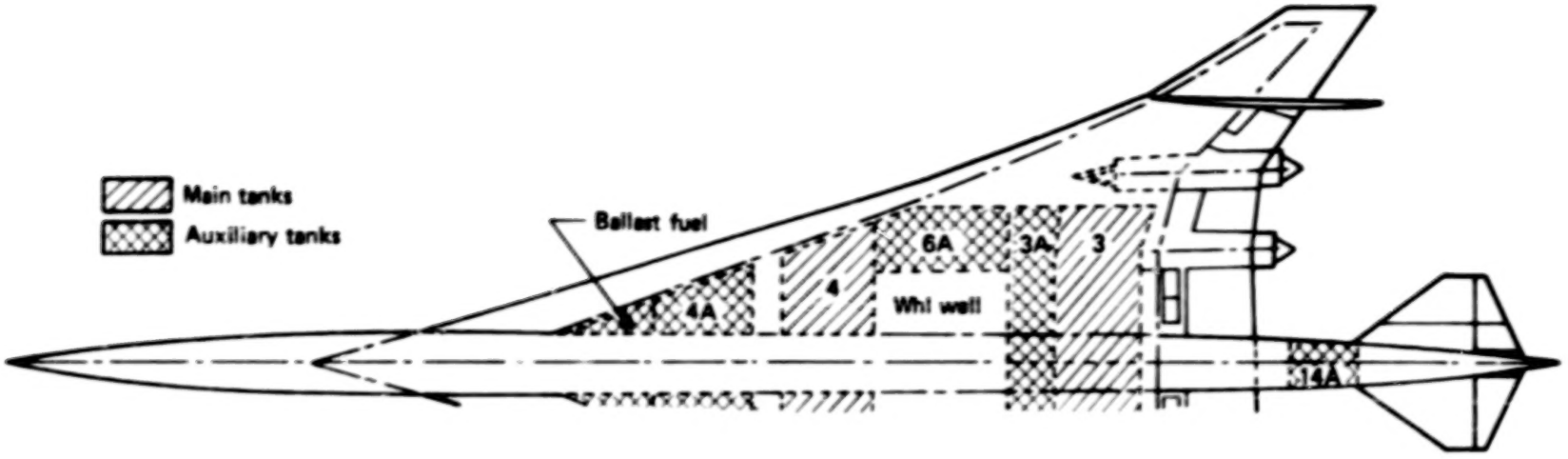

Tank no.		Capacity/airplane		cg body station		Average depth	
Left	Right	kg	lb m	m	in.	m	in.
1	4	45,495	100,300	54.84	2,159	1.10	43.3
2	3	45,450	100,200	70.59	2,779	0.73	28.7
1A	4A	28,894	63,700	47.85	1,884	1.21	47.6
2A	3A	30,481	67,200	66.70	2,626	0.94	37.2
5A	6A	27,805	61,300	61.47	2,420	0.80	31.5
14A		15,059	33,200	84.05	3,309	2.65	104.5
Ballast		13,154	29,000	42.77	1,684	1.27	50.0
Total capacity (excluding ballast)		193,184	425,900	62.80	2,464.6		

Figure 5. – Fuel tank layout, model 969-512B

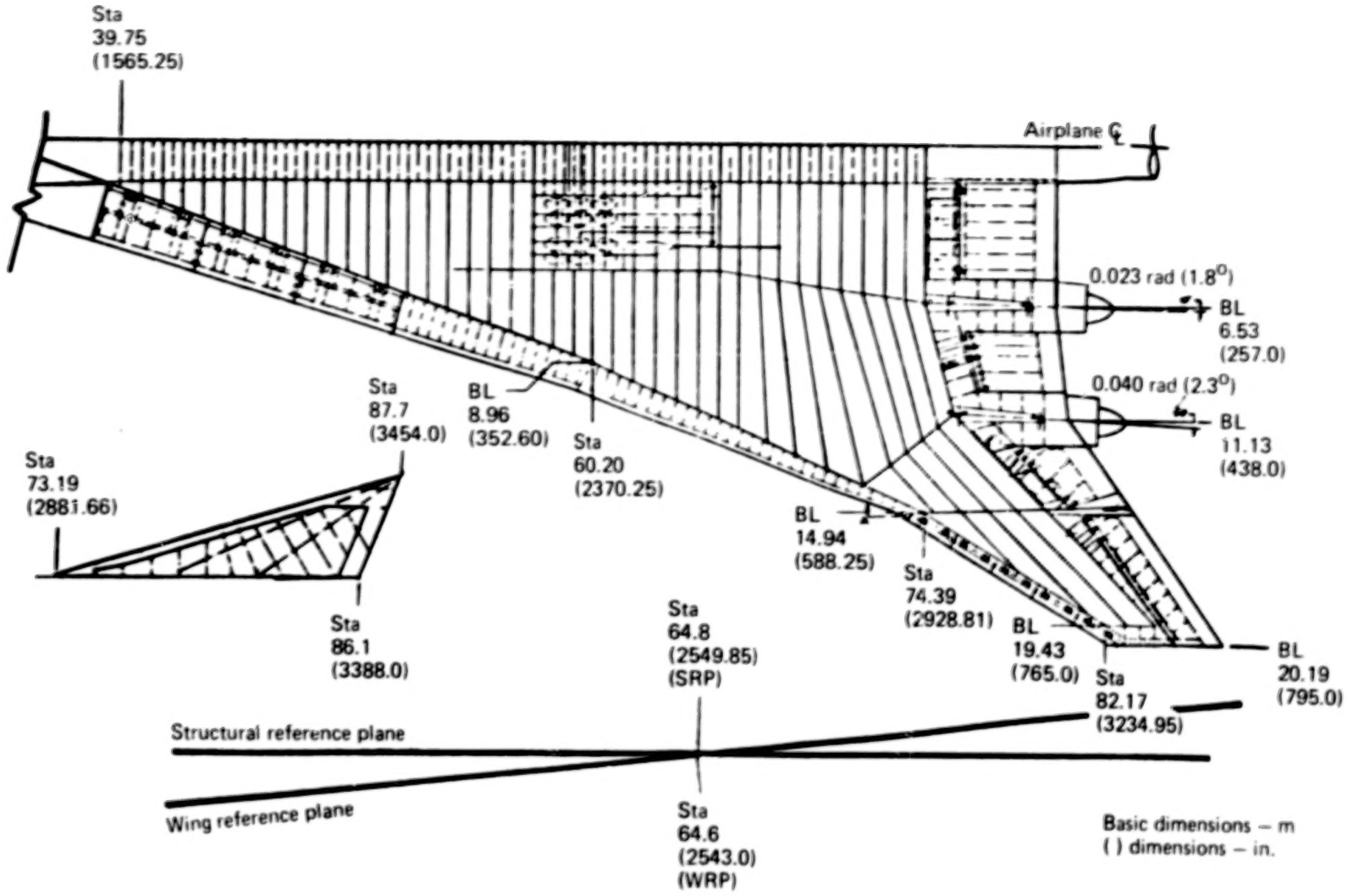

Figure 6. – Wing structural arrangement, model 969-512B

83

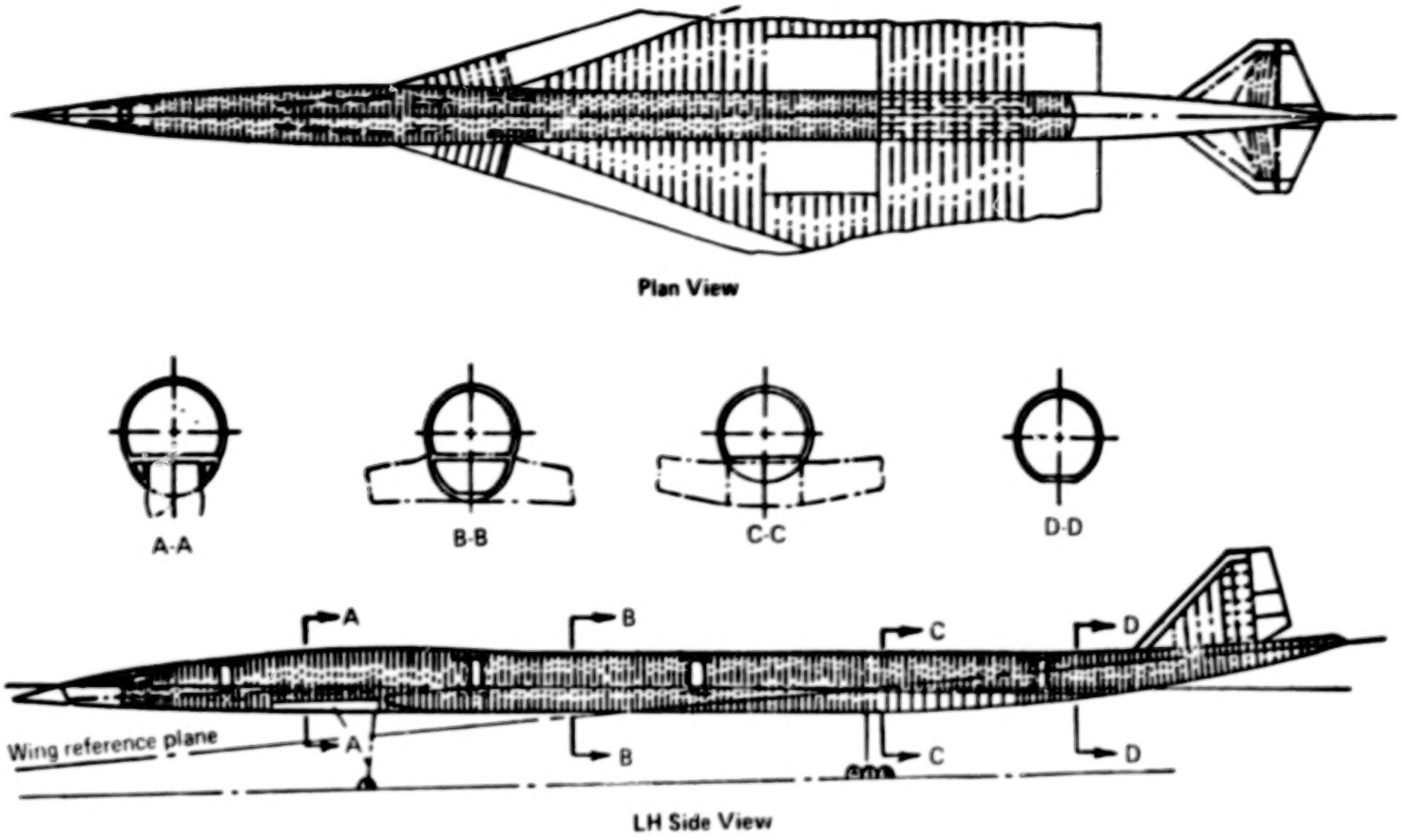

Figure 7. – Body structural arrangement, model 969-512B

Candidate materials	Availability	Environmental effects	Production capability	Cost	Specifications	Selected
Metals						
Titanium						
Ti-6Al-4V	Yes	Yes	Yes	Yes	Yes	Yes
Ti-8Al-1V-1Mo	Yes	No	–	–	–	No
Ti-6Al-6V-2SN	Yes	Yes	Yes	Yes	Yes	Yes
Steel						
Ph 15-7 Mo	Yes	Yes	Yes	Yes	Yes	Yes
15-5 Ph	Yes	Yes	Yes	Yes	Yes	Yes
Custom 455	Yes	Yes	Yes	Yes	Yes	Yes
Metal sandwich						
Al brazed Ti	Yes	Yes	Yes	–	Yes	Yes
Stresskin	Yes	Yes	No	–	–	No
Ag brazed steel	Yes	Yes	Yes	No	–	No
Composites						
Bsc/Al	Yes	Yes	No	–	–	No
B/Pi	Yes	–	–	–	–	No
Gr/Pi	Yes	–	–	–	–	No
B/Ep	Yes	No	–	–	–	No
Gr/Ep	Yes	No	–	–	–	No
Sealants						
DC-94-529	Yes	Yes	Yes	Yes	Yes	Yes
DC-94-530	Yes	No	–	–	–	No
Insulations						
Fluorosilicone	Yes	–	–	–	–	Yes
Ti foil envelope	Yes	–	–	–	–	Yes

Figure 8. – Materials selection process, 1975 technology

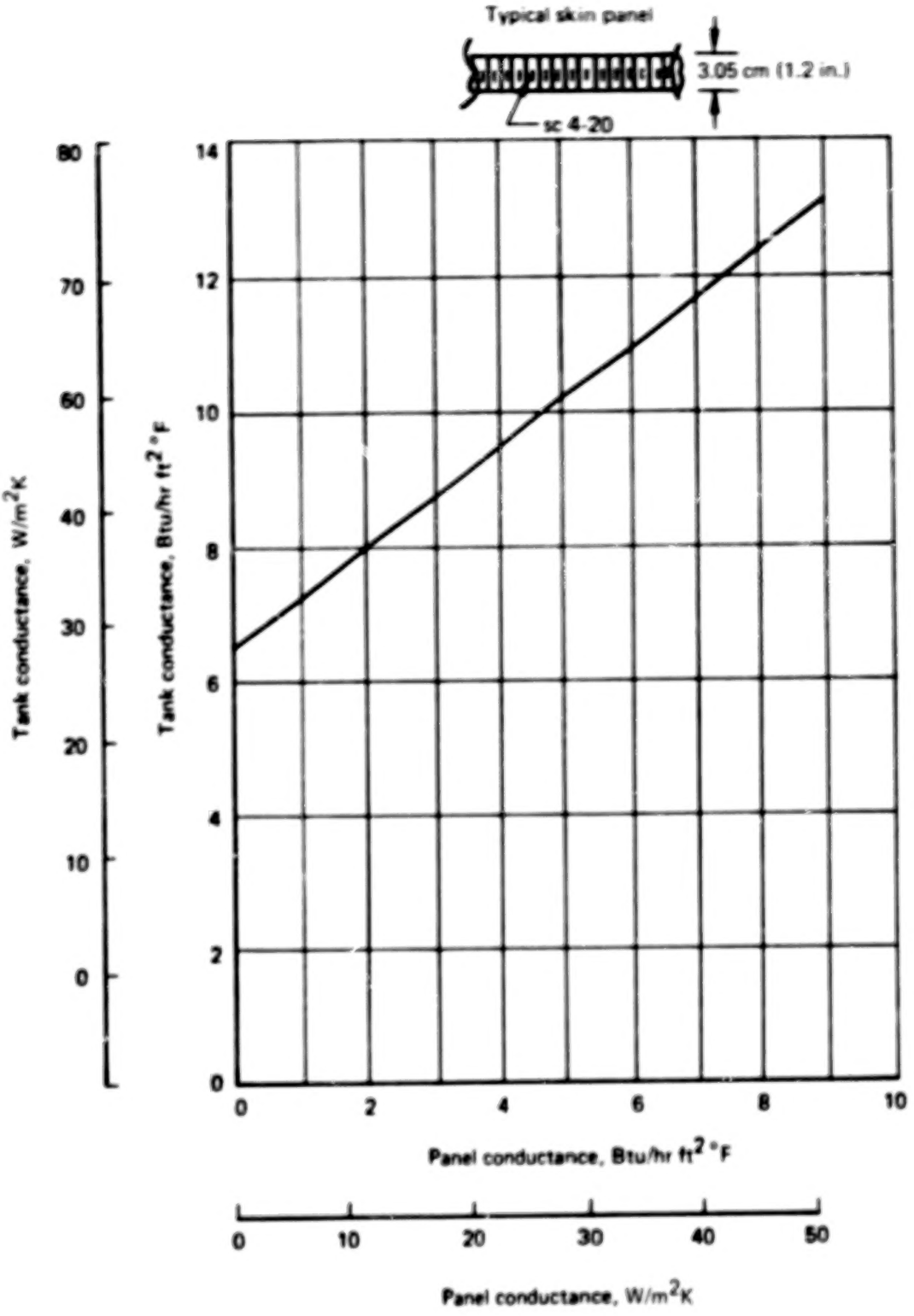

Figure 9. – Panel/tank conductance characteristics

Material	Relative thermal conductivity
Titanium 6Al-4V	1.0
Magnesia	0.35
Pyrolytic graphite	0.26
Pyroceram	0.23
Silica	0.19
Zirconia	0.12
Mica	0.06
Reinforced silicone	0.05
Polytetrafluoroethylene (PTFE)	0.03
Thoria	$\geqslant 0$

Figure 10. – Potential insulating materials

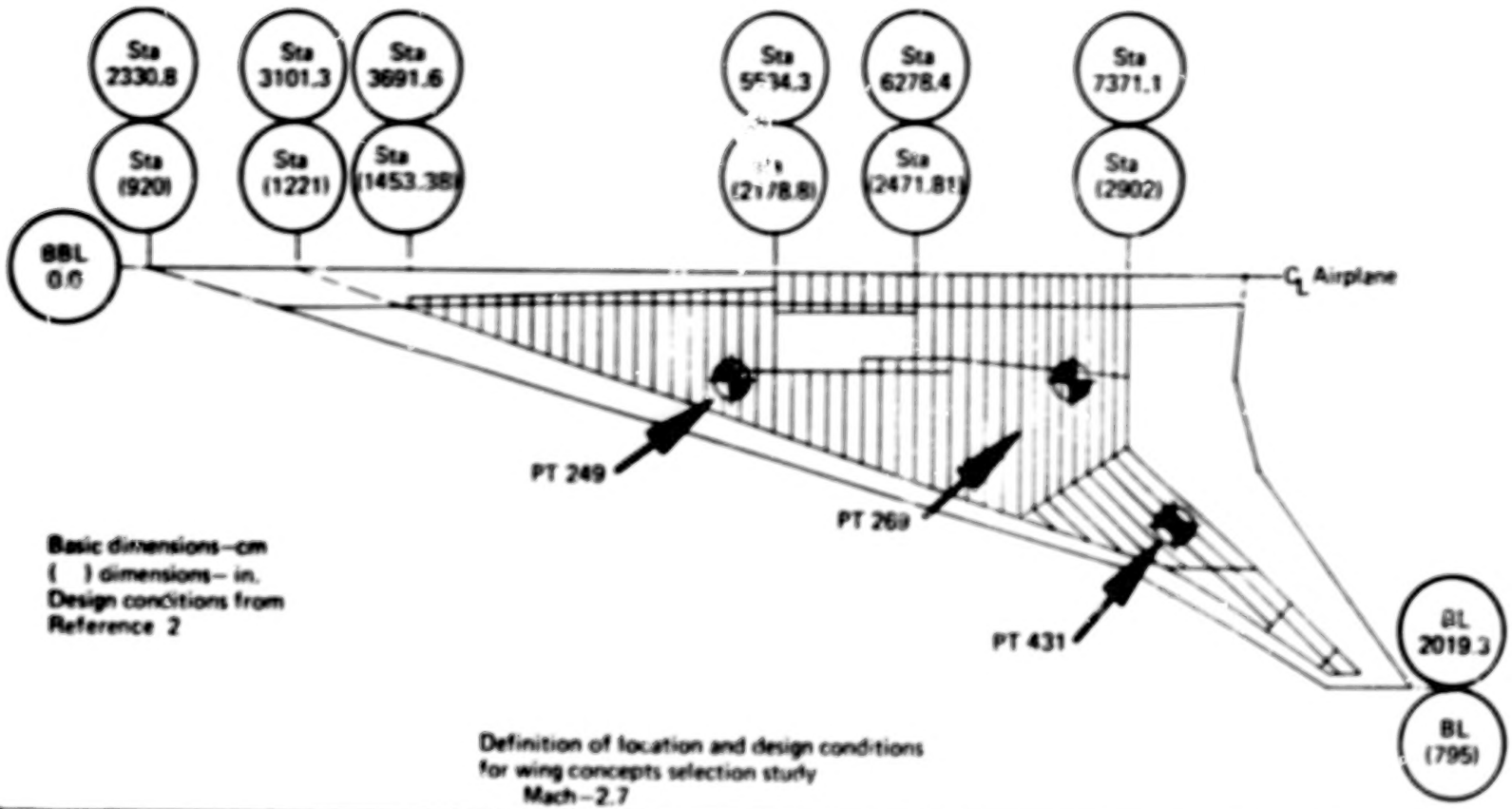

Definition of location and design conditions
for wing concepts selection study
Mach–2.7

Point	Component	Design condition	T °C	T (° F)	N_x kN/m	N_x (kips/in.)	N_y kN/m	N_y (kips/in.)	N_{xy} kN/m	N_{xy} (kips/in.)
249	Upr panel	Refuel overpress	Rt	Rt	–	–	–	–	–	–
249	Lwr panel	Refuel overpress	Rt	Rt	–	–	–	–	–	–
269	Upr panel	Trans descr (1.2-3)	121± 15°	250± 15°	-1908	-10.9	-259	-1.48	1105	0.32
269	Lwr panel	Trans climb(1.2-1)	Rt	Rt	2070	11.82	357	2.04	1205	6.89
431	Upr panel	Trans climb (1.2-1)	Rt	Rt	-3820	-21.8	-184	-1.05	290	1.66
431	Lwr panel	Trans climb (1.2-1)	Rt	Rt	3820	21.8	184	1.05	290	1.66

Figure 11. – Wing structural control panel locations and design conditions

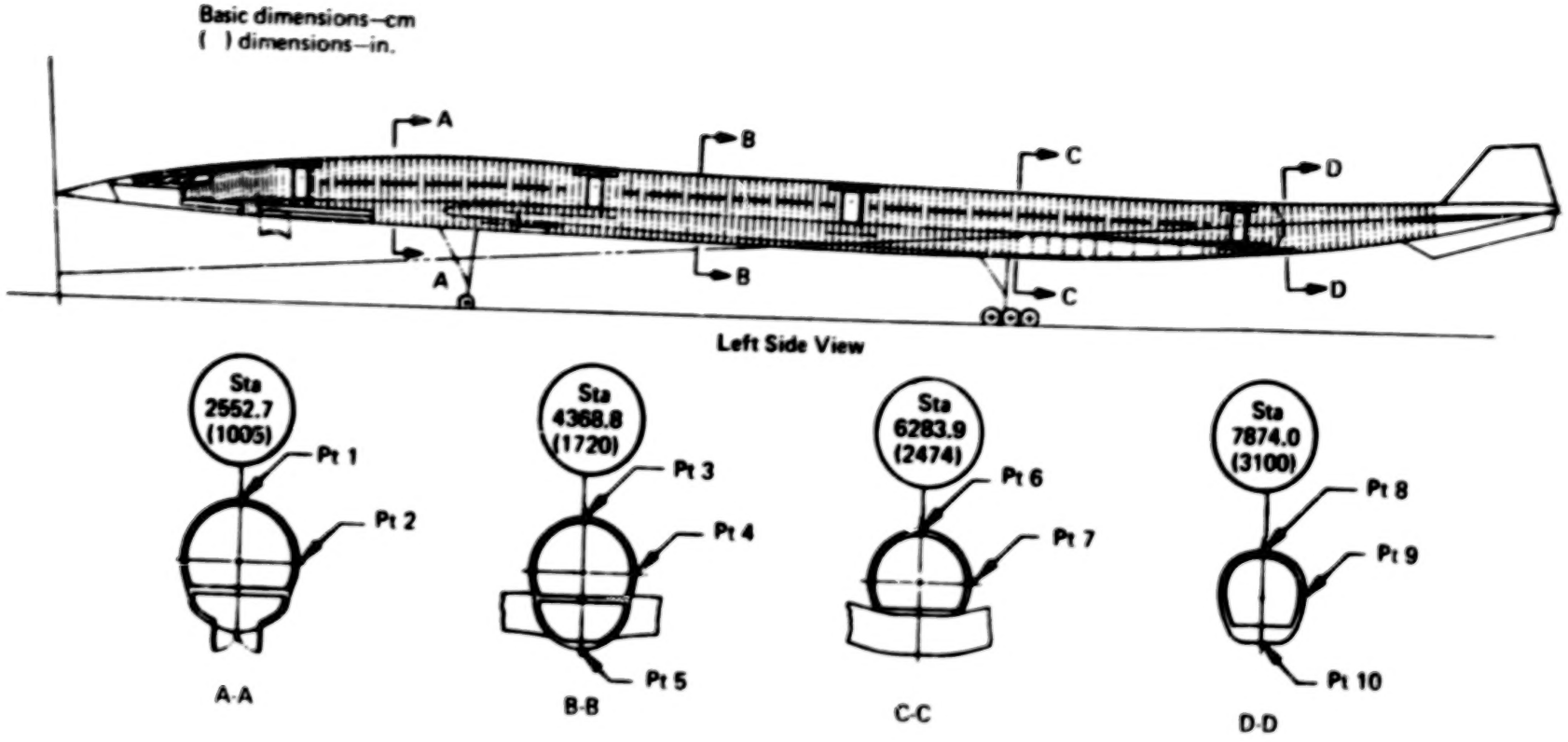

Figure 12. – Body control panel locations

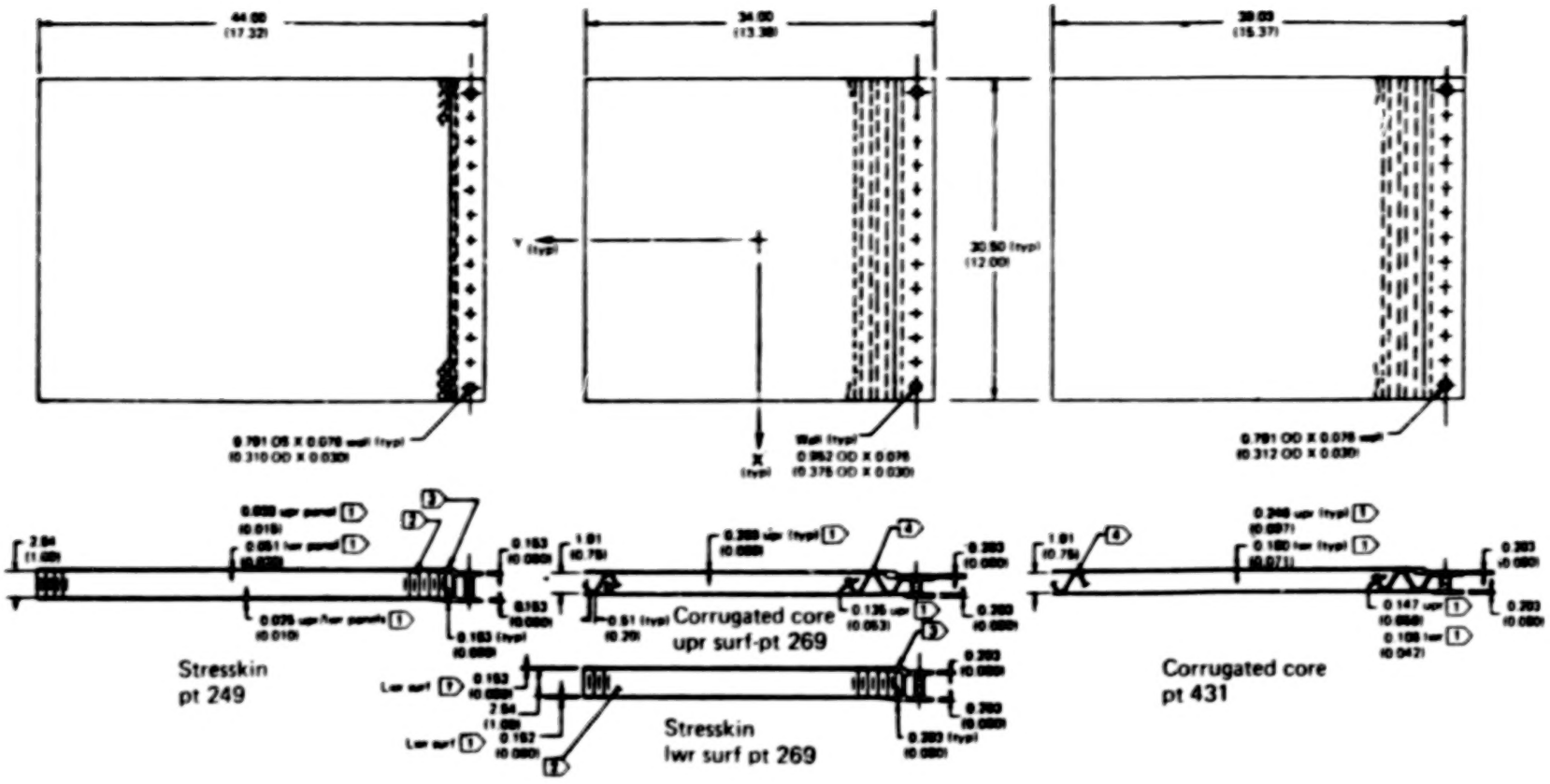

See figure 11 for panel locations
Basic dimensions—cm
( ) dimensions—in.

4 Spotweld
3 Electron beam weld
2 83.29 kg/m^3 (5.2 pcf)·Ti-3Al-2.5V
1 Ti-6Al-4V Cond I

Figure 13. – Wing baseline skin panels

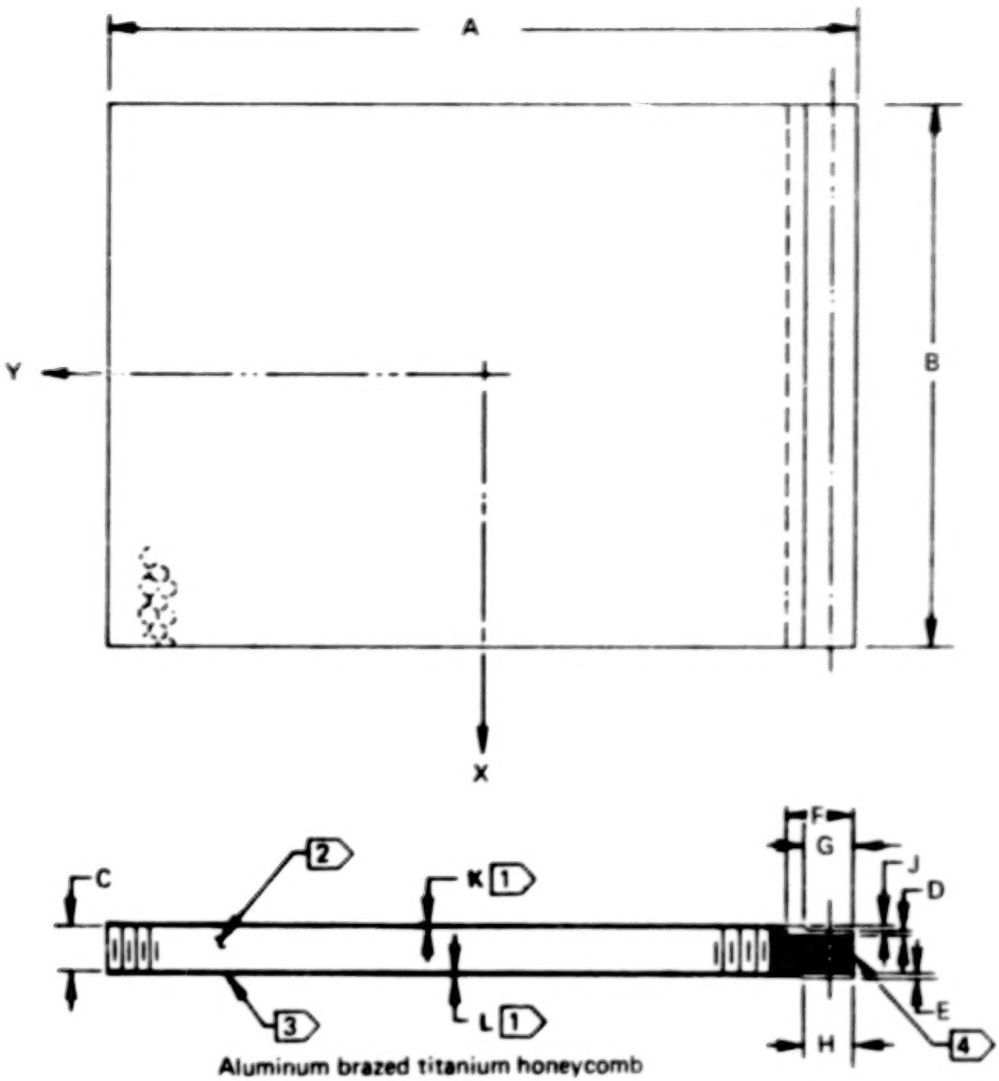

Aluminum brazed titanium honeycomb

See figure 11 for panel point locations

Basic dimensions—cm

( ) dimensions—in.

4 **464.9 kg/m^3** (29 lbm/ft^3) SS2-60 core Ti-6Al-4V

3 **Braze**

2 **78.50 kg/m^3** (4.9 lbm/ft^3) –SCA-20 core Ti-3Al-2.5V

1 **Ti-6Al-4V Cond I**

Point	A	B	C	D	E	F	G	H	J	K	L	
	44.0	30.5	2.54	0.153	0.153	3.80	2.62	3.05	0.228	0.038 (0.015)	0.025 (0.010)	Upr Surf
249	(17.32)	(12.00)	(1.00)	(0.060)	(0.060)	(1.50)	(1.03)	(1.20)	(0.090)	0.051 (0.020)	0.025 (0.010)	Lwr Surf
	34.00	30.50	2.54	0.221	0.221	4.32	3.05	3.05	0.305	0.221 (0.087)	0.221 (0.087)	Upr Surf
269	(13.38)	(12.00)	(1.00)	(0.087)	(0.087)	(1.70)	(1.20)	(1.20)	(0.120)	0.152 (0.060)	0.152 (0.060)	Lwr Surf
	39.03	30.50	2.54	0.246	0.246	4.32	3.05	3.05	0.305	0.246 (0.097)	0.246 (0.097)	Upr Surf
431	(15.37)	(12.00)	(1.00)	(0.097)	(0.097)	(1.70)	(1.20)	(1.20)	(0.120)	0.224 (0.088)	0.224 (0.088)	Lwr Surf

Figure 14. – Wing skin panel, aluminum, brazed titanium honeycomb

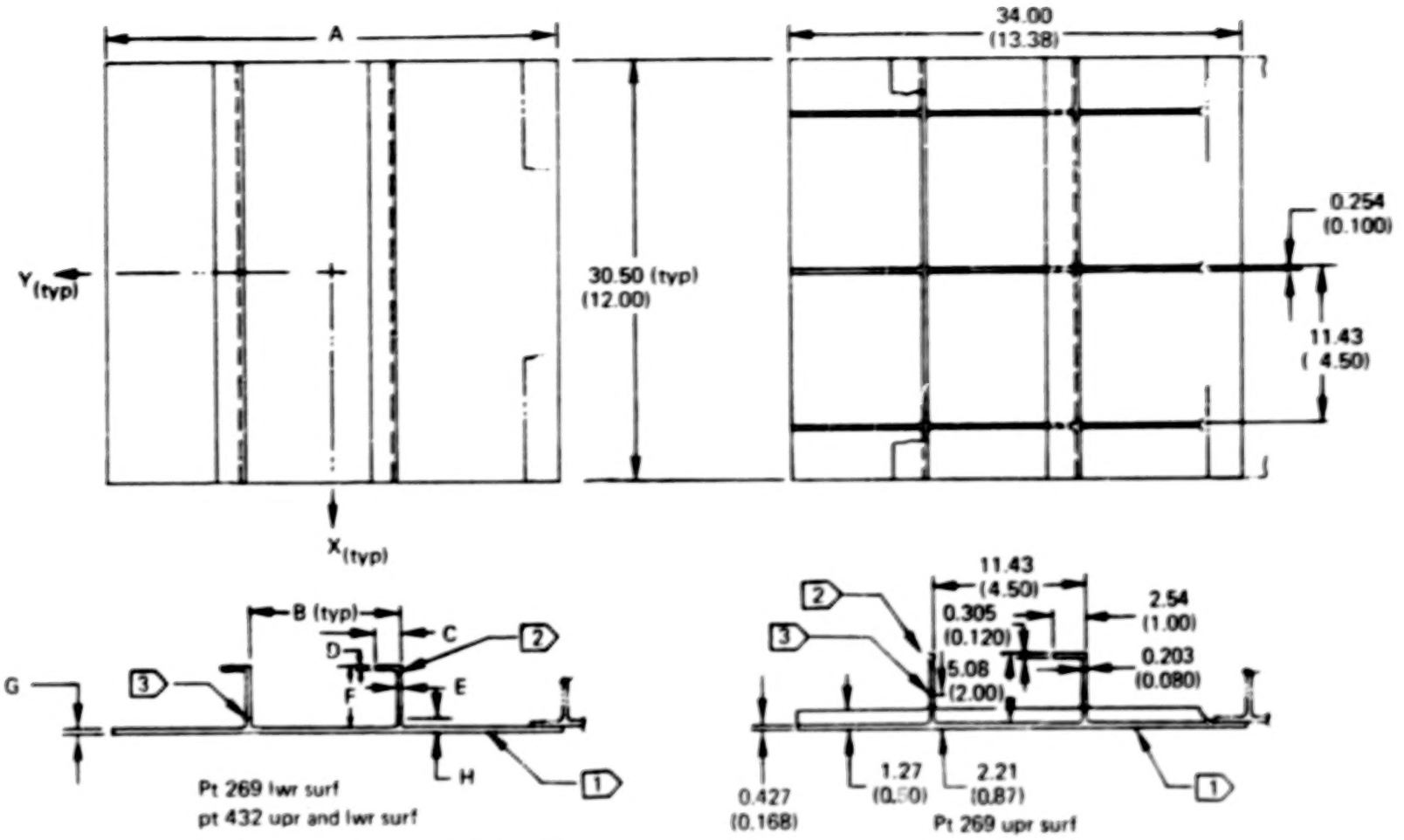

Point	A	B	C	D	E	F	G	H	
249									Upr panel
									Lwr panel
269	34.00 (13.38)	–	–	–	–	–	–	–	Upr panel
		11.43 (4.50)	1.91 (0.75)	0.191 (0.075)	0.178 (0.070)	4.45 (1.75)	0.317 (0.125)	1.232 (0.485)	Lwr panel
431	39.05 (15.37)	14.35 (5.65)	2.54 (1.00)	0.457 (0.180)	0.305 (0.120)	5.08 (2.00)	0.546 (0.215)	1.422 (0.560)	Upr panel
		14.35 (5.65)	2.54 (1.00)	0.356 (0.140)	0.203 (0.080)	4.45 (1.75)	0.394 (0.155)	1.283 (0.505)	Lwr panel

Figure 15. – Wing skin panel, integrally machined and welded – sheet stiffener

92

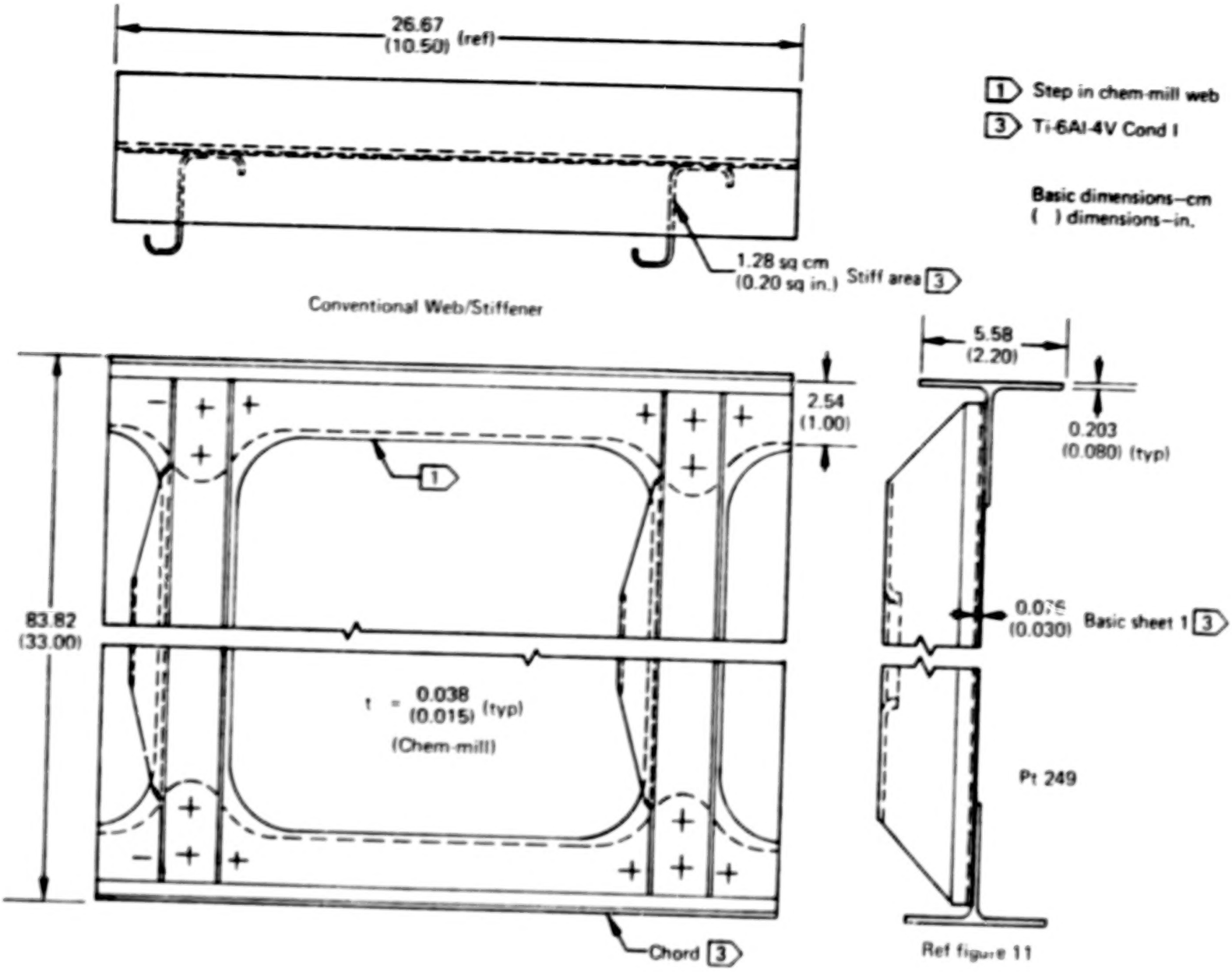

Figure 16. – Wing spar, baseline, PT 249

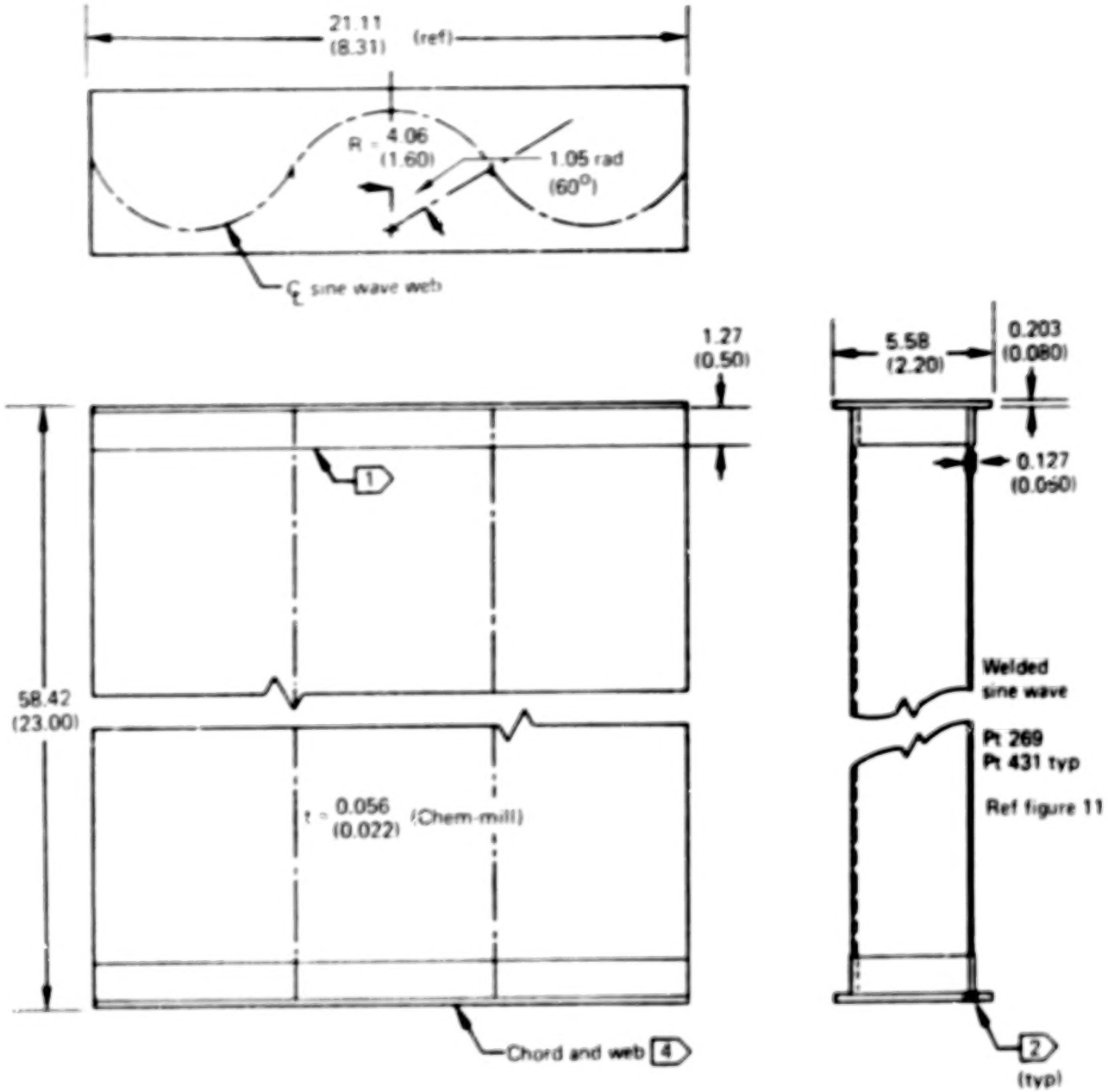

Figure 17. — Wing spar, baseline, PT 269 and 431

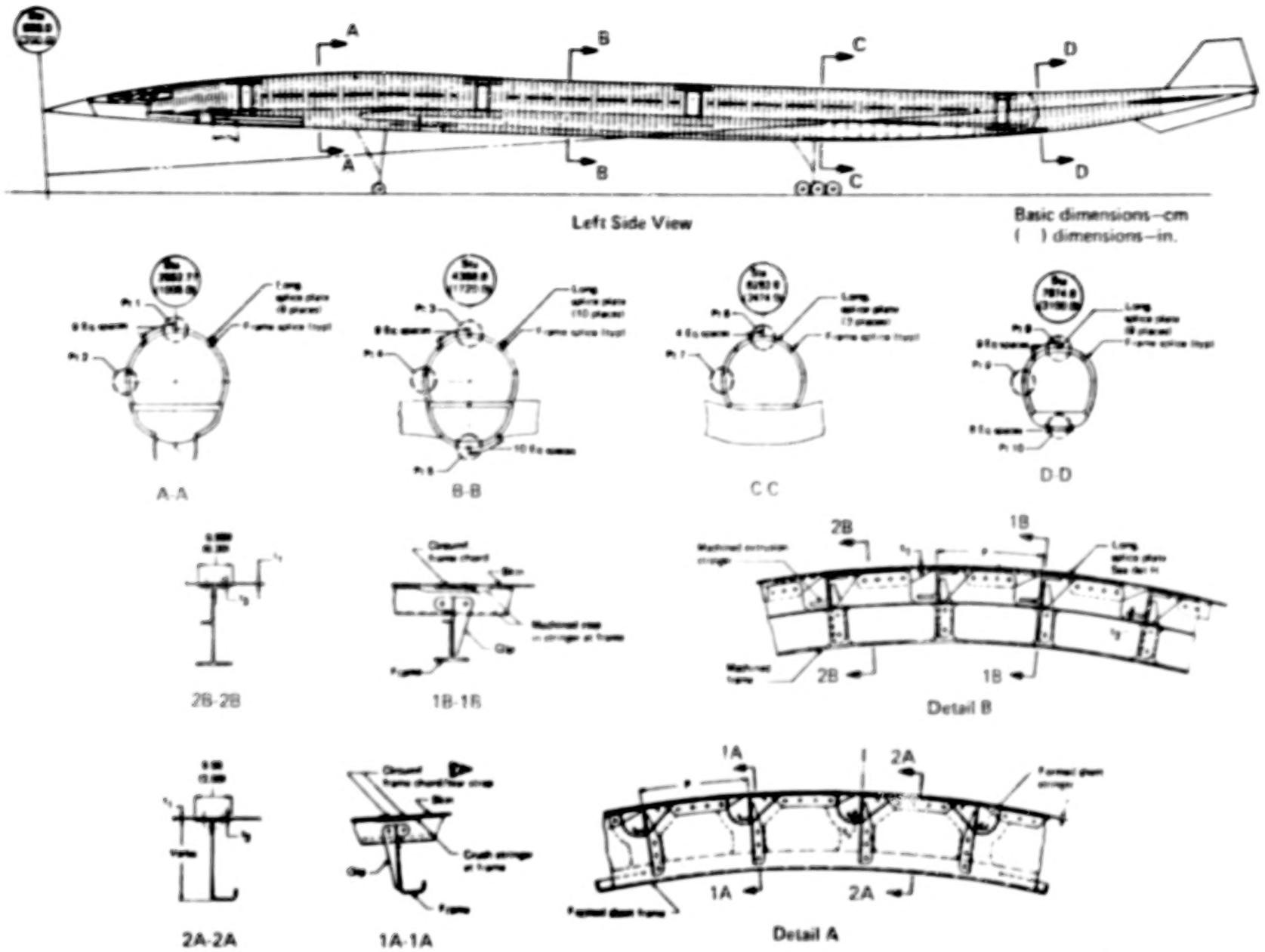

Figure 18. – Body baseline shell arrangement

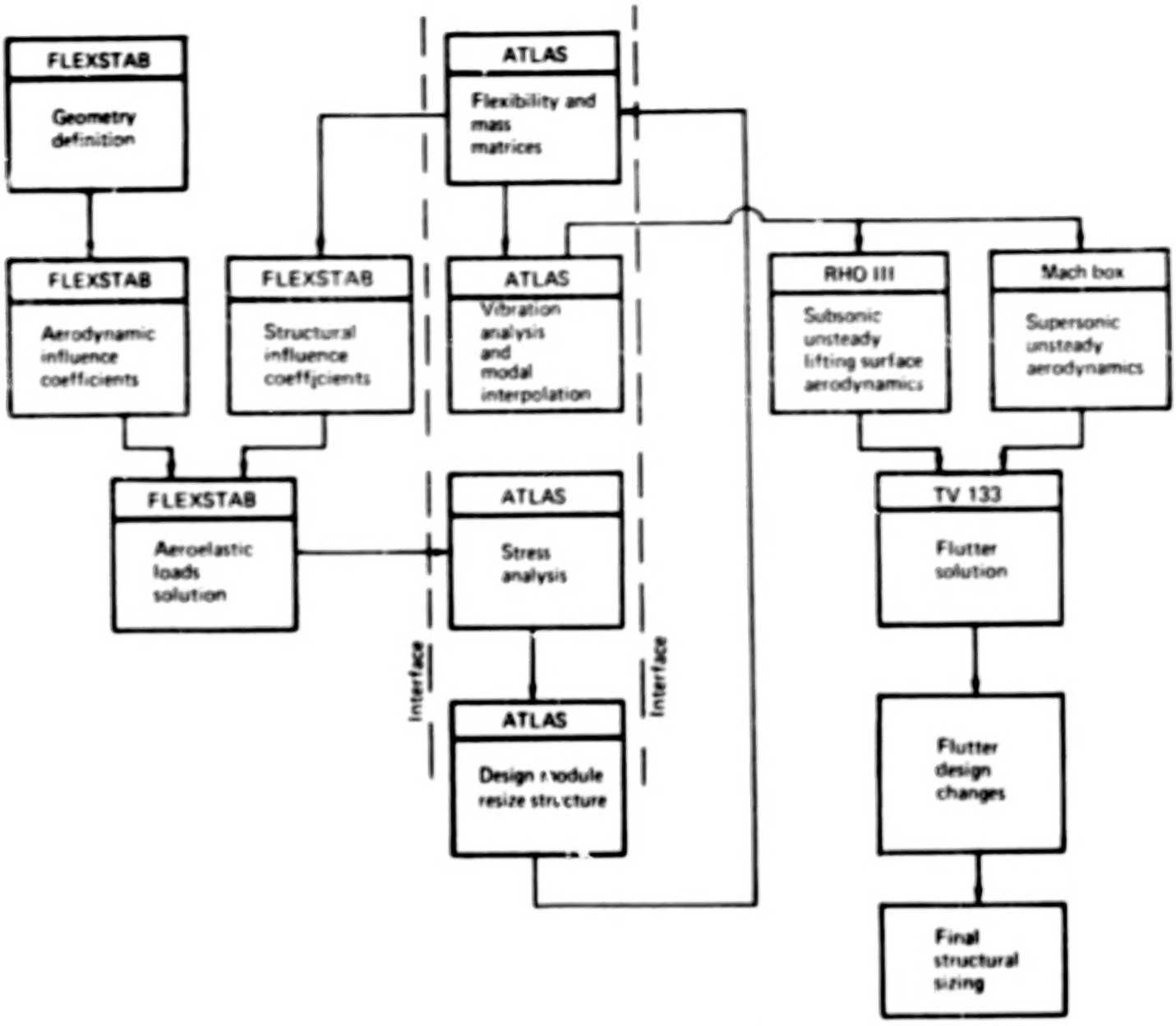

Figure 19. – Structural analysis and design process

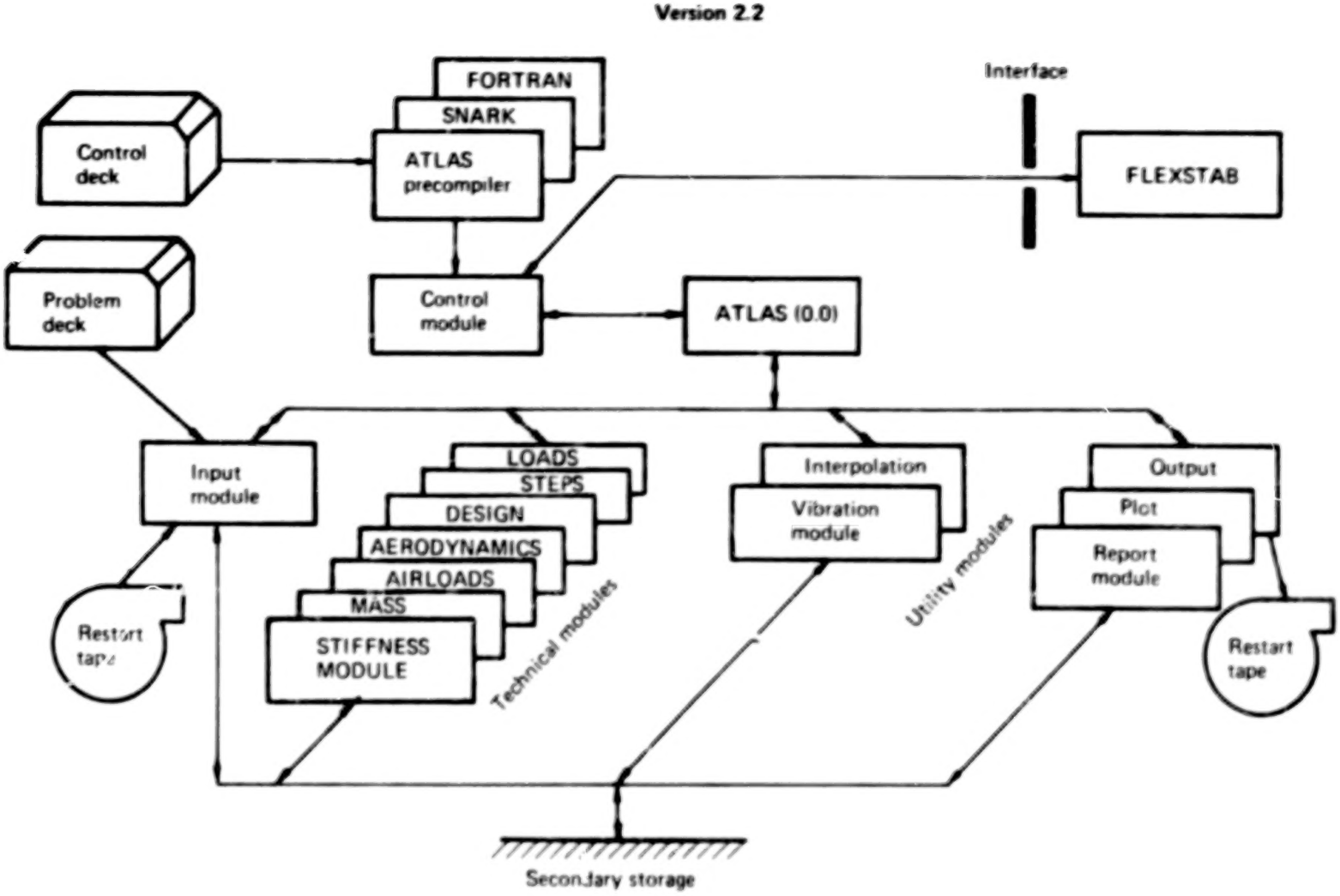

Figure 20. – ATLAS, an integrated structural analysis and design system

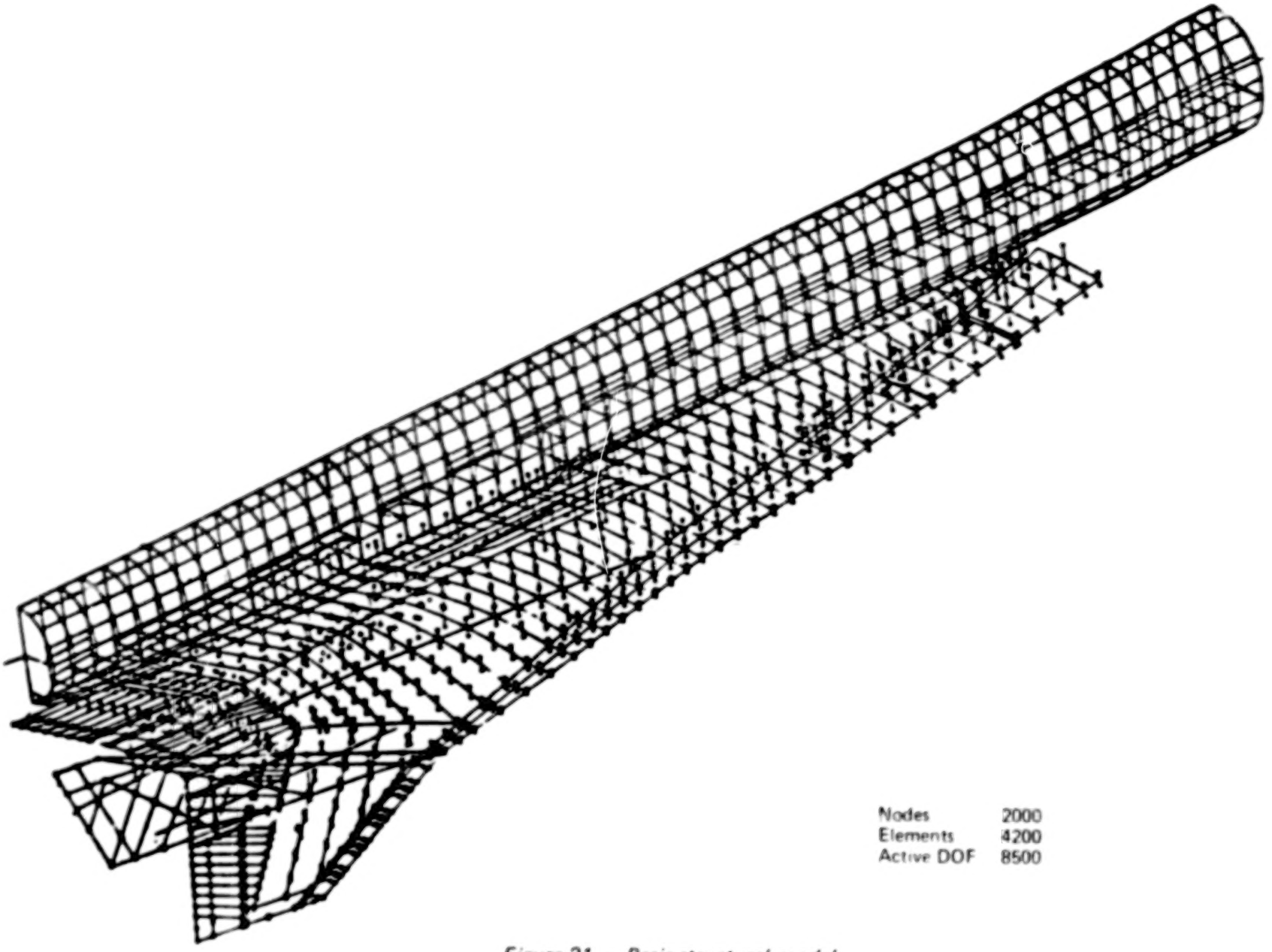

Figure 21. – Basic structural model

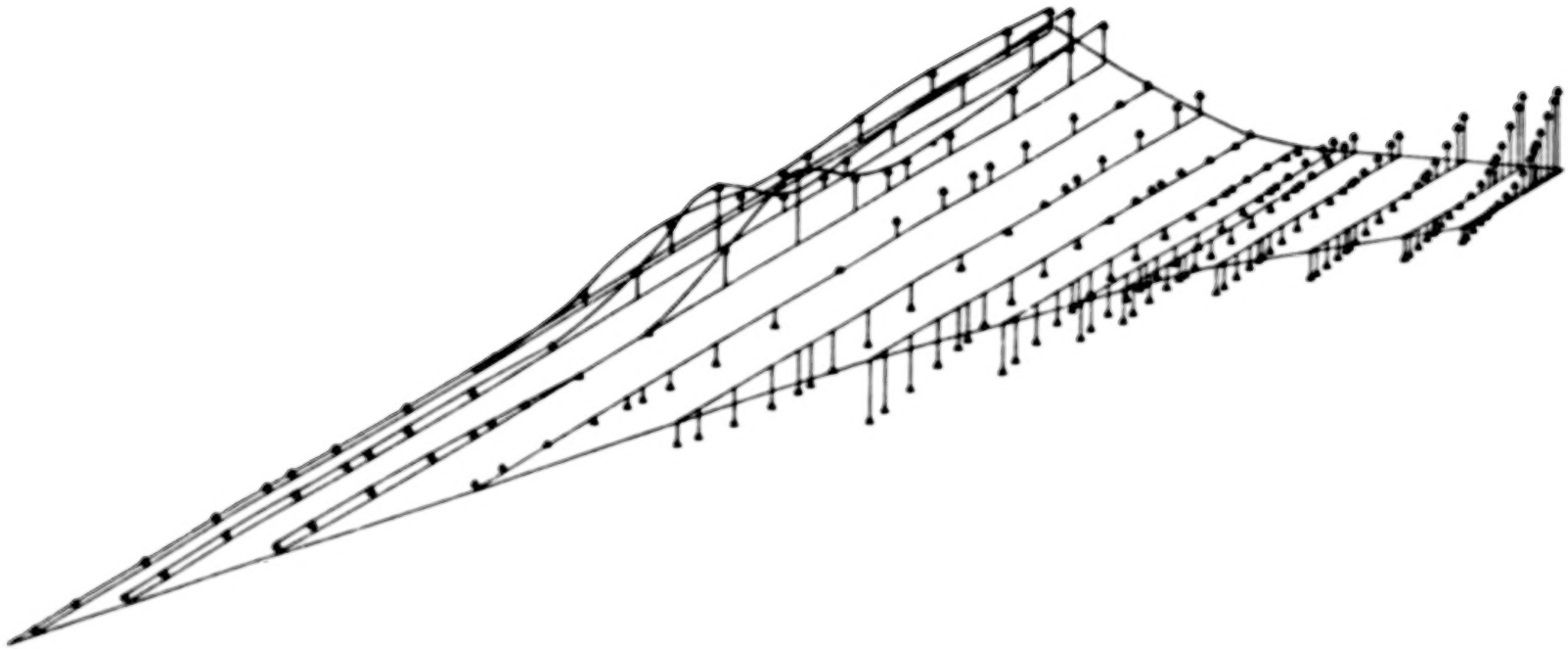

Figure 22. – Resonance of landing gear

Figure 23. — Mass paneling for flutter

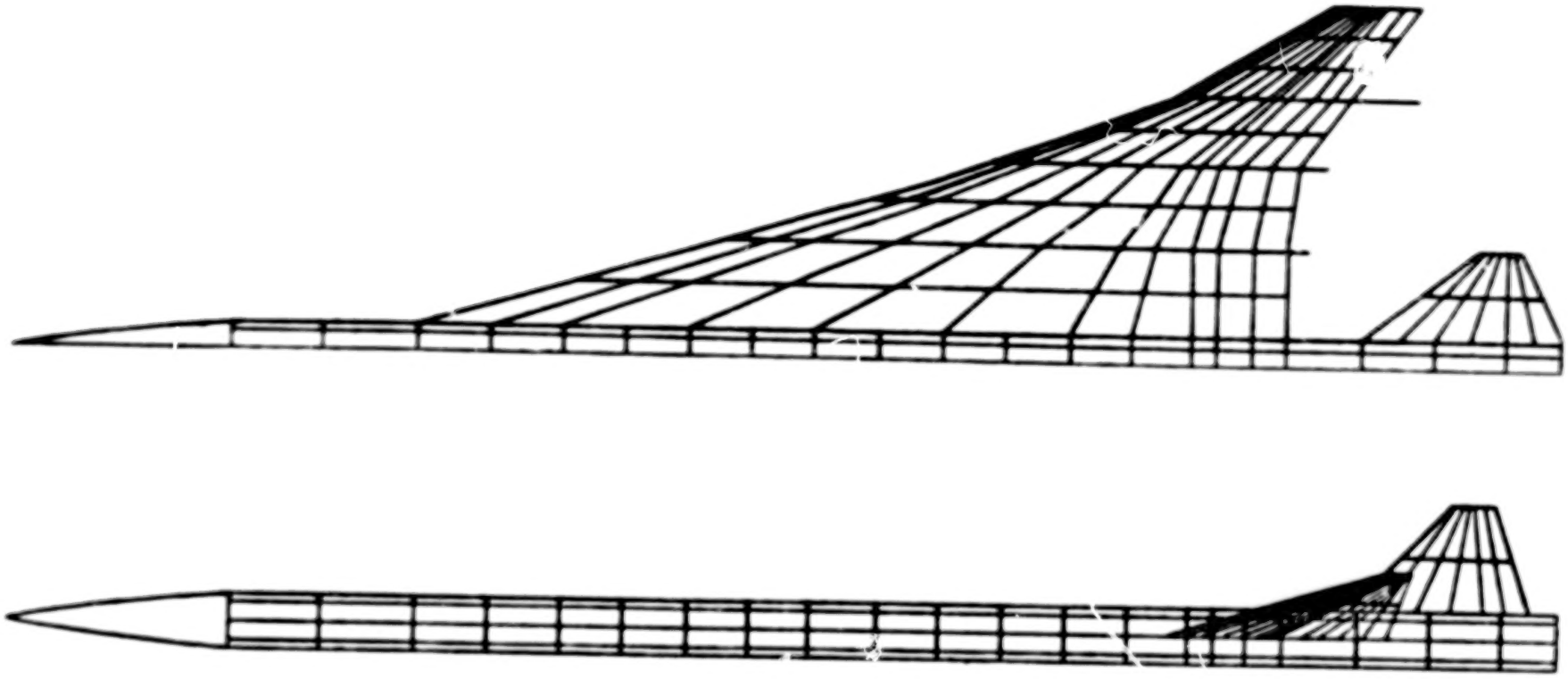

Figure 24. – Aerodynamic paneling for subsonic loads

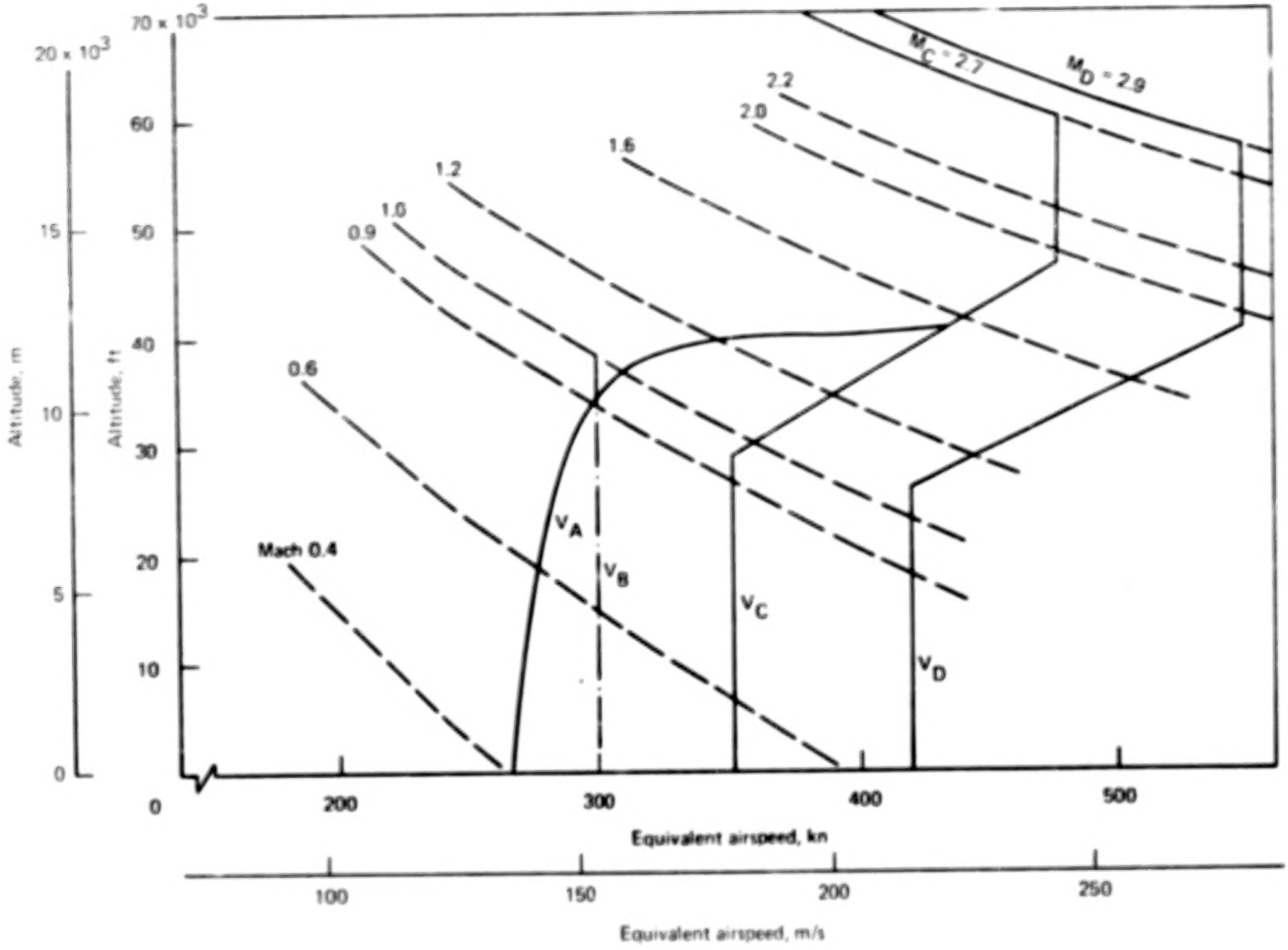

Figure 25. – Design speed-altitude envelope

11.2

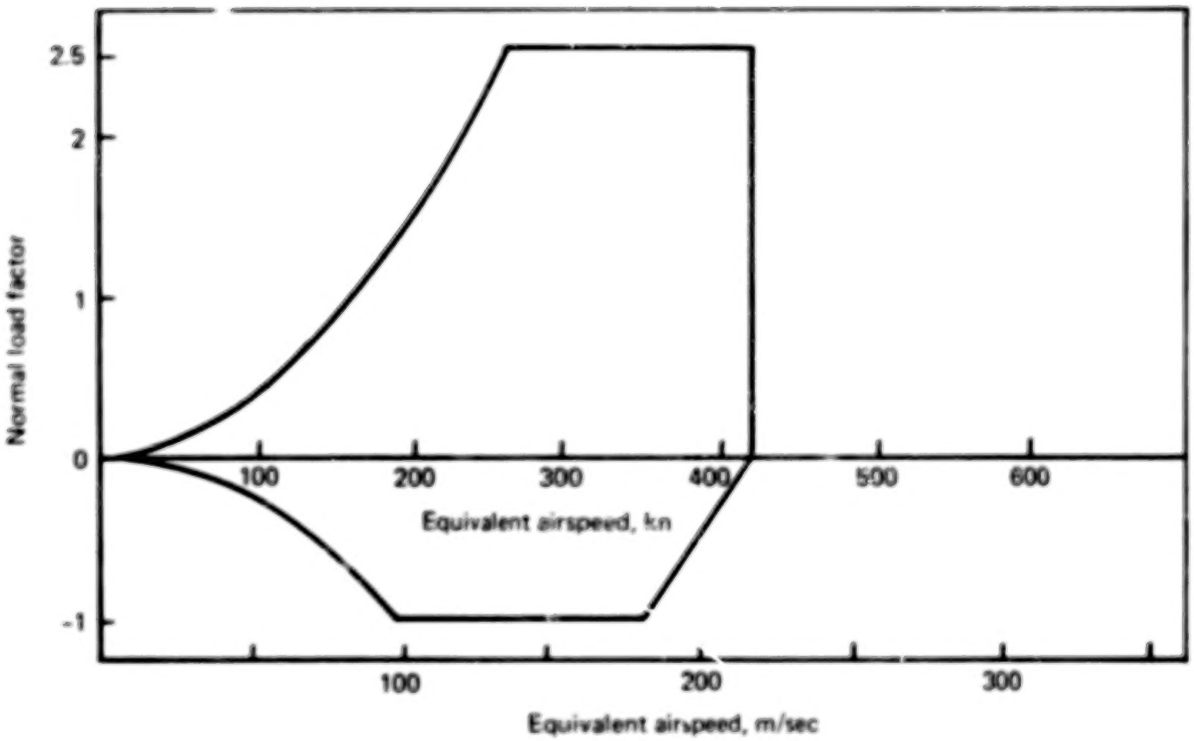

Figure 26. – Maneuver envelope at sea level for maximum flight mass

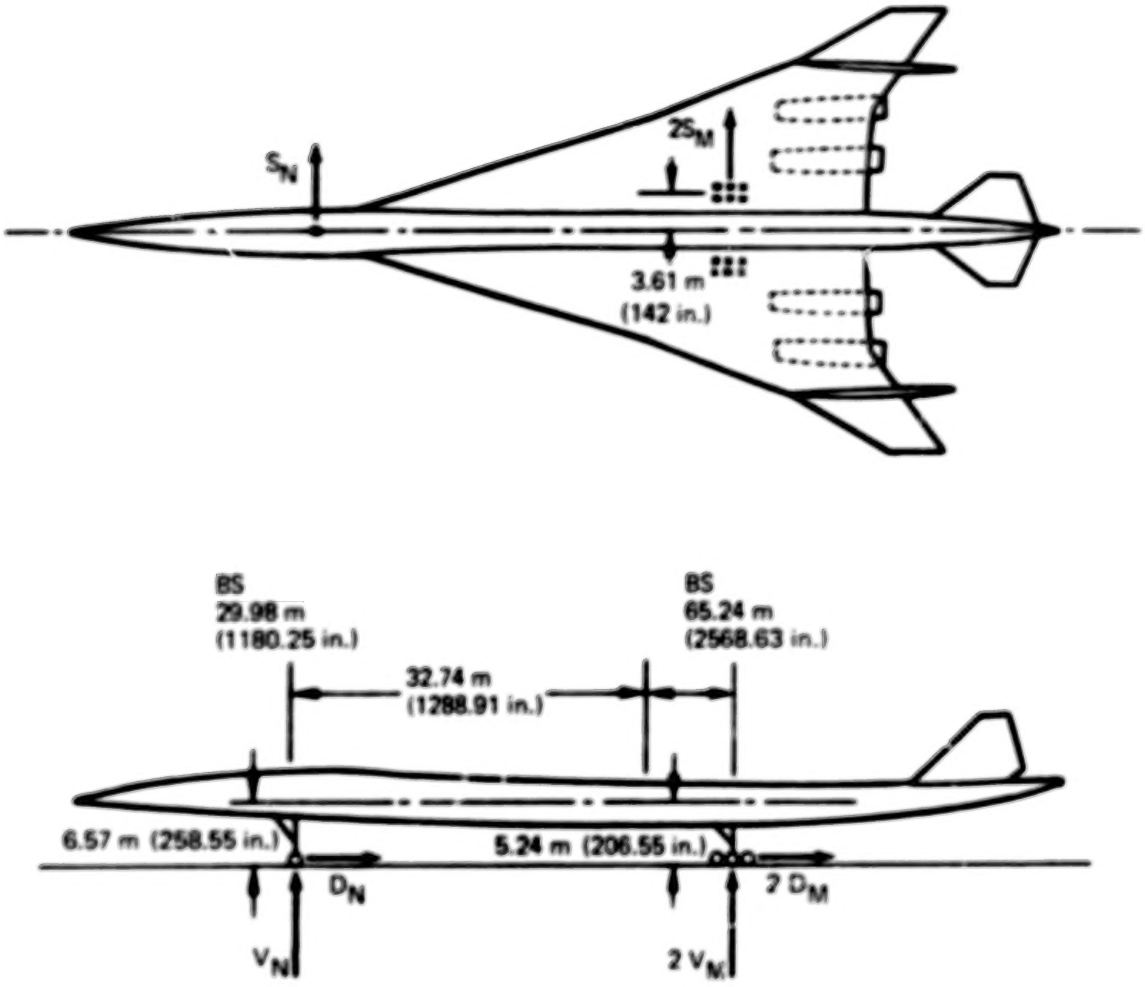

Figure 27. – Geometry and gear reactions for ground loads

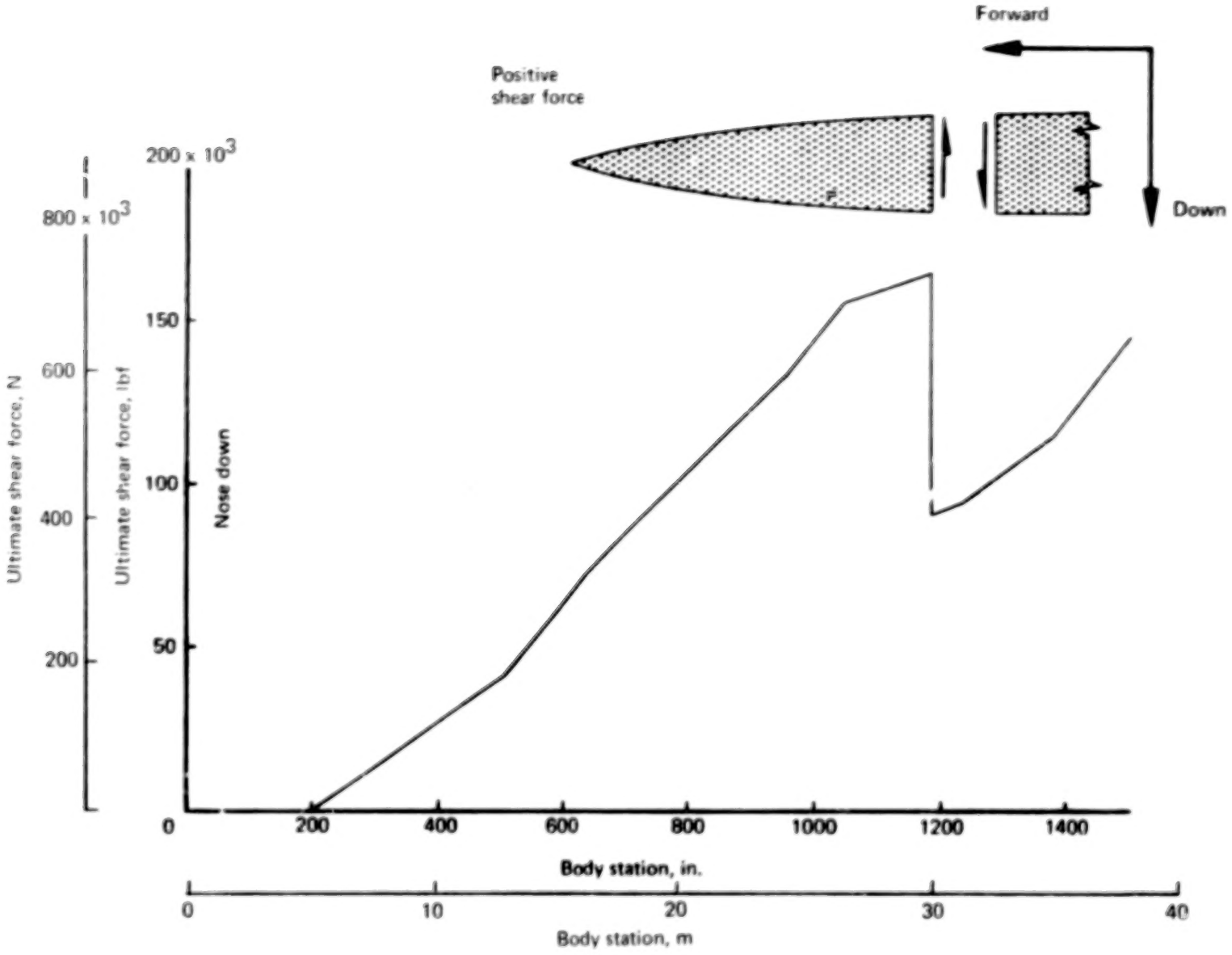

Figure 28.—Forward body ultimate shear force, landing impact

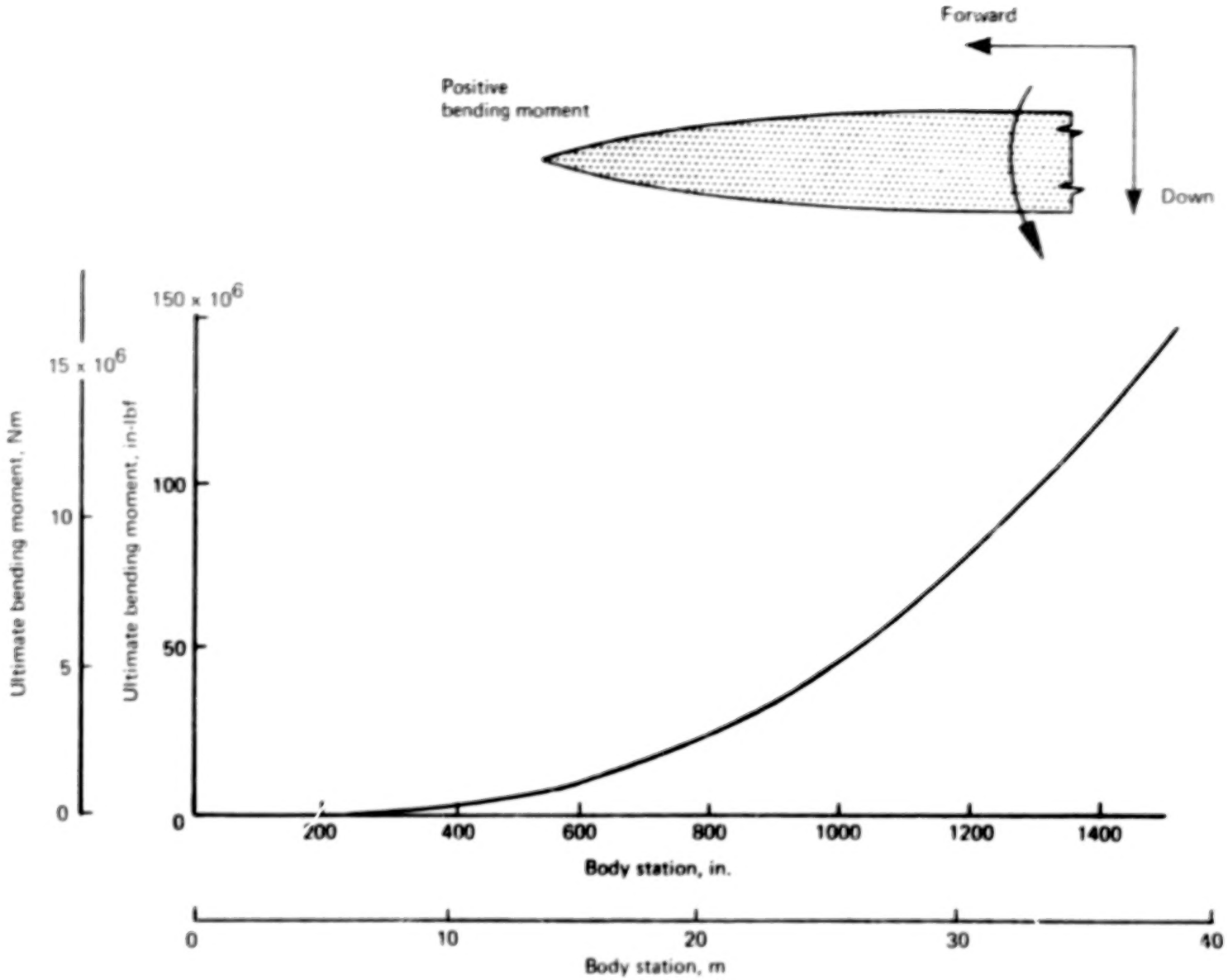

Figure 29. -- Forward body ultimate bending moment, landing impact

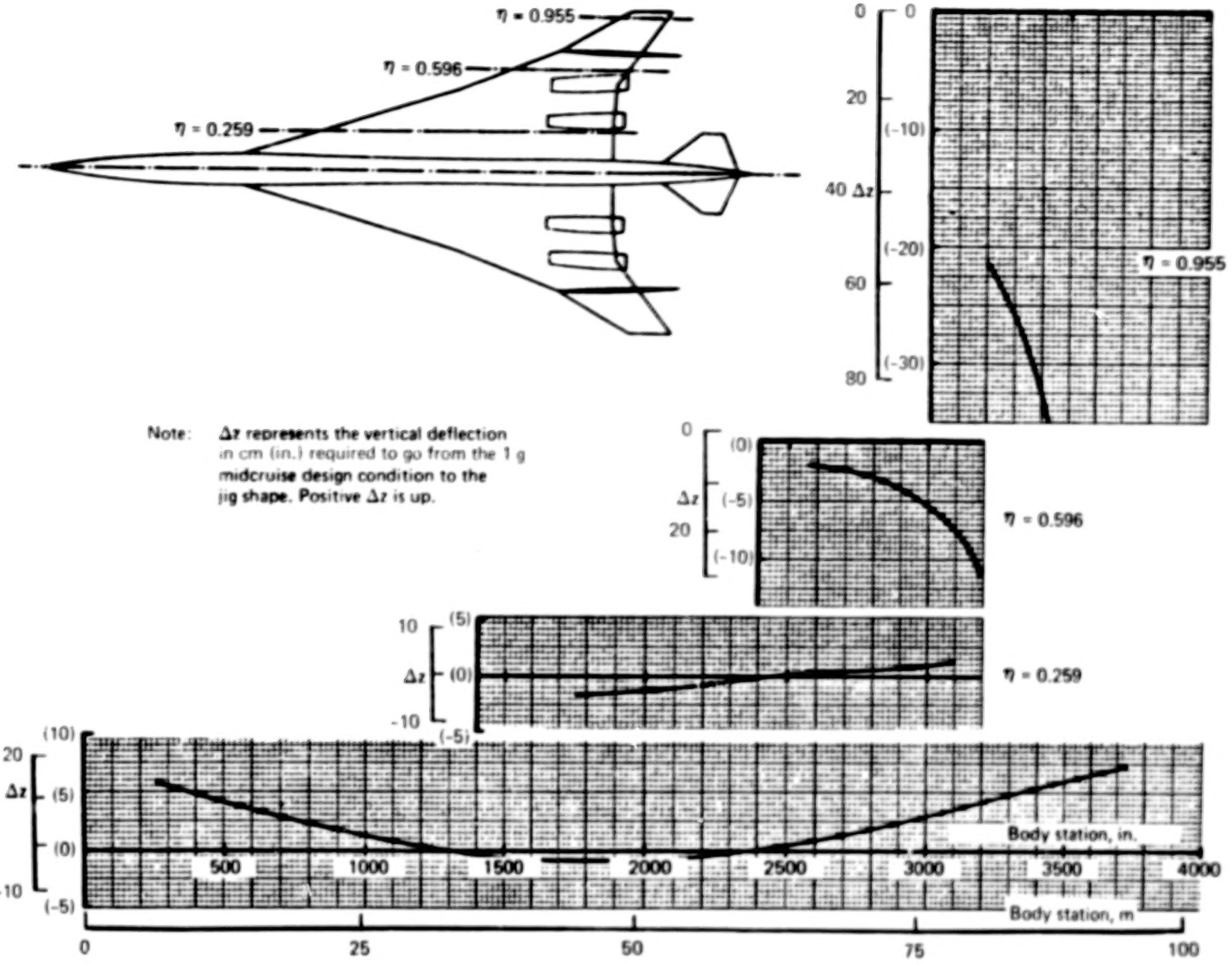

Figure 30. – Jig shape deflections

107

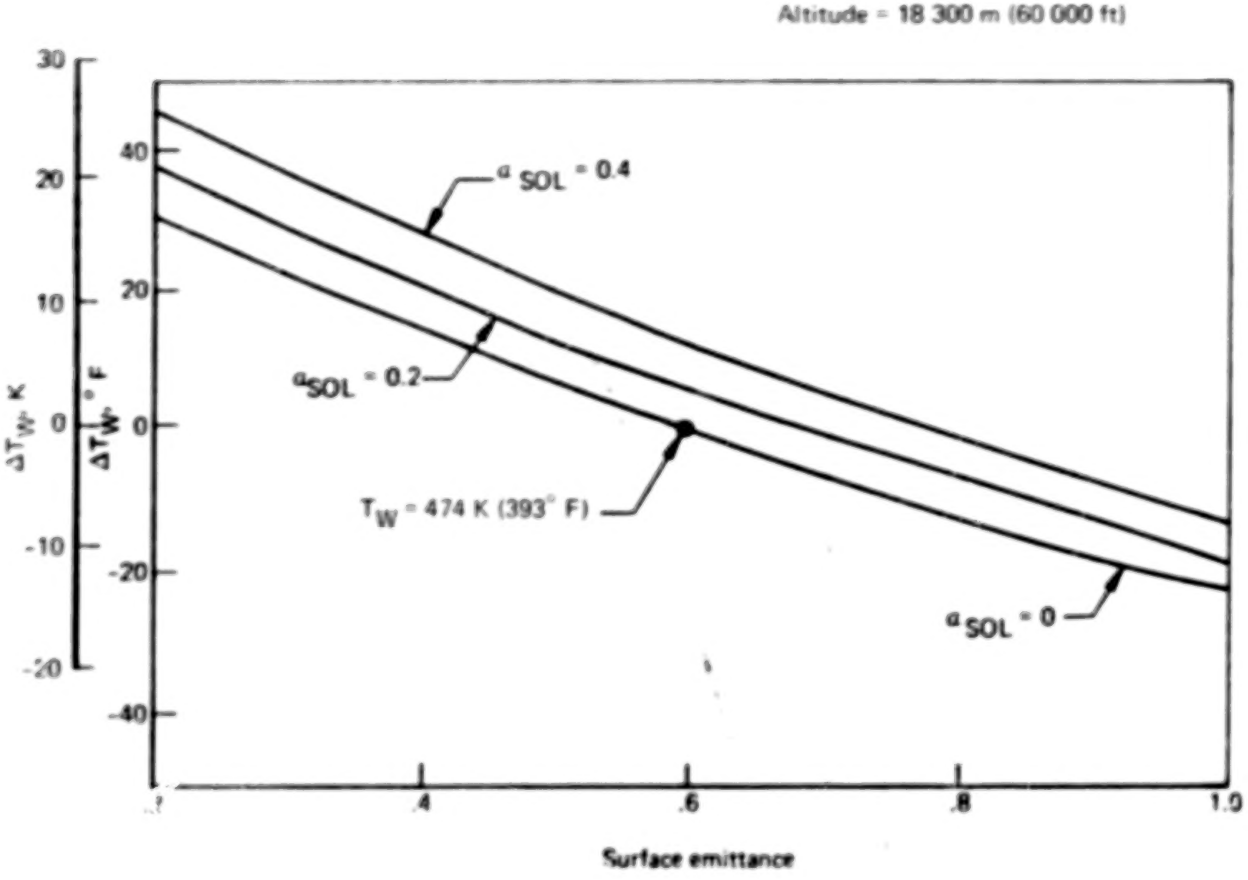

Figure 31. – Solar and emittance effects

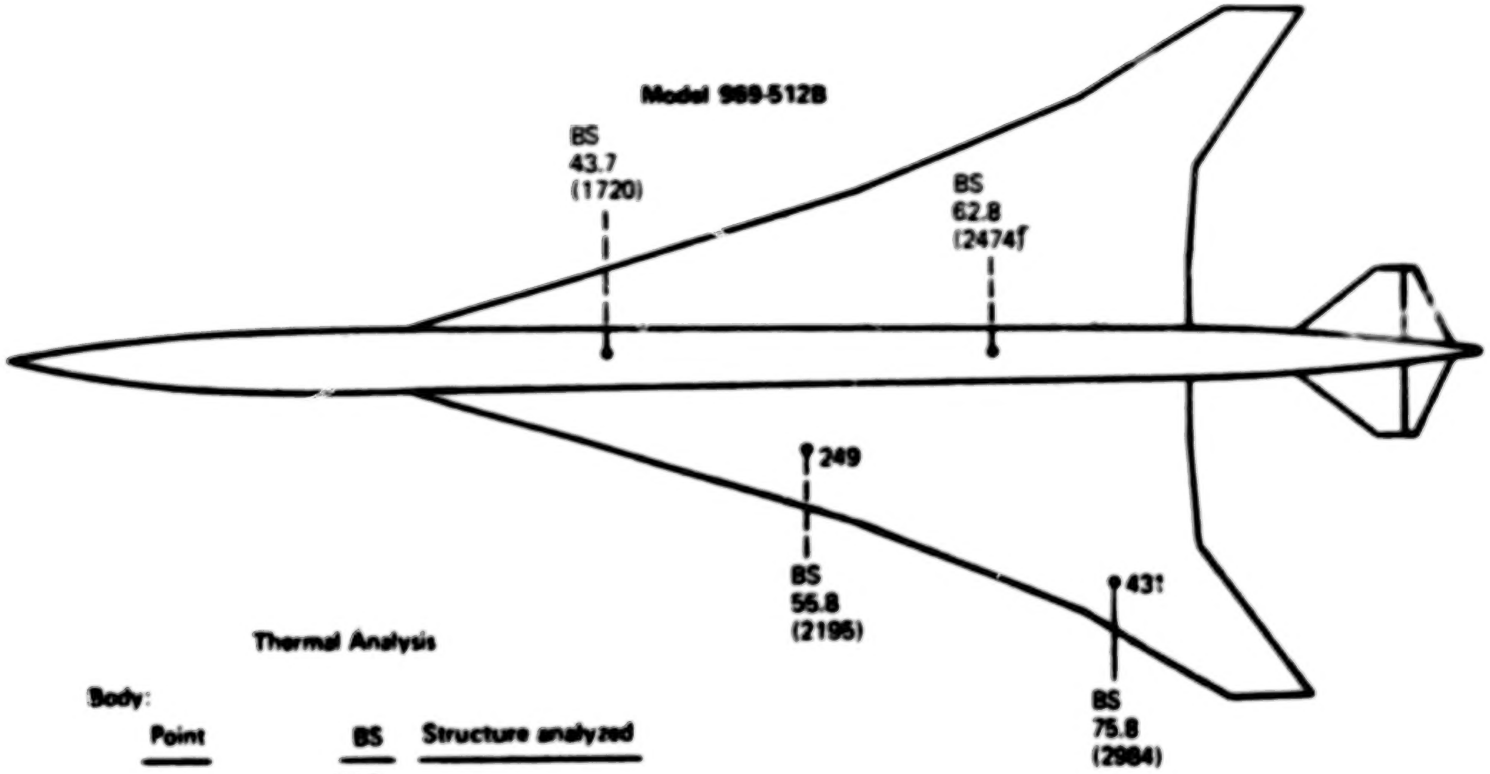

Thermal Analysis

Body:

Point	BS	Structure analyzed
5 (Lower crown)	43.7 (1720)	Body stringer
6 (Upper crown)	62.8 (2474)	Body stringer

Wings:

Point	BS	Structure analyzed
249 (tank I)	55.8 (2195)	(1) panels (2) spar
431 (dry bay)	75.8 (2984)	(1) panels (2) spar

Basic dimensions – m
( ) dimensions – in.

Figure 32. – Control points for thermal analysis

109

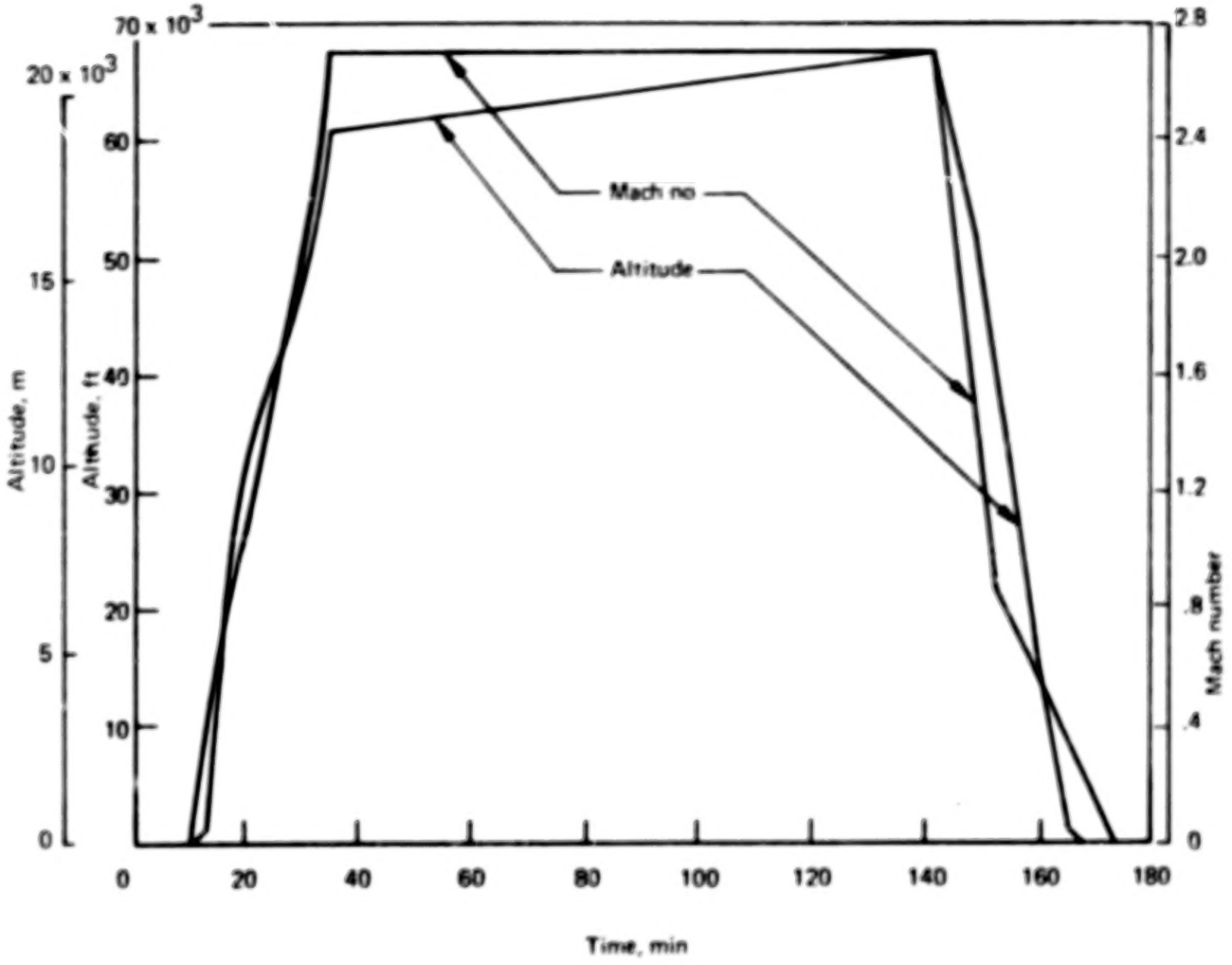

Figure 33. – Mission profile–6190 km (3340 nmi)

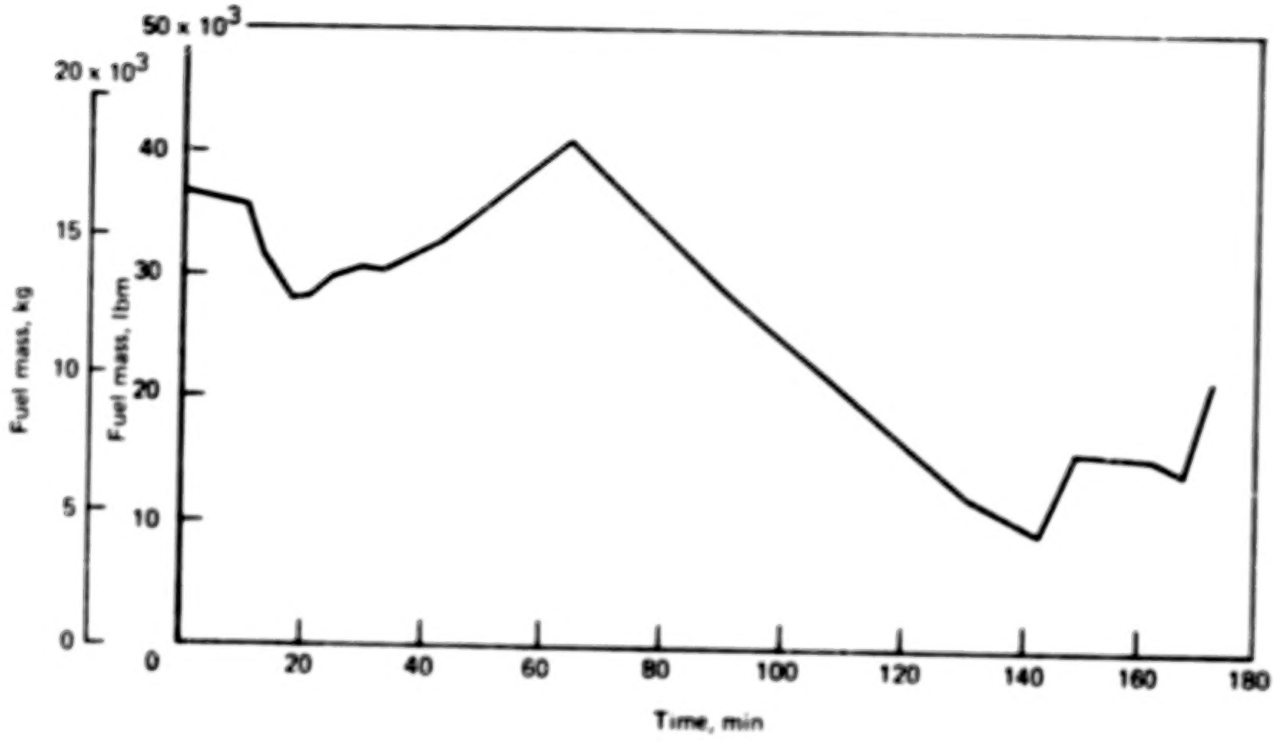

Figure 34. – Fuel tank nos. 1 and 2, fuel management

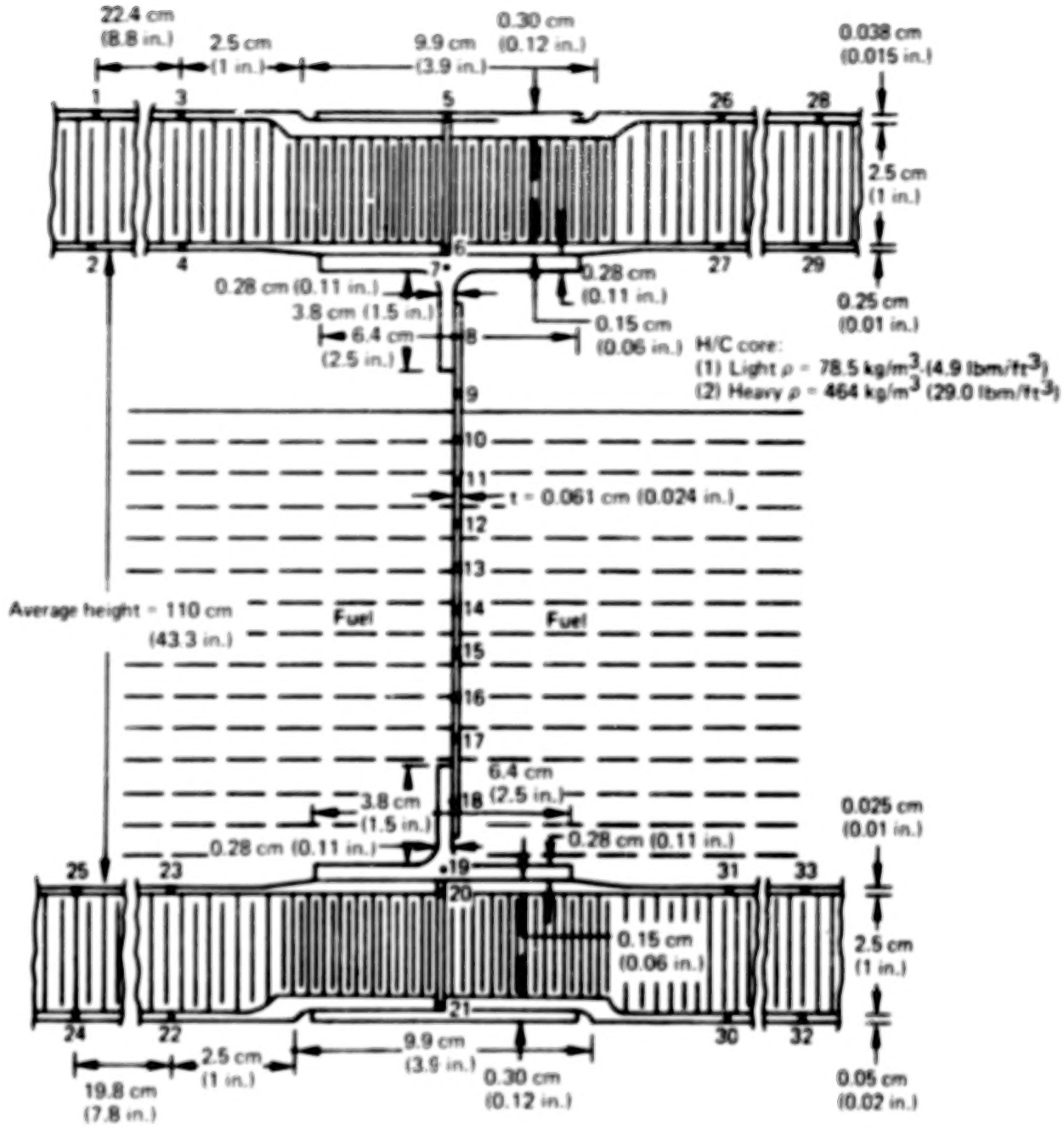
22.4 cm (8.8 in.)
2.5 cm (1 in.)
9.9 cm (3.9 in.)
0.30 cm (0.12 in.)
0.038 cm (0.015 in.)
2.5 cm (1 in.)
0.25 cm (0.01 in.)
0.28 cm (0.11 in.)
3.8 cm (1.5 in.)
6.4 cm (2.5 in.)
0.15 cm (0.06 in.)
H/C core:
(1) Light ρ = 78.5 kg/m3 (4.9 lbm/ft3)
(2) Heavy ρ = 464 kg/m3 (29.0 lbm/ft3)
t = 0.061 cm (0.024 in.)
Average height = 110 cm (43.3 in.)
Fuel
Fuel
0.025 cm (0.01 in.)
2.5 cm (1 in.)
0.05 cm (0.02 in.)
19.8 cm (7.8 in.)
Average spar spacing, 88.9 cm (35 in.)

Figure 35. – Fuel tank no. 1, point 249

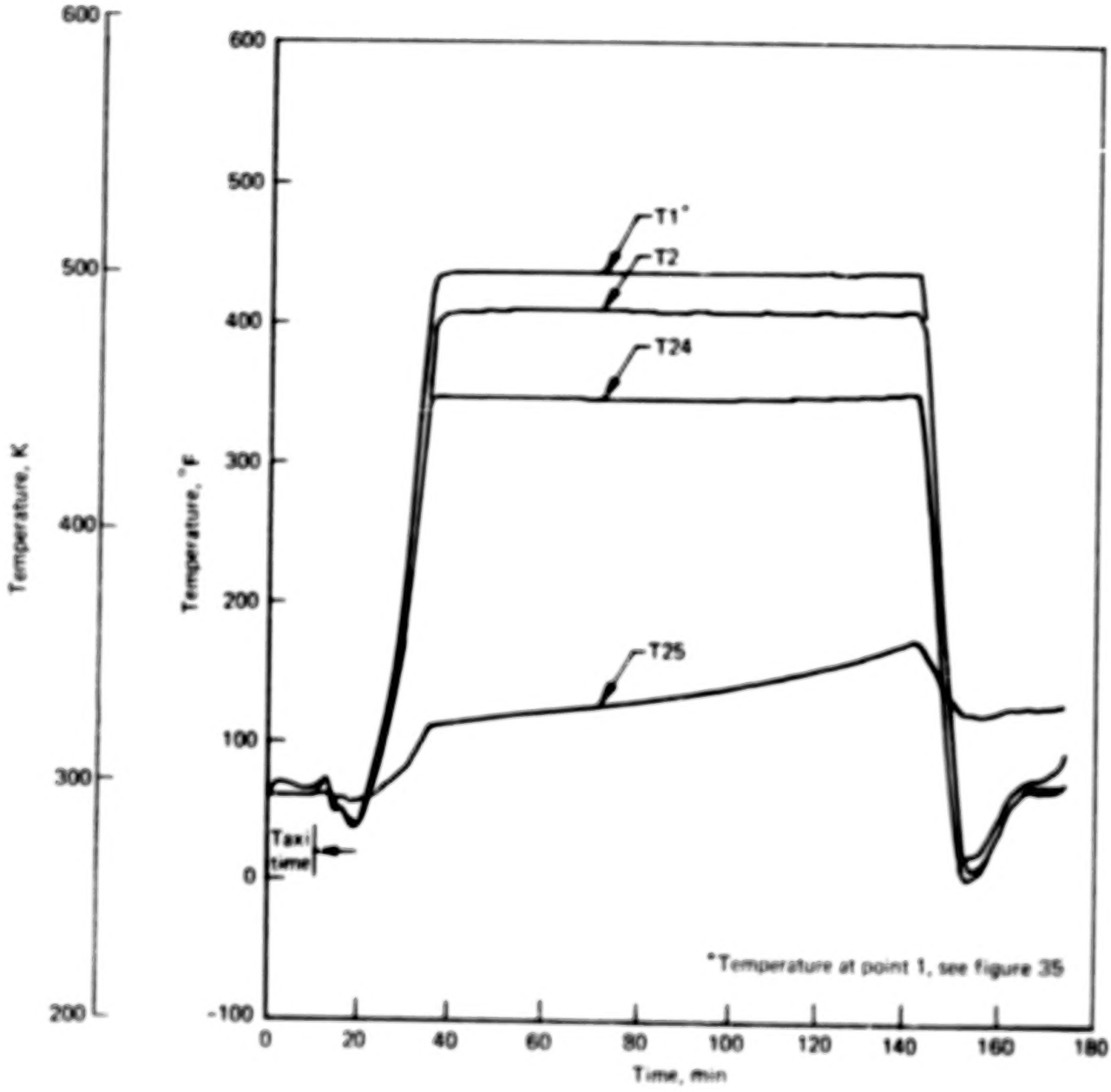

Figure 36. – Fuel tank no. 1 temperatures, point 249, case 1

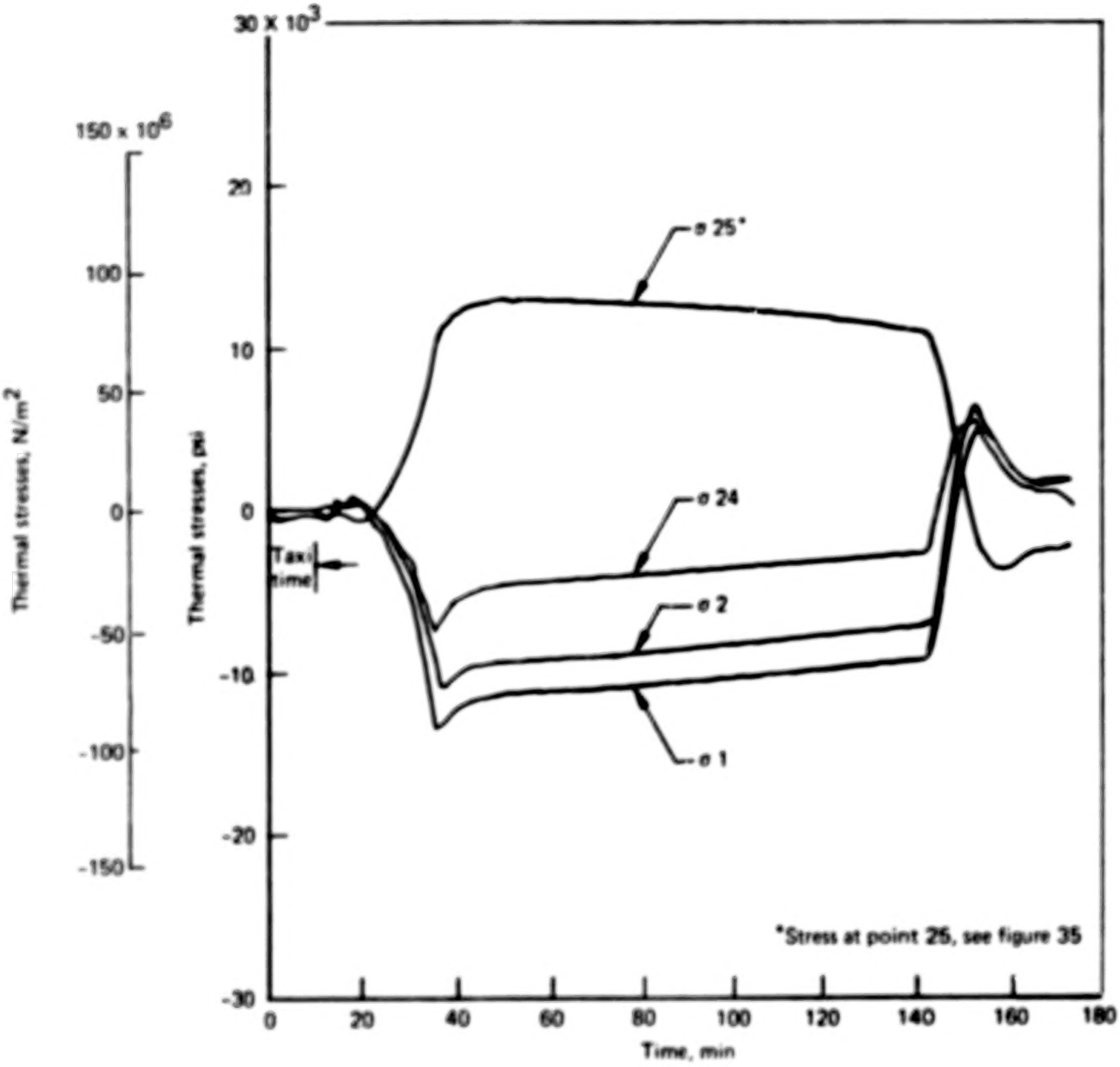

Figure 37. – Fuel tank no. 1 thermal stresses, point 249, case 1

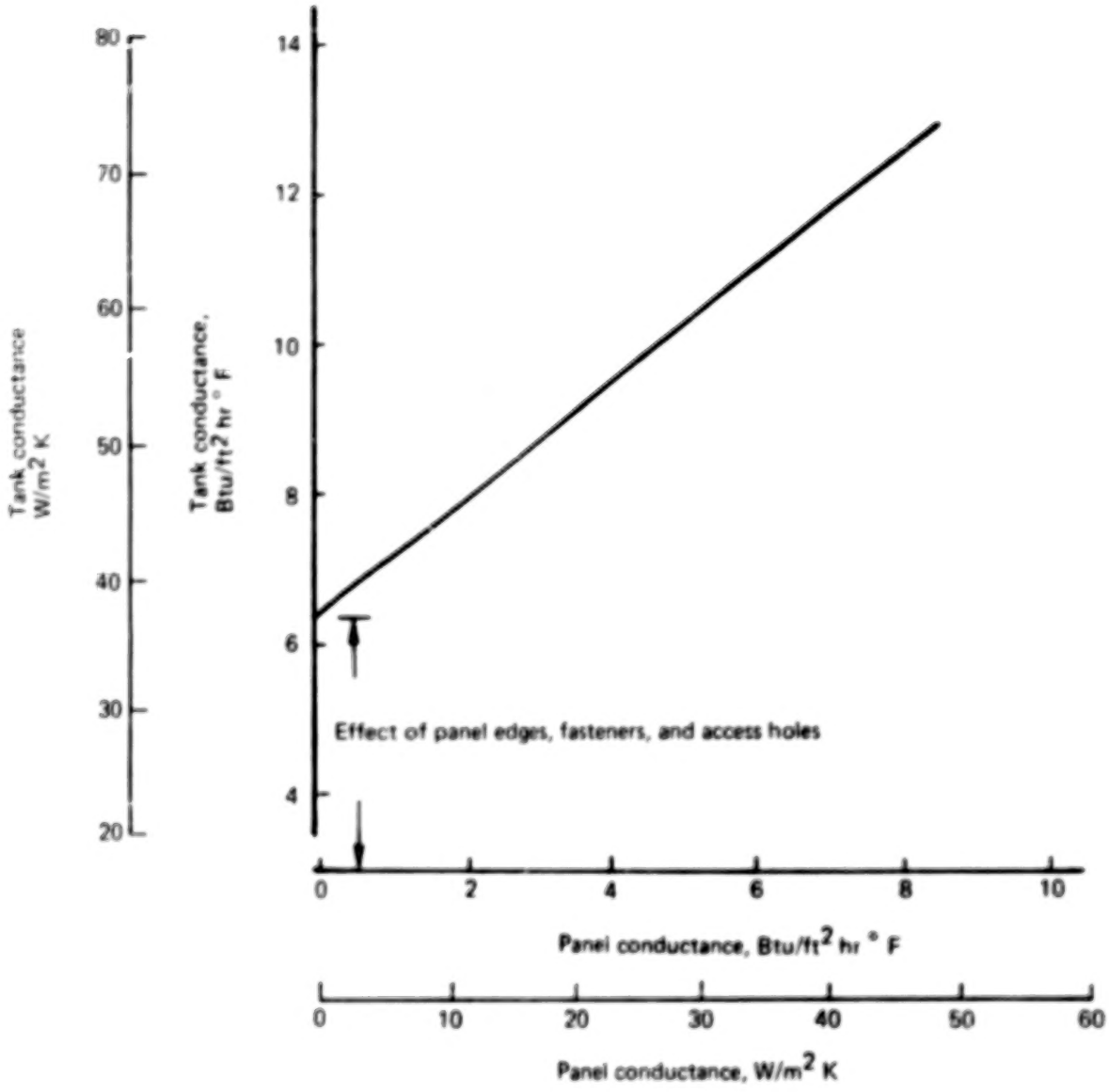

Figure 38. – Effect of panel thermal conductance on fuel tank conductance

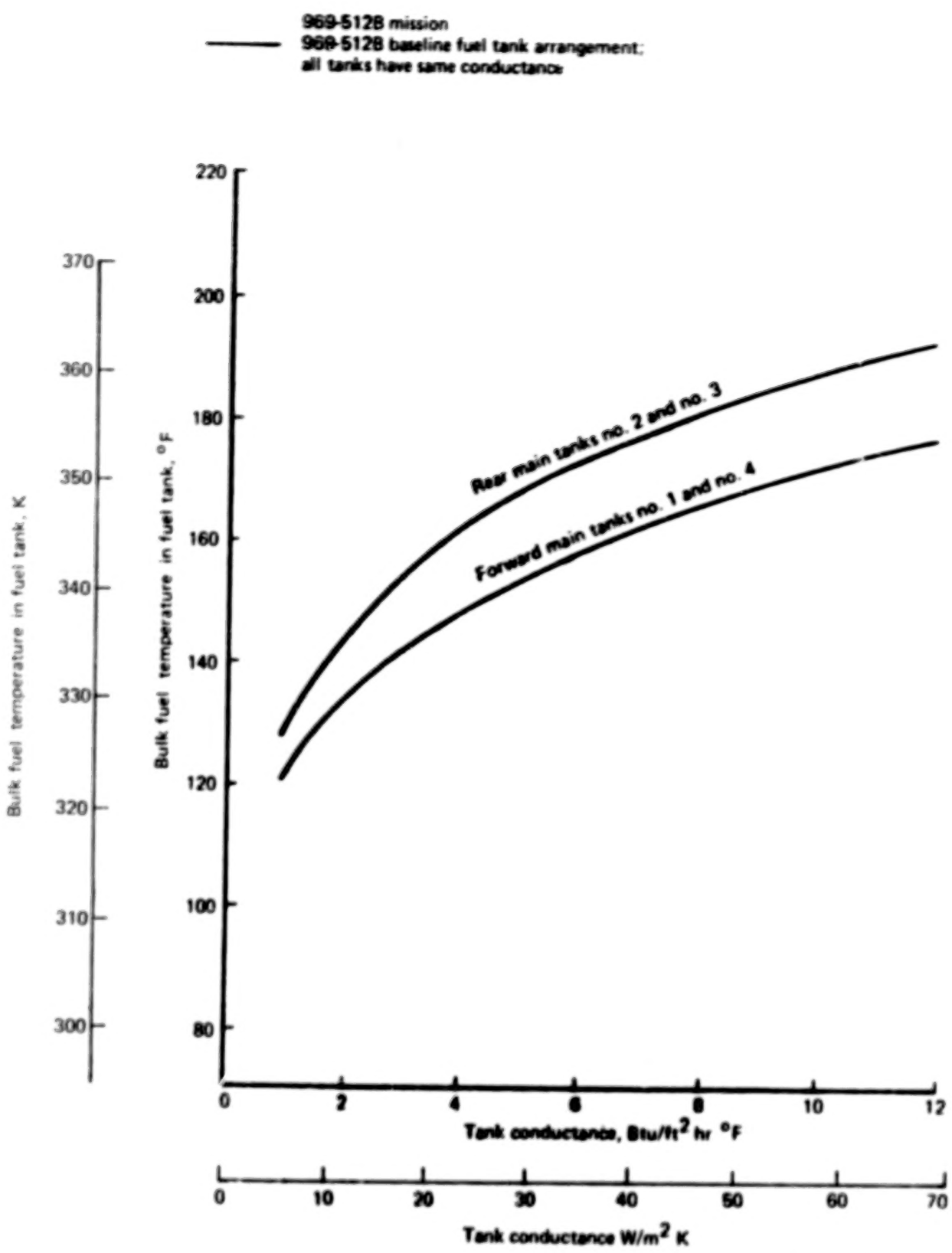
969-5128 mission
969-5128 baseline fuel tank arrangement; all tanks have same conductance
Bulk fuel temperature in fuel tank, K
Bulk fuel temperature in fuel tank, °F
Rear main tanks no. 2 and no. 3
Forward main tanks no. 1 and no. 4
Tank conductance, Btu/ft² hr °F
Tank conductance W/m² K

Figure 39. – Maximum temperature of fuel in main tanks at end of second supersonic cruise mission baseline configuration

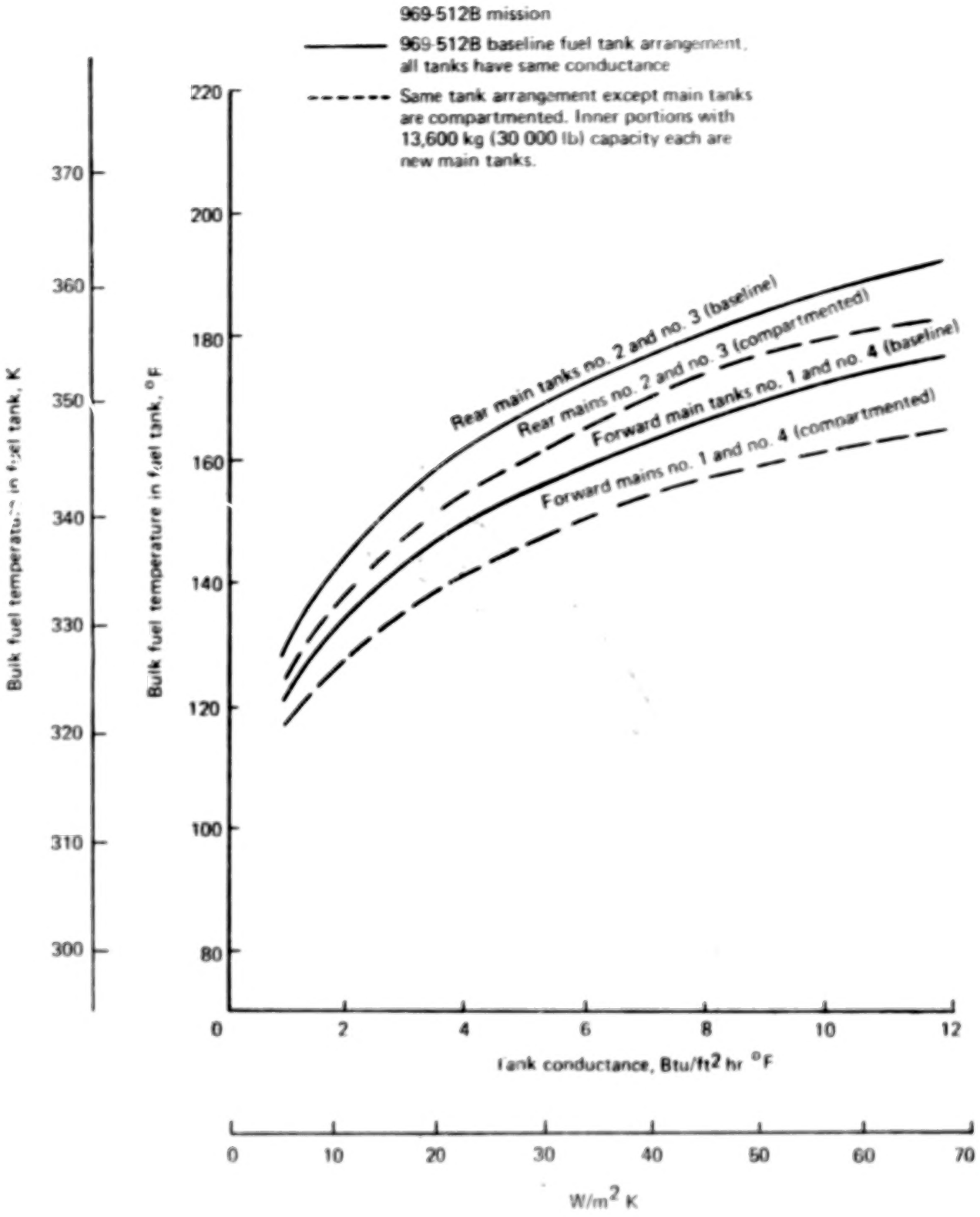
969-512B mission
969-512B baseline fuel tank arrangement, all tanks have same conductance
Same tank arrangement except main tanks are compartmented. Inner portions with 13,600 kg (30 000 lb) capacity each are new main tanks.
Bulk fuel temperature in fuel tank, K
Bulk fuel temperature in fuel tank, °F
Rear main tanks no. 2 and no. 3 (baseline)
Rear mains no. 2 and no. 3 (compartmented)
Forward main tanks no. 1 and no. 4 (baseline)
Forward mains no. 1 and no. 4 (compartmented)
Tank conductance, Btu/ft2 hr °F
W/m2 K

Figure 40. — Maximum temperature of fuel in main tanks at end of supersonic cruise, second trip, compartmented configuration

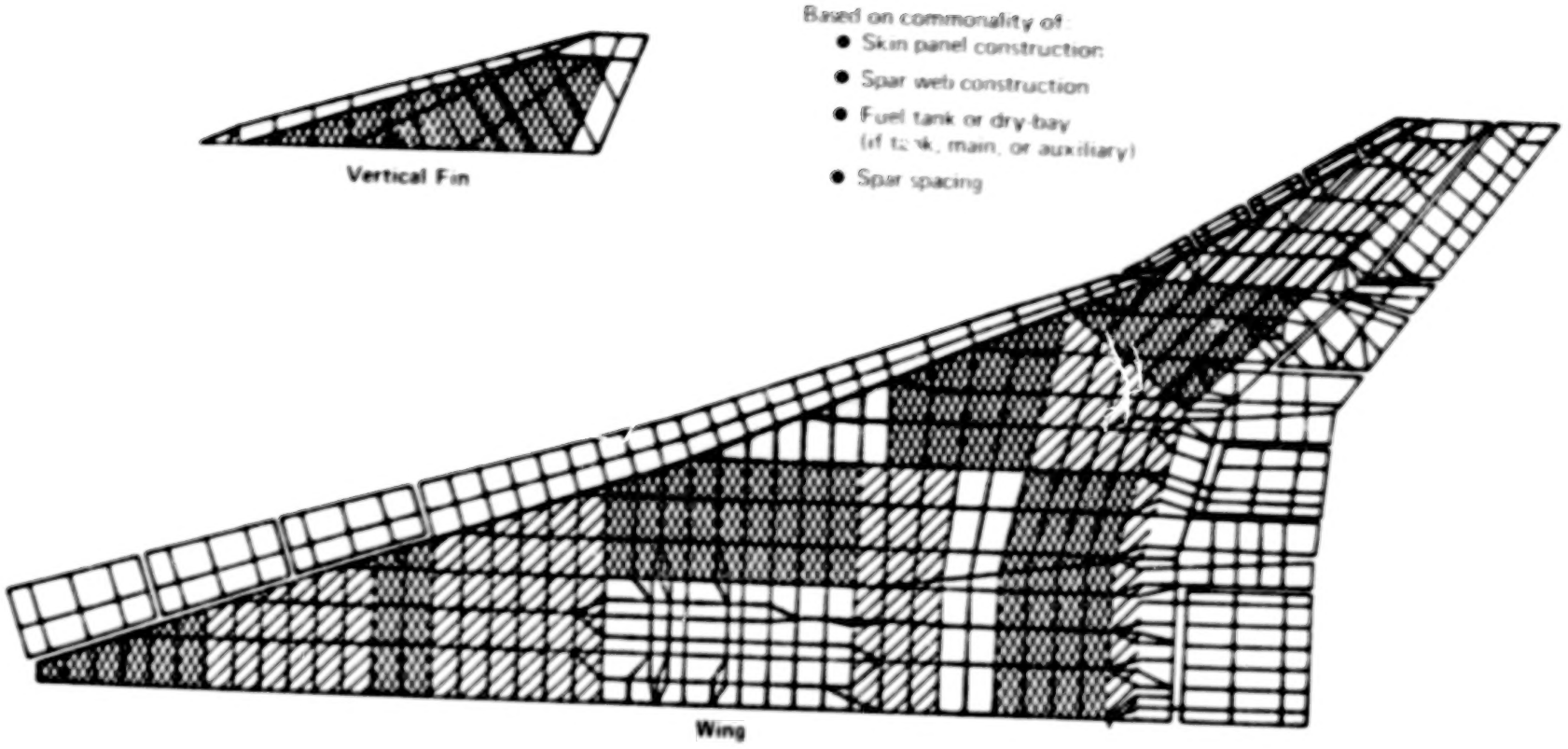

Figure 41. – Wing structure regions

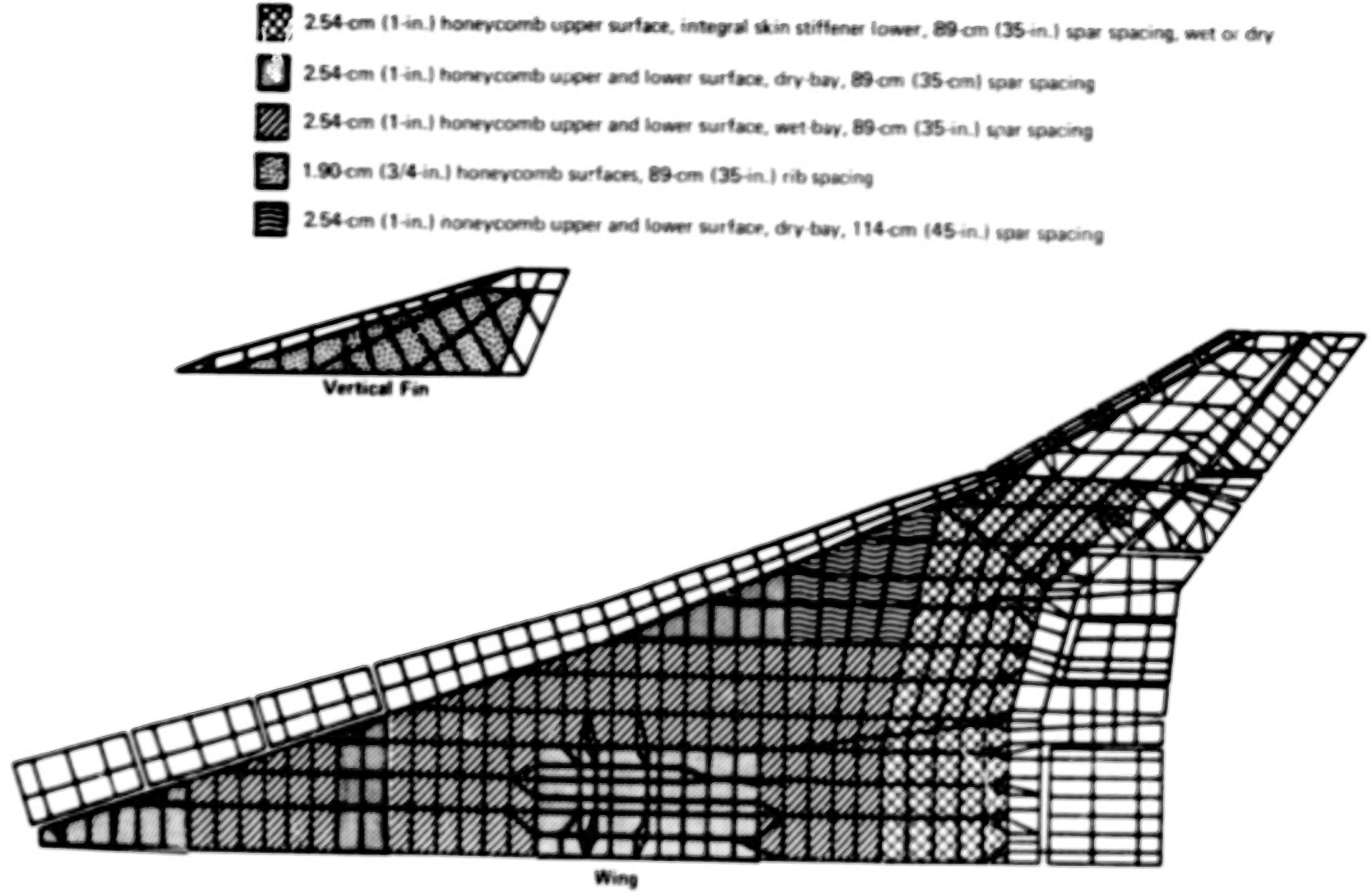
2.54-cm (1-in.) honeycomb upper surface, integral skin stiffener lower, 89-cm (35-in.) spar spacing, wet or dry
2.54-cm (1-in.) honeycomb upper and lower surface, dry-bay, 89-cm (35-cm) spar spacing
2.54-cm (1-in.) honeycomb upper and lower surface, wet-bay, 89-cm (35-in.) spar spacing
1.90-cm (3/4-in.) honeycomb surfaces, 89-cm (35-in.) rib spacing
2.54-cm (1-in.) honeycomb upper and lower surface, dry-bay, 114-cm (45-in.) spar spacing
Vertical Fin
Wing

Figure 42. – Wing cover element subsets

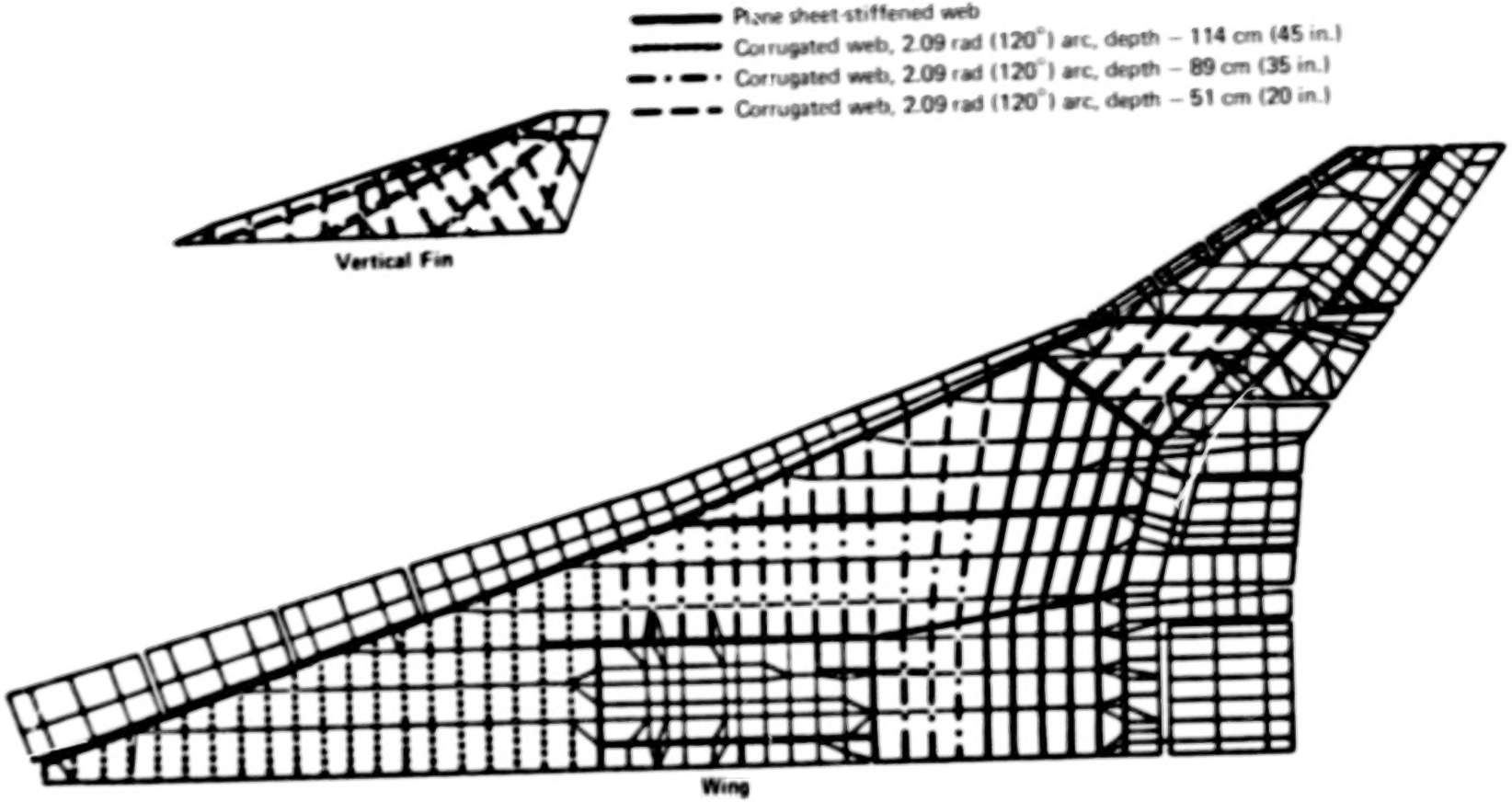
Plane sheet-stiffened web
Corrugated web, 2.09 rad (120°) arc, depth – 114 cm (45 in.)
Corrugated web, 2.09 rad (120°) arc, depth – 89 cm (35 in.)
Corrugated web, 2.09 rad (120°) arc, depth – 51 cm (20 in.)
Vertical Fin
Wing

Figure 43. – Wing spar element subsets

	Honeycomb panel face sheet		Integral skin-stiffener panel		Corrugated or sheet-stiffener spar	
Design cycle	Inner thickness, cm (in.)	Outer thickness, cm (in.)	Skin thickness, cm (in.)	Stiffener-to-skin area ratio	Web gage, cm (in.)	Chord area, cm^2 ($in.^2$)
1	0.025 (0.010)	0.051 (0.020) (lower surface) 0.038 (0.015) (upper surface and fin)	0.147 (0.058	0.20	0.051 (0.020)	As initially sized
2				2.41t−0.016[b]	(a)	0.25 of area of larger adjacent skin panel
3				Cycle 2 value		Cycle 2 value

[a] 0.051 (0.020) except for corrugated webs in fuel tanks which are designed by 6-g crash or refueling overpressure.

[b] Based on data in NACA TN 2873

Figure 44. – Lower bound data

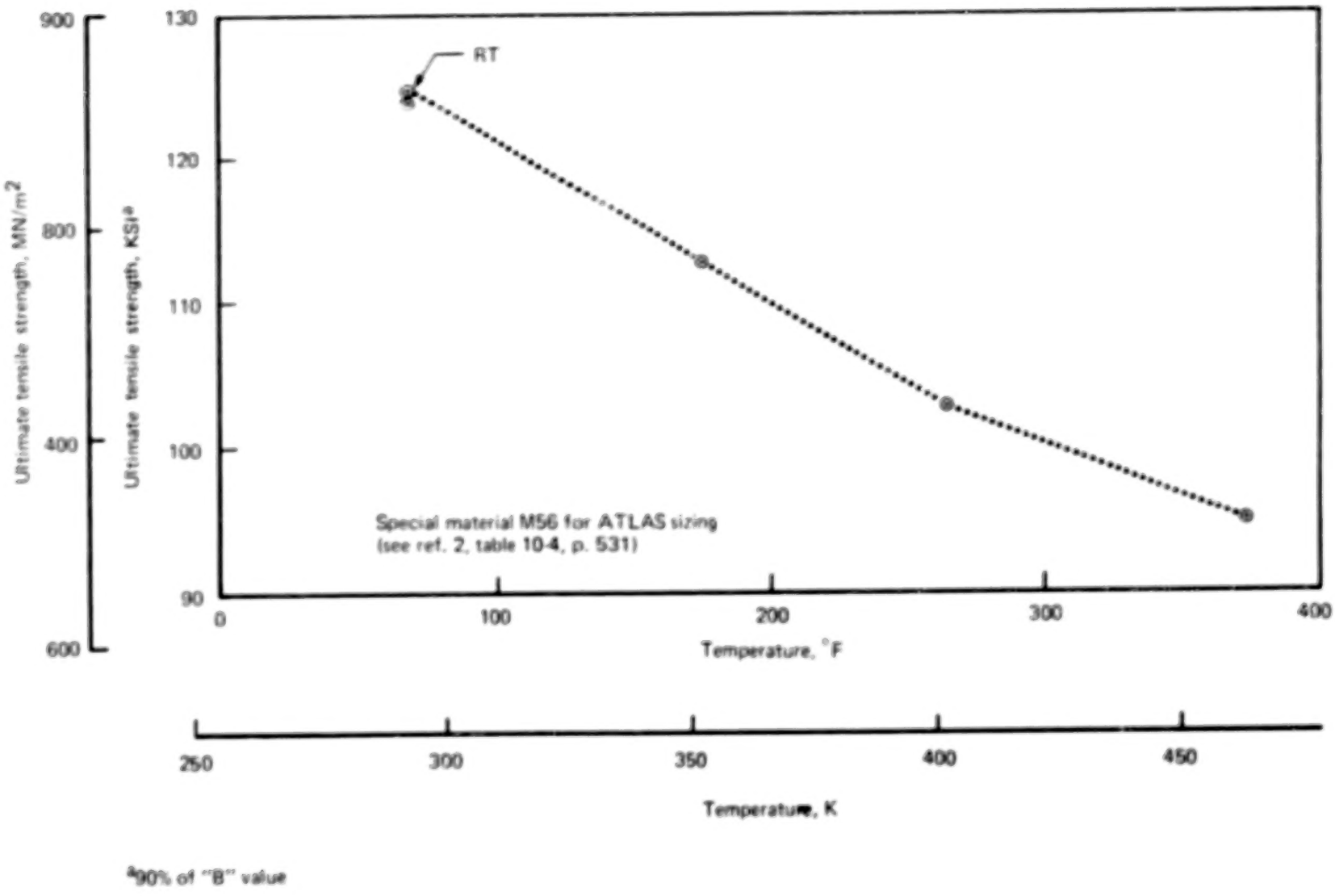

[a]90% of "B" value

Figure 45. — Typical mechanical properties (including thermal stress decrements) Ti-6Al-4V, condition 1

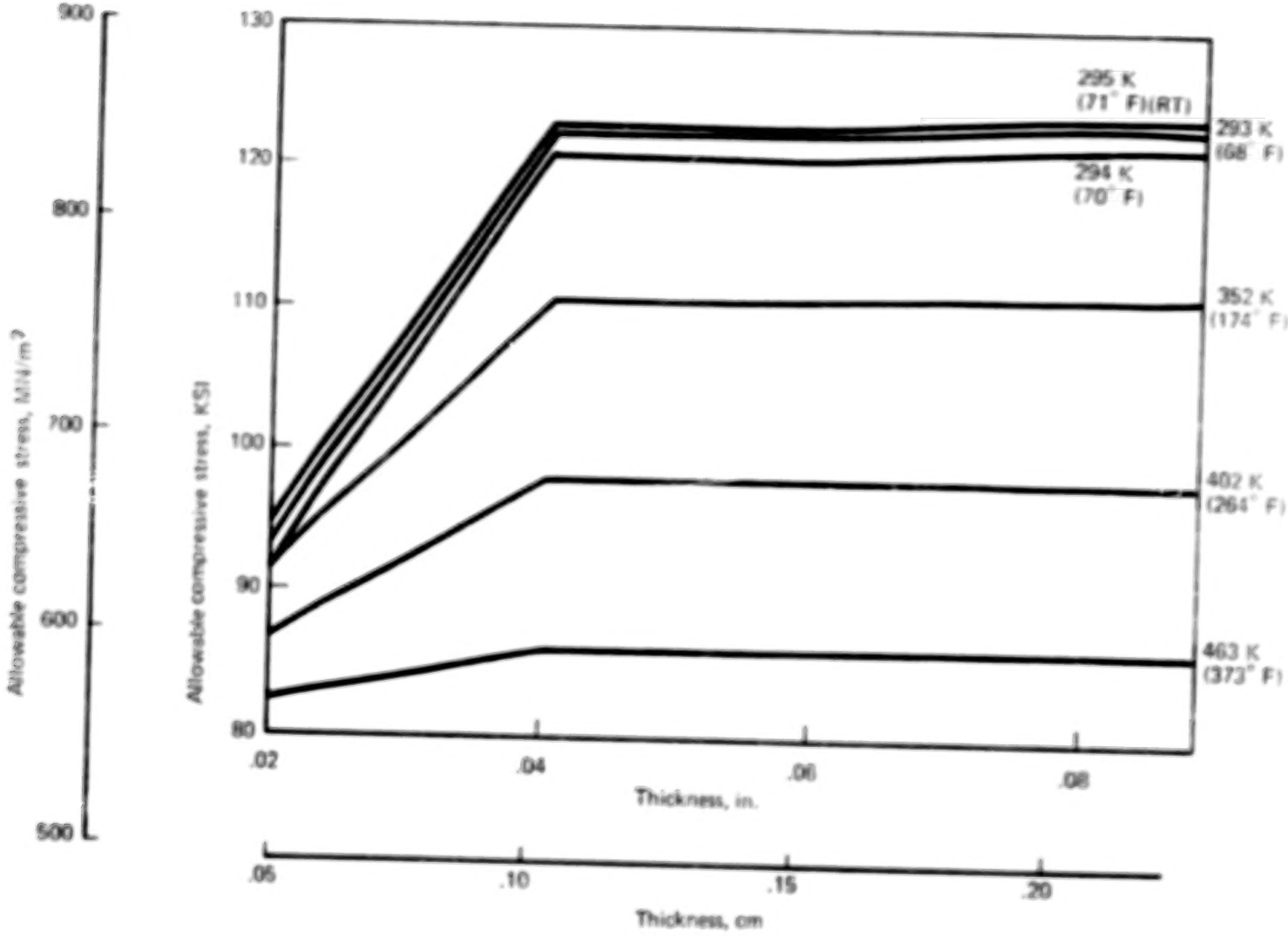

Figure 46. – Typical instability allowables (including thermal stress decrements), Ti-6Al-4V, condition A

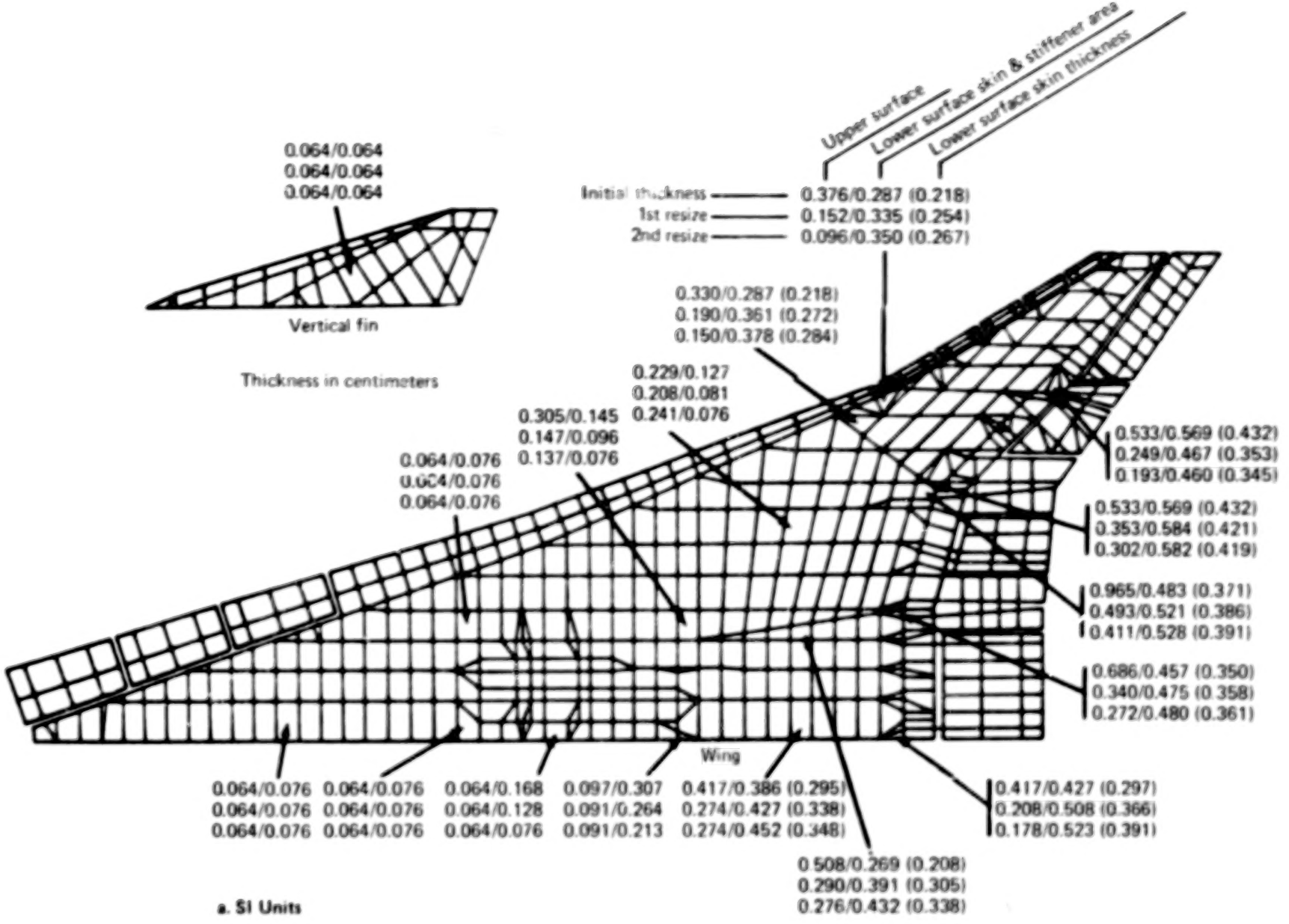

Figure 47. – Typical wing panel resizing results

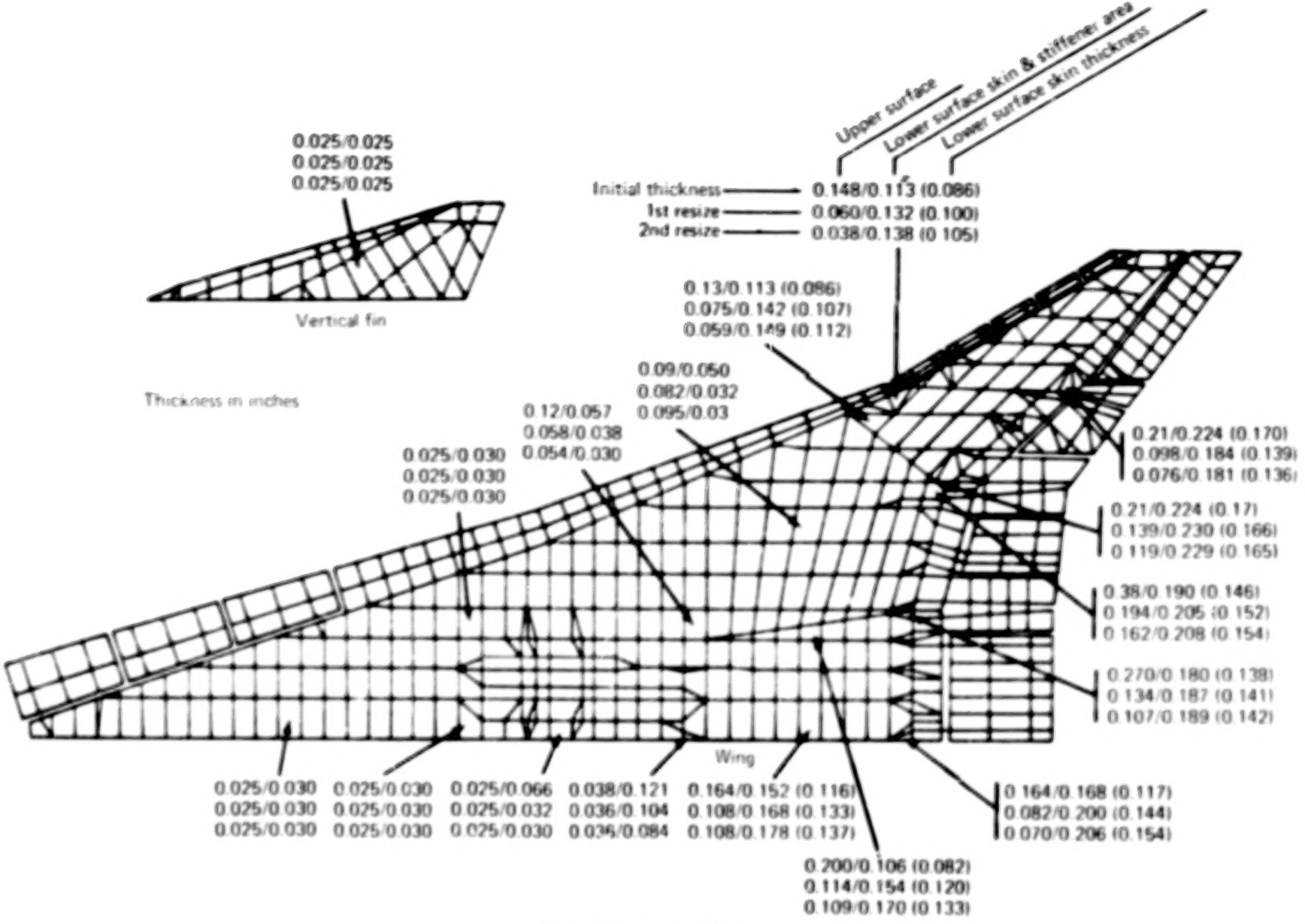

b. U.S. Customary Units

Figure 47. – (Concluded)

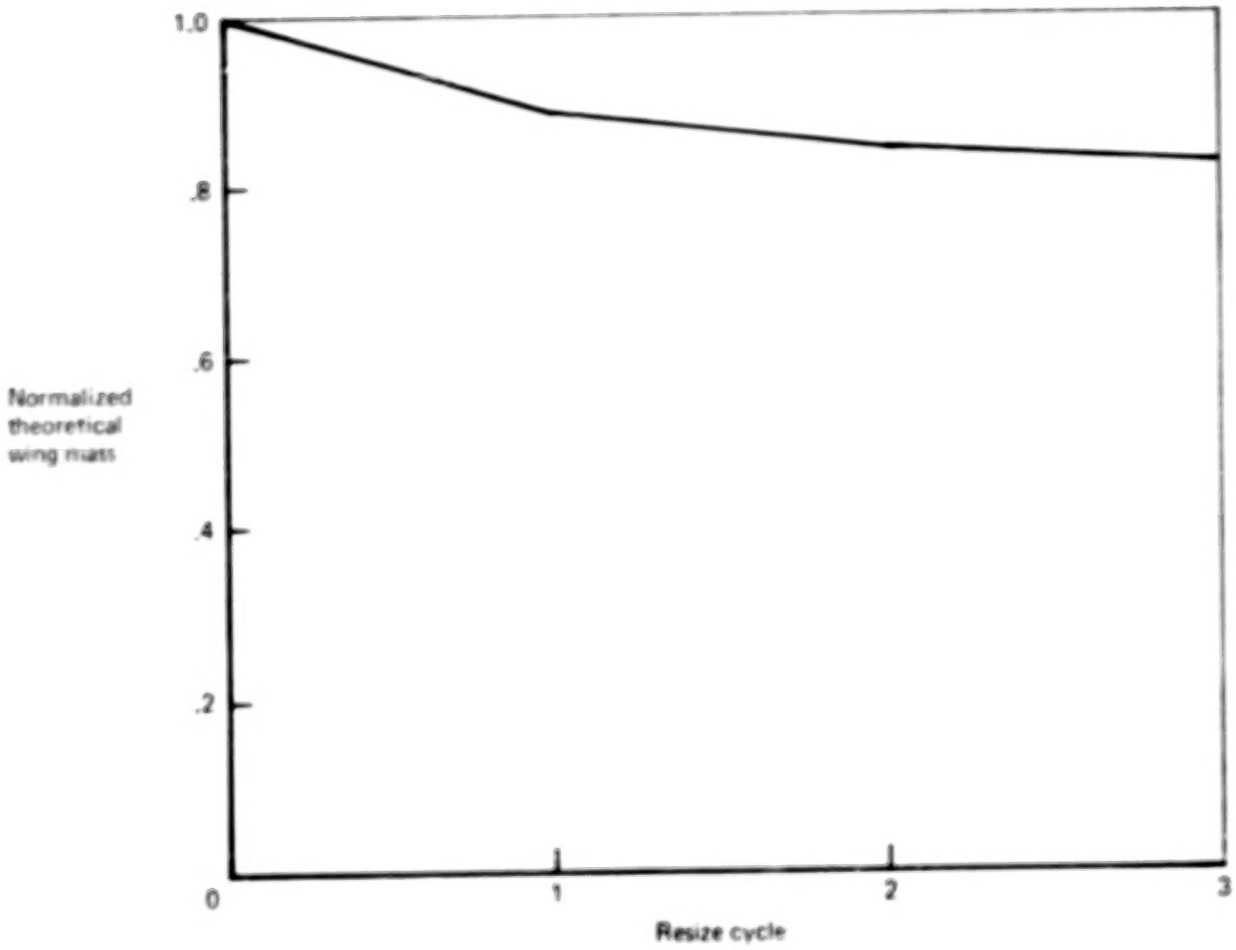

Figure 48. – Effect of resizing on theoretical wing mass

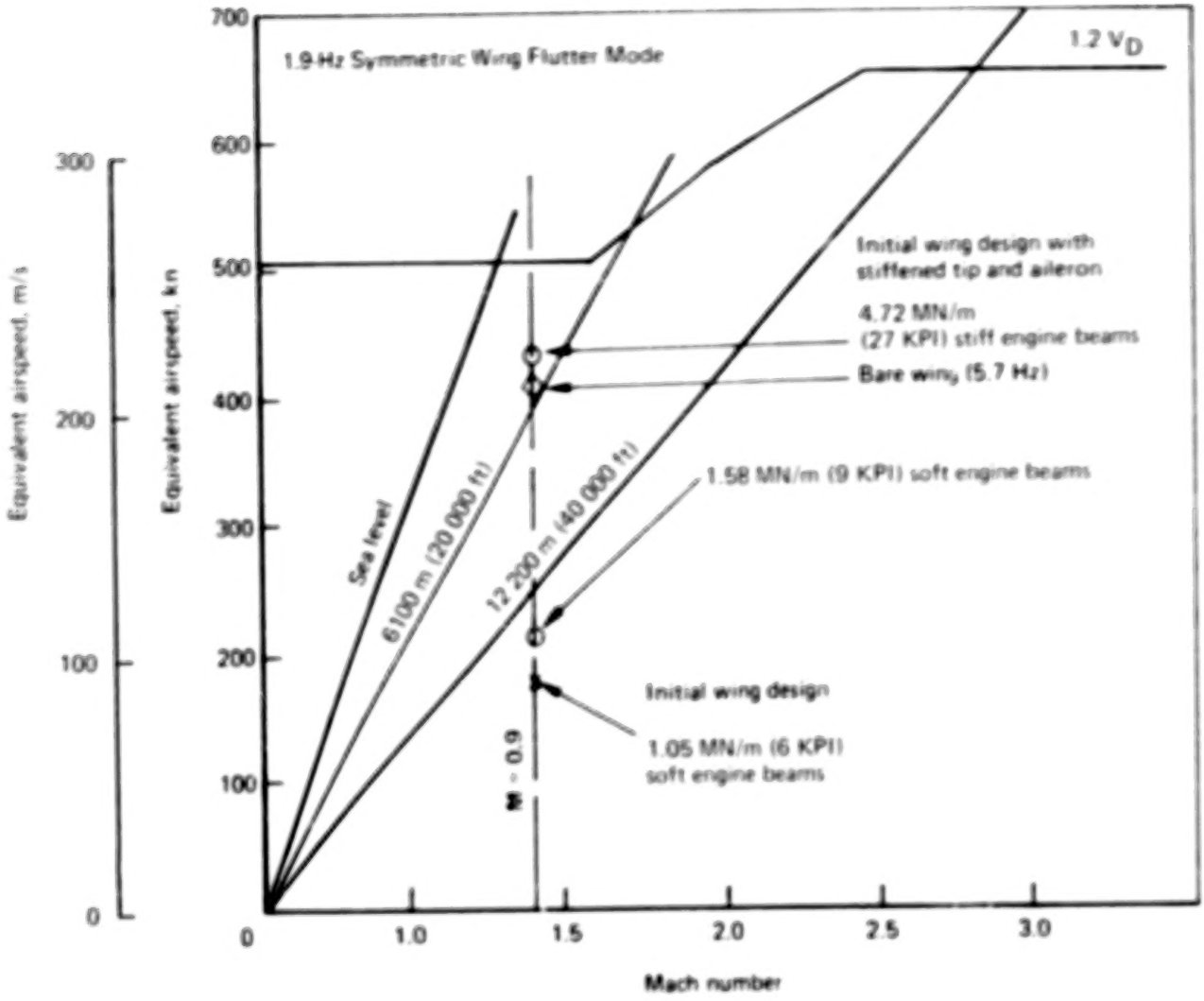

Figure 49. – Preliminary flutter speeds

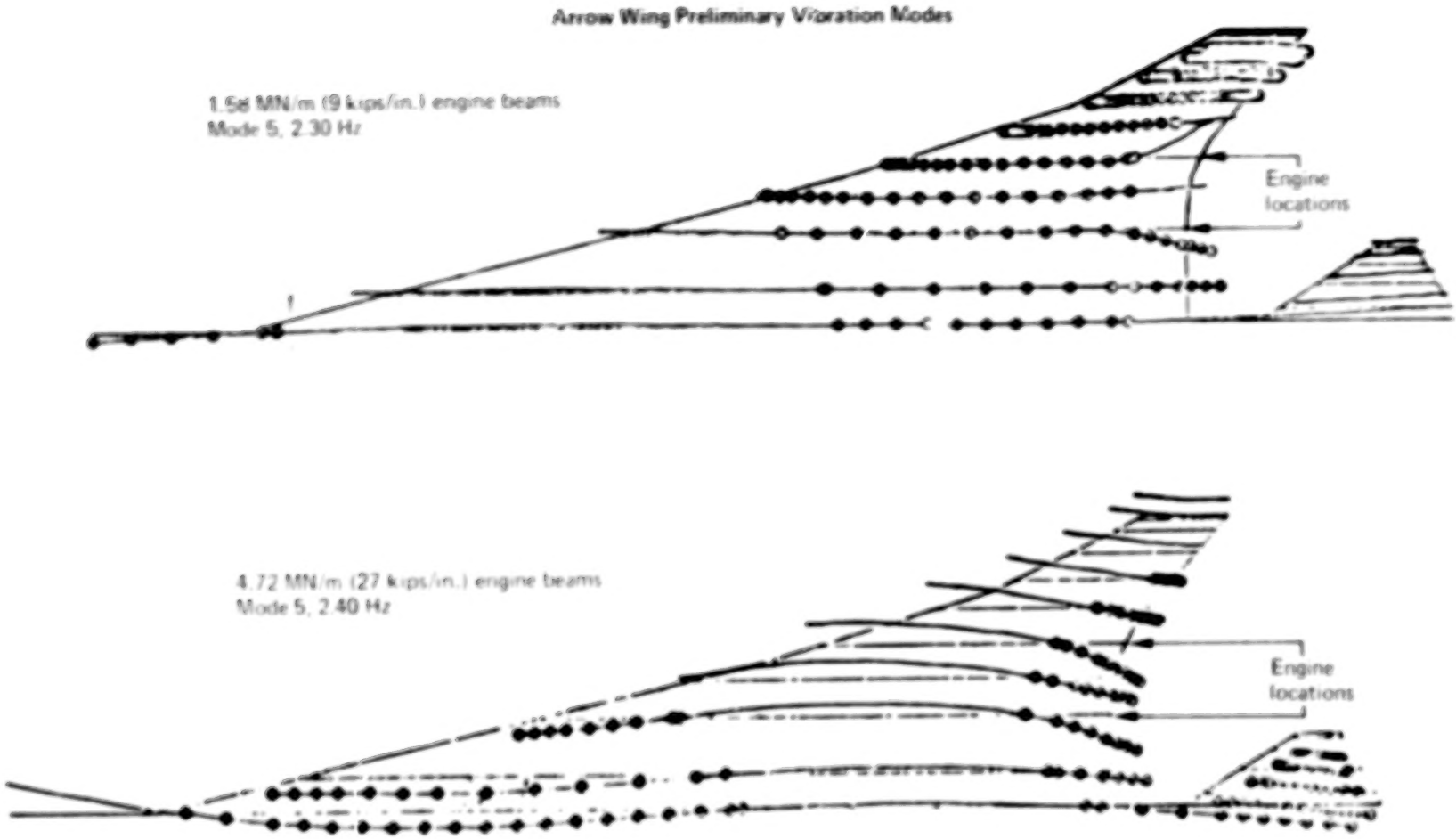
Arrow Wing Preliminary Vibration Modes
1.58 MN/m (9 kips/in.) engine beams
Mode 5, 2.30 Hz
Engine locations
4.72 MN/m (27 kips/in.) engine beams
Mode 5, 2.40 Hz
Engine locations

Figure 50. – Effect of nacelle beam stiffening on modal coupling

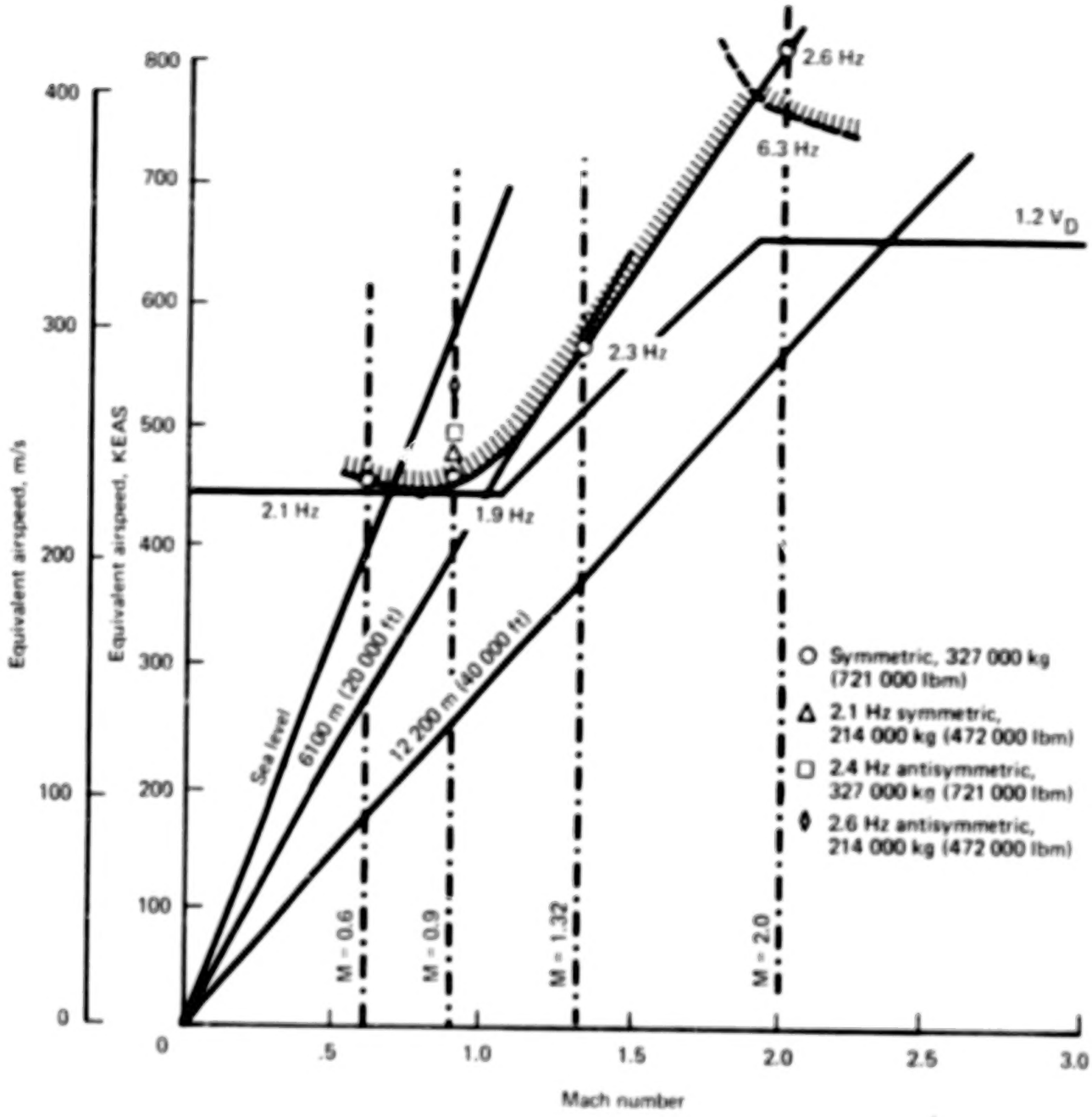
Equivalent airspeed, m/s
Equivalent airspeed, KEAS
Mach number
2.6 Hz
6.3 Hz
1.2 V_D
2.3 Hz
2.1 Hz
1.9 Hz
Sea level
6100 m (20 000 ft)
12 200 m (40 000 ft)
M = 0.6
M = 0.9
M = 1.32
M = 2.0
Symmetric, 327 000 kg (721 000 lbm)
2.1 Hz symmetric, 214 000 kg (472 000 lbm)
2.4 Hz antisymmetric, 327 000 kg (721 000 lbm)
2.6 Hz antisymmetric, 214 000 kg (472 000 lbm)

Figure 51. – Arrow wing flutter boundary, 969-512B

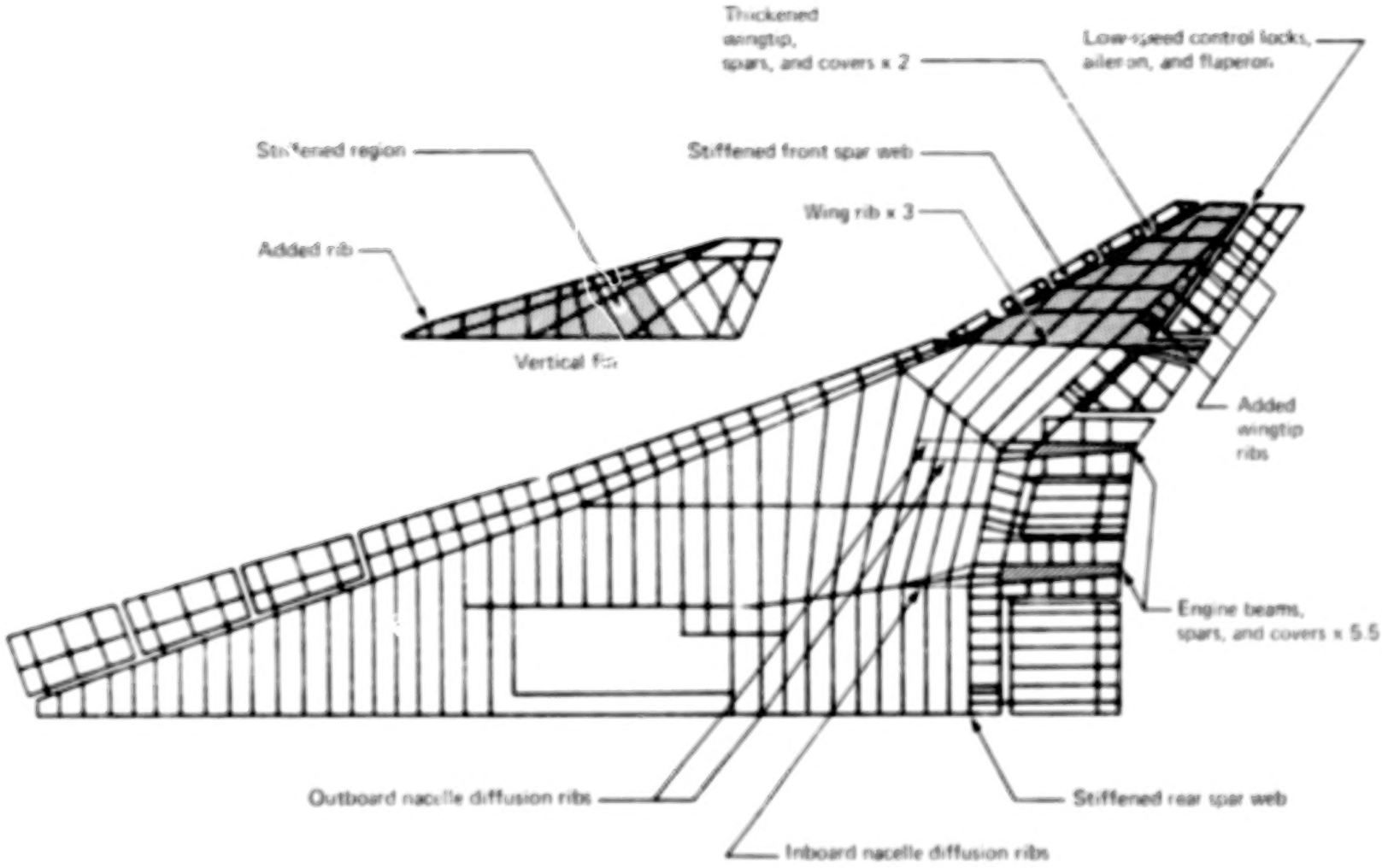

Figure 52. – Final design modification for stiffness

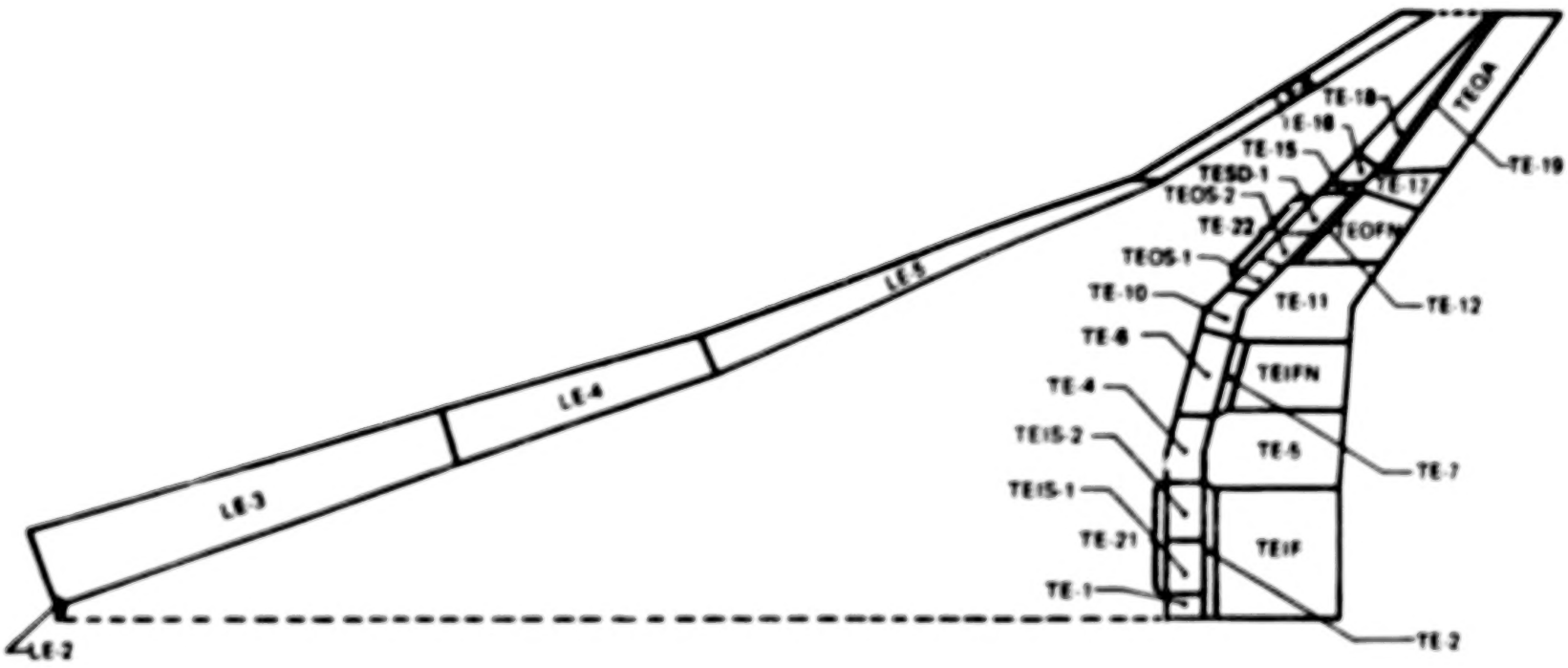

Figure 53. – Wing leading edge and trailing edge structure, mass input elements

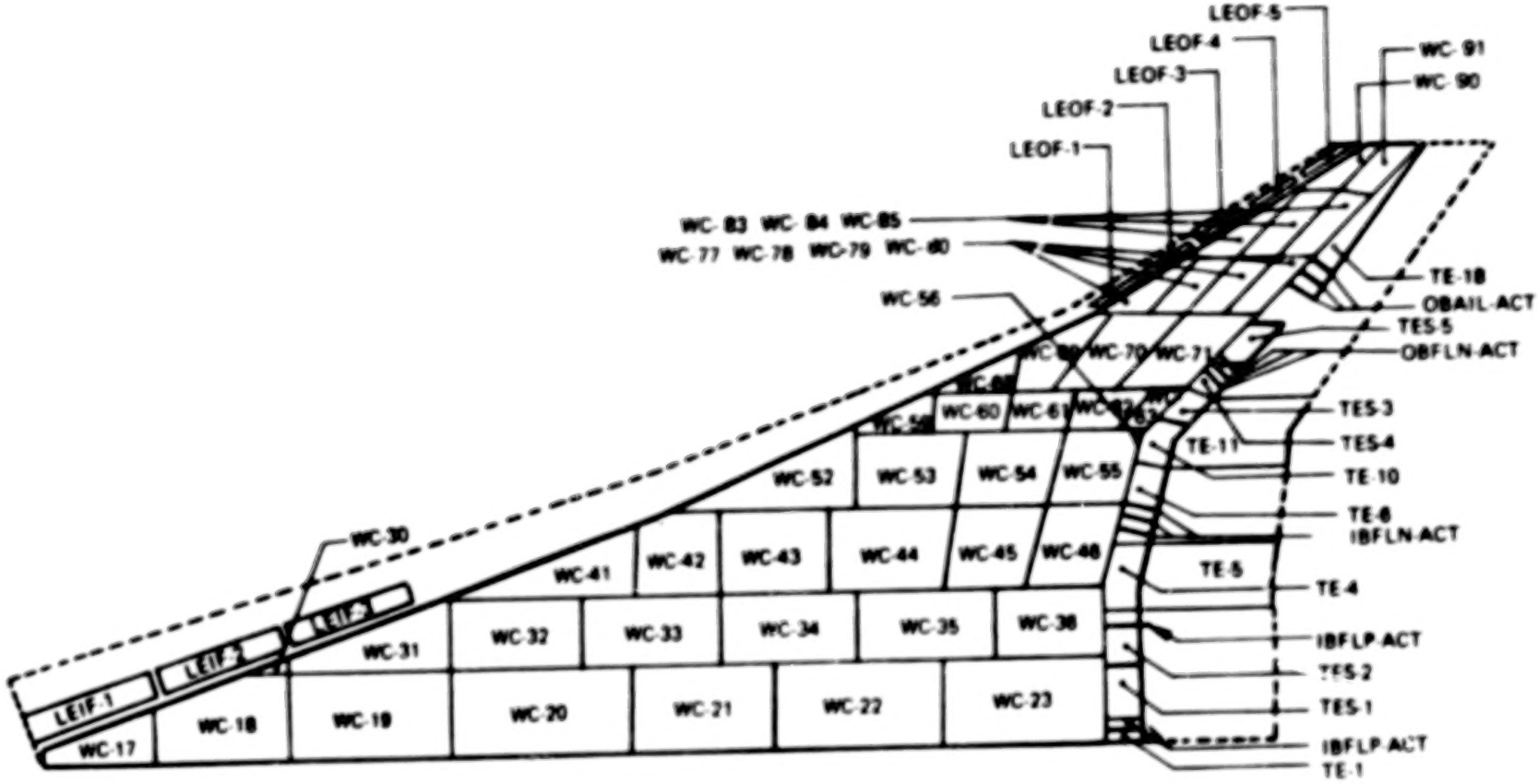

Figure 54. – Wing contents, mass input elements

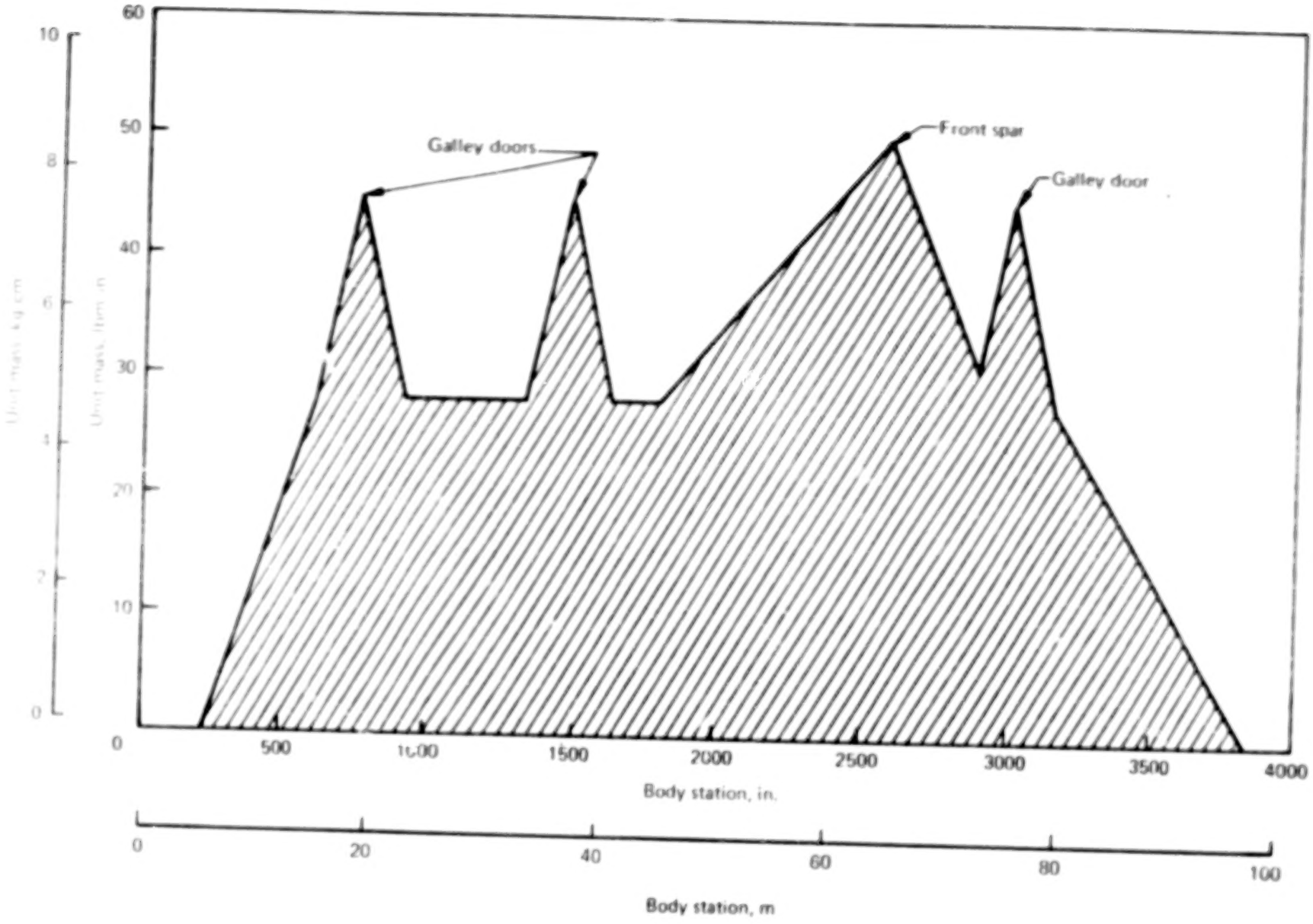

Figure 55. — Body structure and contents, mass distribution

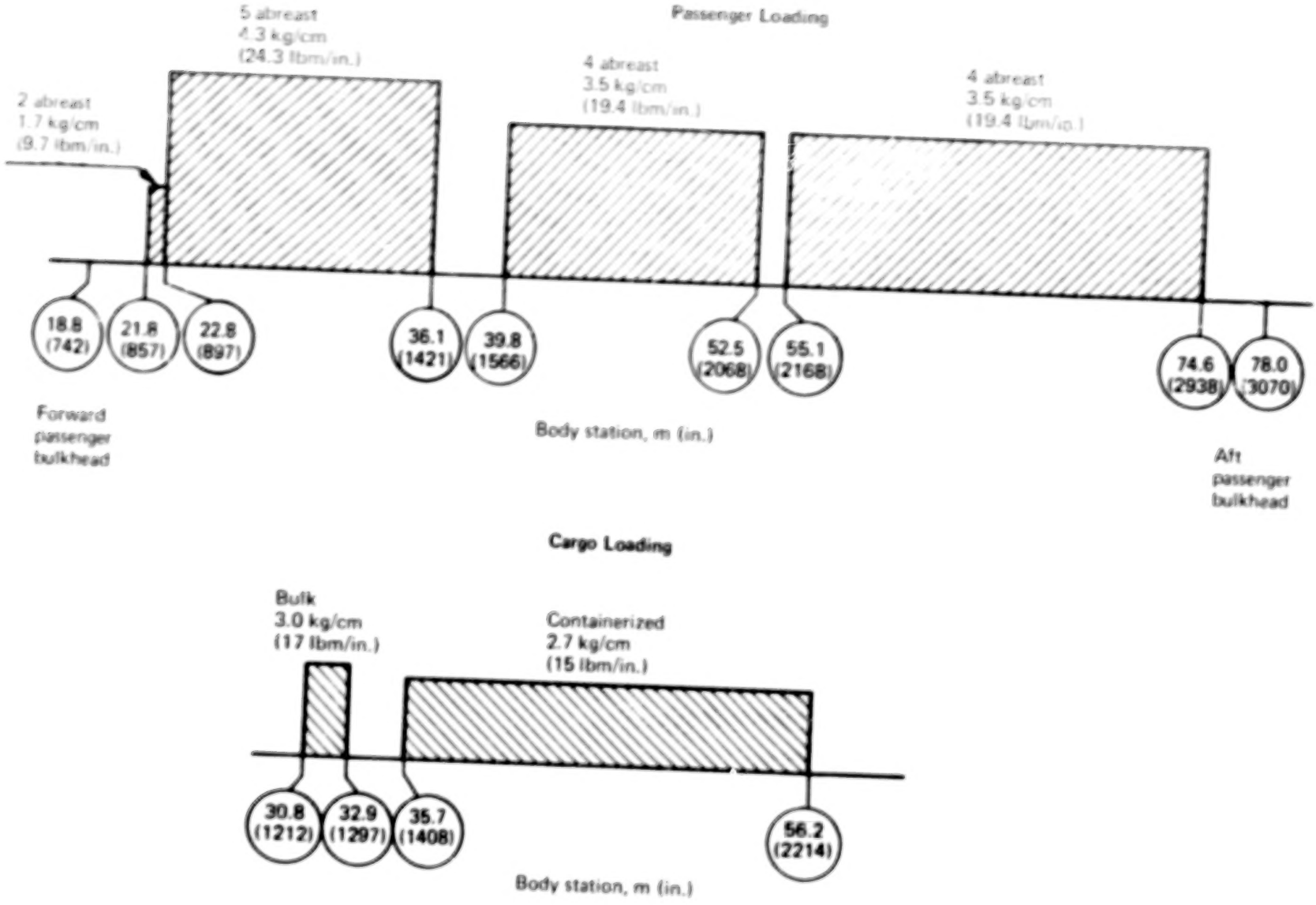

Figure 56. – Body payload, mass distribution

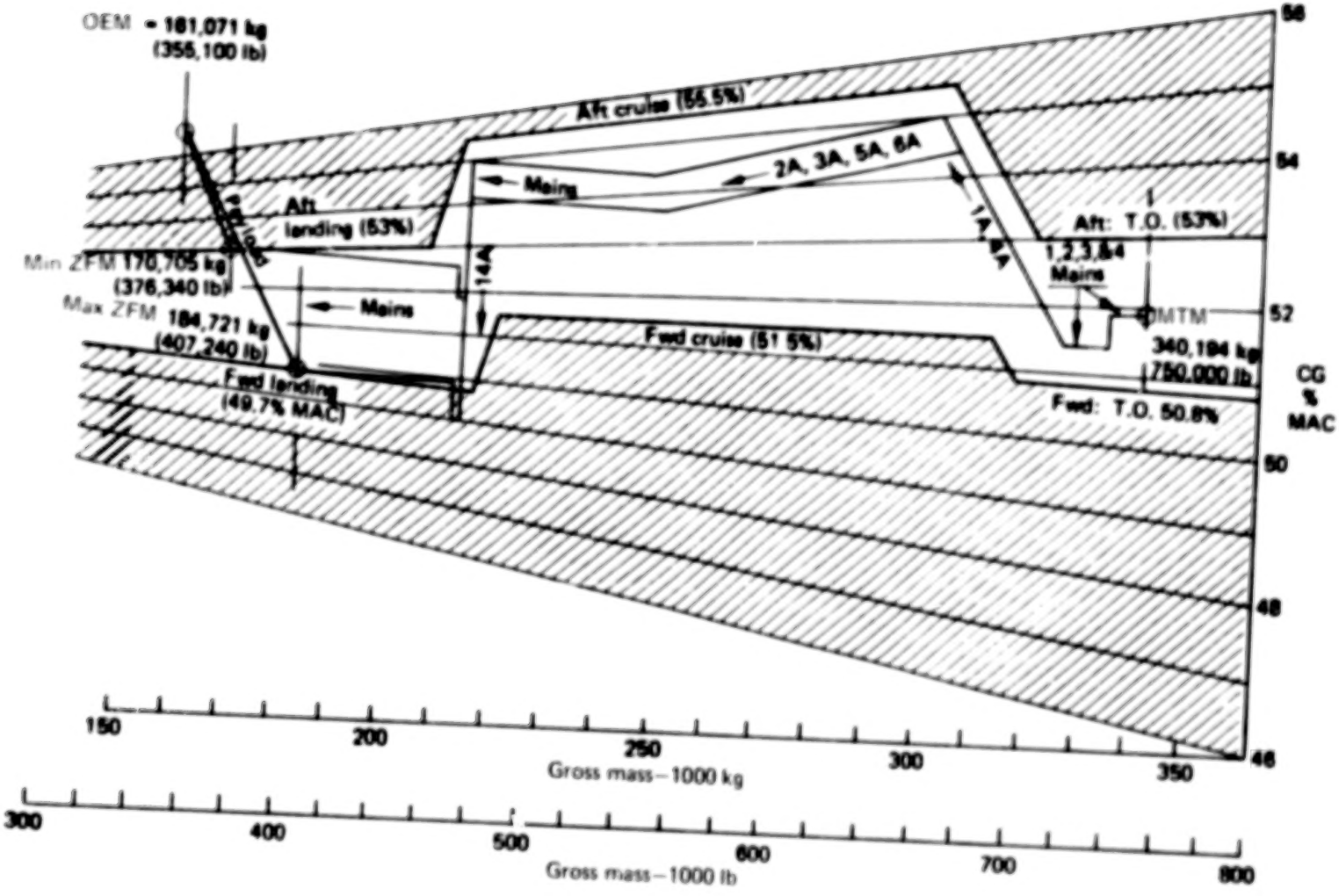

Figure 57. – Fuel management – model 969-512B

135

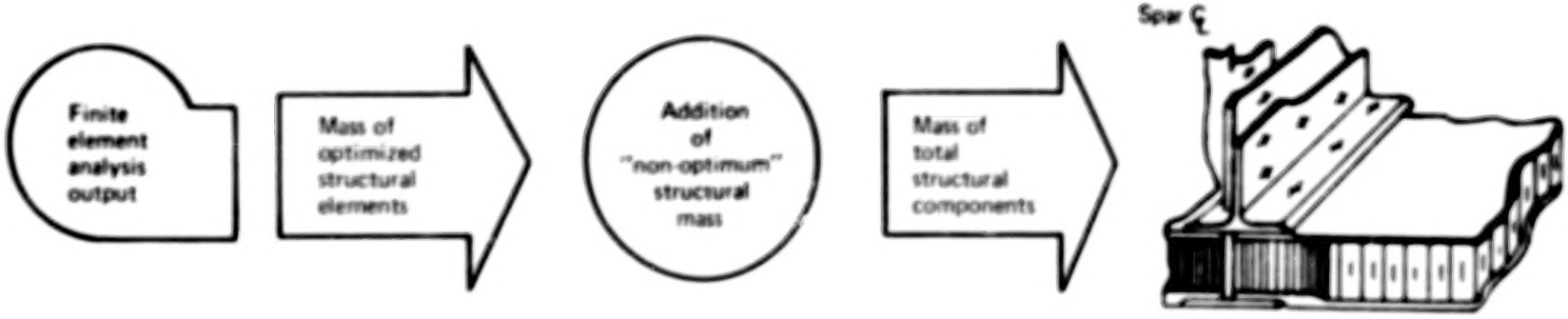
Finite element analysis output
Mass of optimized structural elements
Addition of "non-optimum" structural mass
Mass of total structural components
Spar ℄

Figure 58. – Structural mass estimation

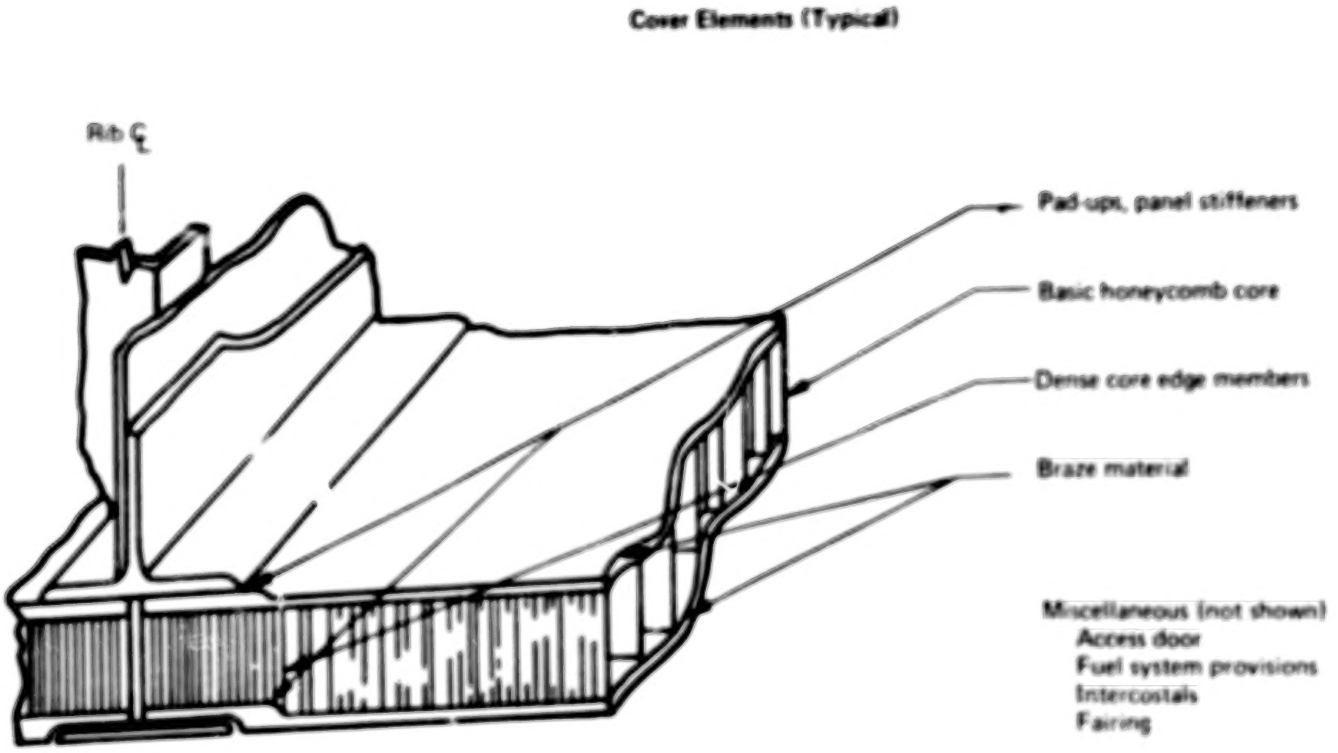

Figure 59. — Typical wing panel elements

137

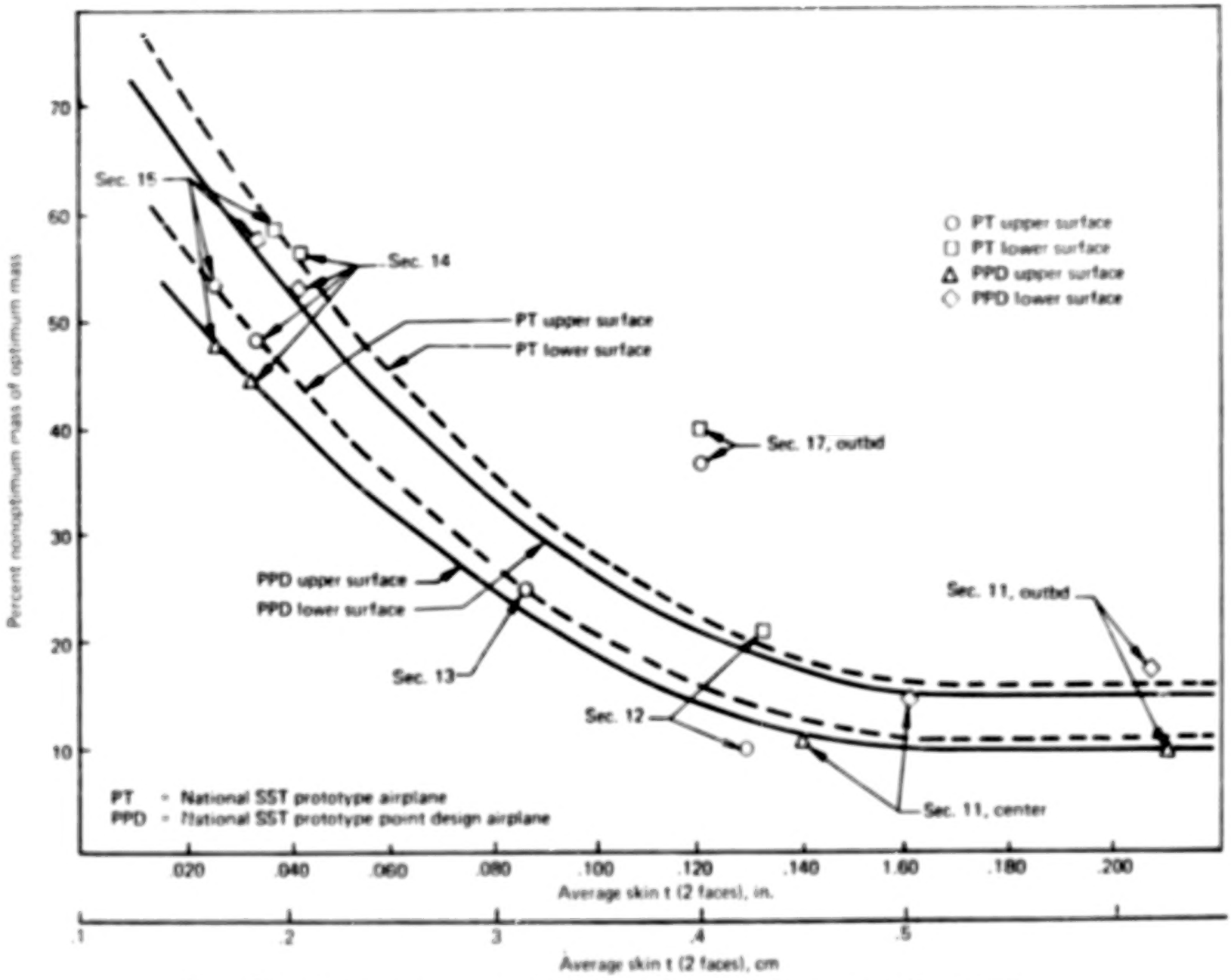

Figure 60. – Aluminum brazed titanium honeycomb panels–skin t vs nonoptimum mass

158

CONTENTS

	Page	
SUMMARY	1	1/A9
INTRODUCTION	3	1/A11
SYMBOLS AND ABBREVIATIONS	5	1/A13
CONFIGURATION DEFINITION	12	1/B6
Engine Definition	12	1/B6
969-512B Configuration	12	1/B6
Stability and Control	14	1/B9
Longitudinal Control	14	1/B9
Longitudinal Stability	14	1/B9
Lateral-Directional Stability and Control	16	1/B11
Fuel Tank Arrangements	17	1/B12
STRUCTURAL DESCRIPTION	19	1/B14
Materials Evaluation and Selection	20	1/C1
Metals	20	1/C1
Advanced Composites/Adhesives	20	1/C1
Fuel Tank Sealant	21	1/C2
Fuel Tank Insulation	21	1/C2
Structural Concepts	22	1/C3
Wing Skin Panel Concepts	27	1/C11
Wing Spar Concepts	29	1/C13
Fuselage Panel Concepts	30	1/C14
STRUCTURAL ANALYSIS AND DESIGN	32	1/D2
The Integrated Computer Program System	32	1/D2
The ATLAS System	32	1/D2
FLEXSTAB System	34	1/D4
Flutter Modules	36	1/D6
Analytical Models	36	1/D6
Structural Model	36	1/D6
Structural Model Verification	37	1/D7
Mass Model	38	1/D8
Aerodynamic Model	38	1/D8
Structural Design Loads	38	1/D8
Structural Design Airspeeds	38	1/D8
Design Gross Masses	39	1/D9
Engine Thrust	39	1/D9
Maneuver and Gust Criteria	39	1/D9
Landing, Taxi, and Ground Handling Loads Criteria	41	1/D11
Aerodynamic Loads Analysis	41	1/D11

CONTENTS (Concluded)

	Page
Structural Load Conditions	43 1/D14
Jig Shape	45 1/E2
Thermal Analyses	45 1/E2
Aerodynamic Heating	45 1/E2
Solar Absorptance and Surface Emittance	46 1/E3
Transient Thermal Analysis	46 1/E3
Fuel Temperature Analysis	48 1/E5
Mission Description	48 1/E5
Temperature Limits	49 1/E6
Fuel System	49 1/E6
Fuel Temperature	49 1/E6
Stress Analysis and Strength Sizing	52 1/E10
Flutter Analysis and Resizing	55 1/E13
Flutter Analysis Procedure	55 1/E13
Preliminary Flutter Analysis and Stiffness Resize	55 1/E13
Final Flutter Analysis and Stiffness Redesign	57 1/F1
Mass Analysis	58 1/F2
Wing and Contents	59 1/F3
Correction of Mass Analysis	59 1/F3
Body and Contents	62 1/F6
Empennage and Wing-Mounted Fin	62 1/F6
Fuel	62 1/F6
Wing Box Mass Estimation Method	62 1/F6
Mass Changes Resulting From Redesign for Strength	63 1/F7
Additional Mass Required to Satisfy Flutter Criteria	65 1/F10
Final Group Mass Statement	65 1/F10
EFFECTS OF REDESIGN ON AIRPLANE PERFORMANCE	67 1/F13
RECOMMENDATIONS	69 1/G1
Further Applications of the Arrow Wing Model	691 /G1
Research on Prediction of Aerodynamic Pressure Distributions	69 1/G1
Advanced Titanium Alloys	70 1/G2
Fabrication Techniques	70 1/G2
CONCLUDING REMARKS	72 1/G4
REFERENCES	74 1/G6

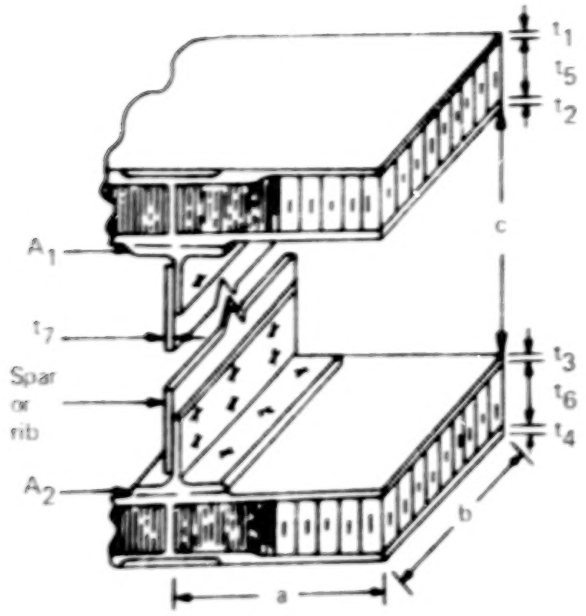

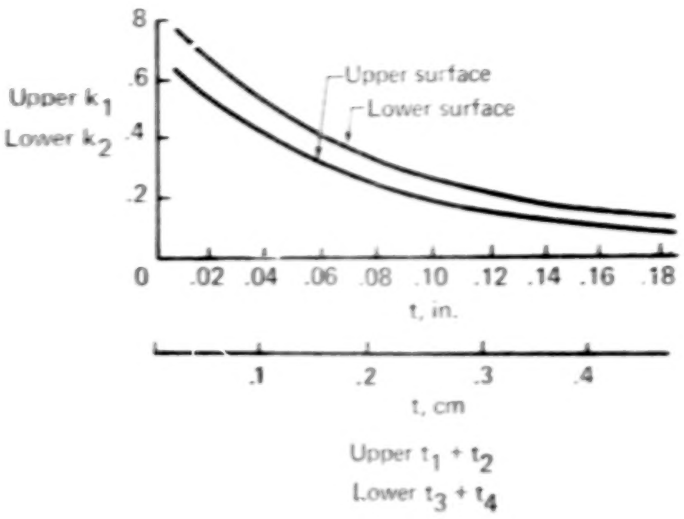

Cover Elements

Optimum mass

		Area		ATLAS sizing		Density
● Upper skin	=	(a)(b)	x	(t_1+t_2)	x	(ρ_1)
● Lower skin	=	(a)(b)	x	(t_3+t_4)	x	(ρ_1)

Nonoptimum mass

				Nonoptimum factor
● Upper skin	=	(Optimum mass)	x	(K_1)
● Lower skin	=	(Optimum mass)	x	(K_2)

		Area		Thickness		Density		Theoretical to actual
● Upper core	=	(a)(b)	x	(t_5)	x	(ρ_2)	x	(1.25)
● Lower core	=	(a)(b)	x	(t_6)	x	(ρ_6)	x	(1.30)
				Unit mass				
● Upper braze	=	(a)(b)	x	(w_1)	x			(1.25)
● Lower braze	=	(a)(b)	x	(w_2)	x			(1.30)

Spar and Rib Elements

Optimum mass

- Chords = ATLAS area/(A_1+A_2) x Length/(b) x Density/(ρ_1)
- Webs = Area/(b)(c) x ATLAS sizing/(t_7) x (ρ_1)

Nonoptimum mass

			Nonoptimum factor
● Spar	=	(Optimum mass)	x (.15)
● Rib	=	(Optimum mass)	x (.18)

Miscellaneous mass

Nonoptimum mass

- Fairing, fence, fuel system provisions, intercostals, jacking provisions, access doors, etc.

Figure 61. – Structural wing box mass estimation method

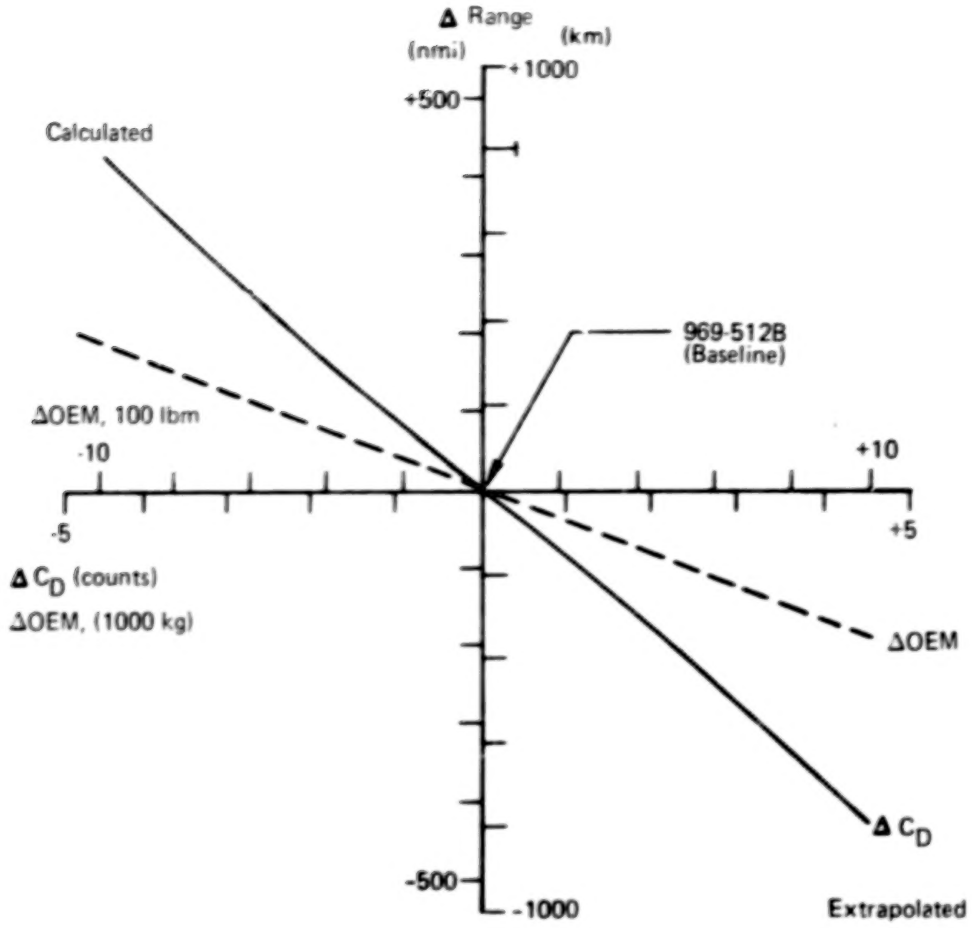

Figure 62. – Range sensitivity to OEM and supersonic drag

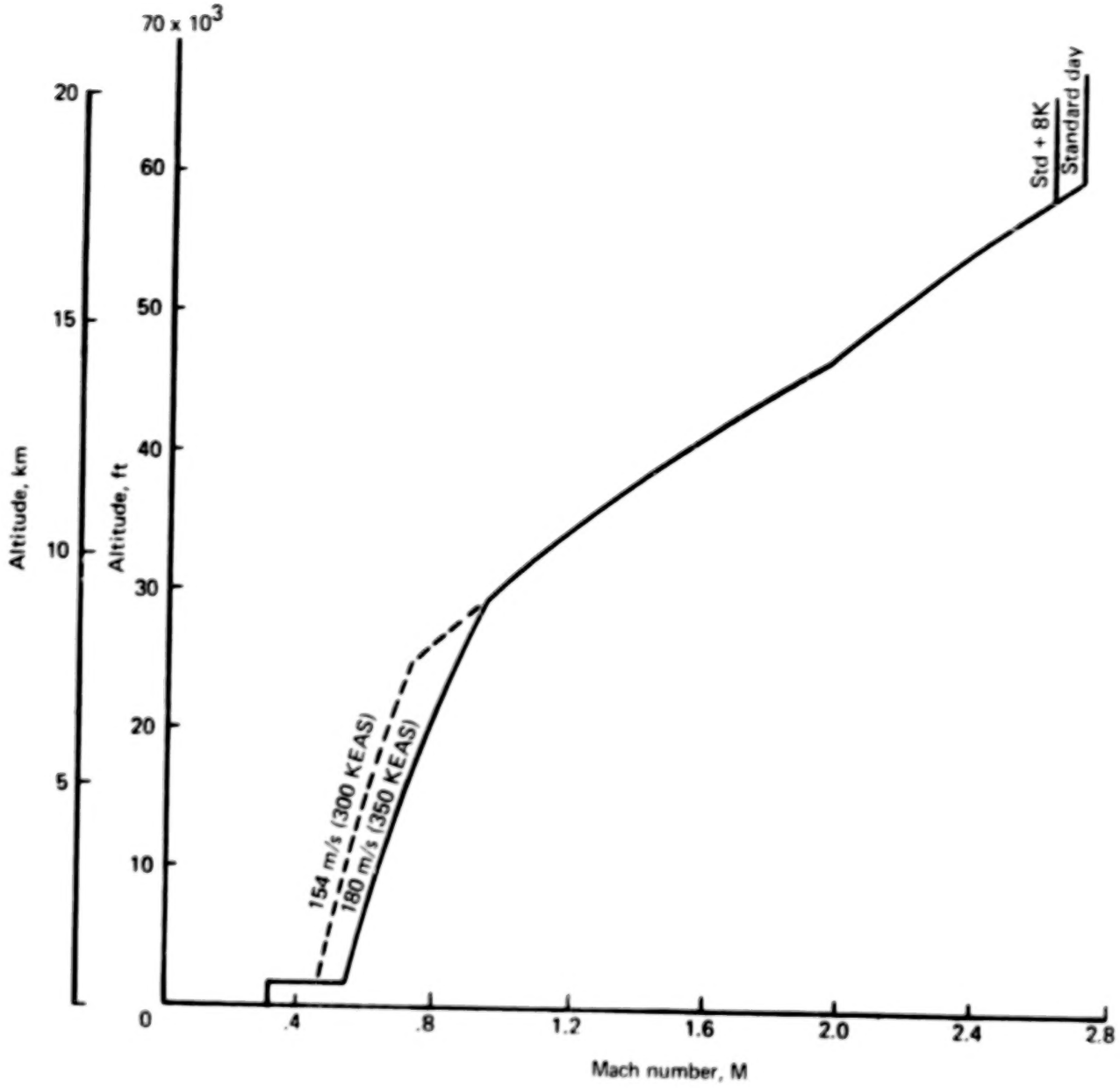

Figure 63. – SST performance climb placards

1. Report No.	2. Government Accession No.	3. Recipient's Catalog No.
NASA CR-2743		

4. Title and Subtitle	5. Report Date
STUDY OF METALLIC STRUCTURAL DESIGN CONCEPTS FOR AN ARROW WING SUPERSONIC CRUISE CONFIGURATION	December 1977
	6. Performing Organization Code
7. Author(s): M. J. Turner and D. L. Grande	8. Performing Organization Report No. D6-42438-3
9. Performing Organization Name and Address: Boeing Commercial Airplane Company, P.O. Box 3707, Seattle, Washington 98124	10. Work Unit No.
	11. Contract or Grant No. NAS1-12287
12. Sponsoring Agency Name and Address: National Aeronautics and Space Administration, Langley Research Center, Hampton, Virginia 23665	13. Type of Report and Period Covered: Tasks I and II Final Report
	14. Sponsoring Agency Code

15. Supplementary Notes

Langley Contract Monitors: James C. Robinson and E. Carson Yates, Jr.

Final Report (Tasks I and II)

16. Abstract

A structural design study was made, based on a 1975 level of technology, to assess the relative merits of various metallic structural concepts and materials for an advanced supersonic aircraft cruising at Mach 2.7. Preliminary studies were made to ensure compliance of the configuration with general design criteria, integrate the propulsion system with the airframe, select structural concepts and materials, and define an efficient structural arrangement. An advanced computerized structural design system was used, in conjunction with a relatively large, complex finite element model, for detailed analysis and sizing of structural members to satisfy strength and flutter criteria. A baseline aircraft design was developed for assessment of current technology as well as for use in future studies of aerostructural trades and in application of advanced technology. Criteria, analysis methods, and results are presented. The effect on design methods of using the computerized structural design system is appraised, and recommendations are presented concerning further development of design tools, development of materials and structural concepts, and research on basic technology.

17. Key Words (Suggested by Author(s))	18. Distribution Statement
Arrow wing, supersonic cruise SCAR technology NASA SCAT-15F	Unclassified–Unlimited Subject Category 05

19. Security Classif. (of this report)	20. Security Classif. (of this page)	21. No. of Pages	22. Price*
Unclassified–Unlimited	Unclassified–Unlimited	148	$7.25

* For sale by the National Technical Information Service, Springfield, Virginia 22161

END

DEC 11 1978